NASA/TM-2007-214894

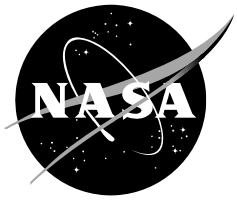

Overview of Supersonic Aerodynamics Measurement Techniques in the NASA Langley Unitary Plan Wind Tunnel

Gary E. Erickson
Langley Research Center, Hampton, Virginia

August 2007

The NASA STI Program Office ... in Profile

Since its founding, NASA has been dedicated to the advancement of aeronautics and space science. The NASA Scientific and Technical Information (STI) Program Office plays a key part in helping NASA maintain this important role.

The NASA STI Program Office is operated by Langley Research Center, the lead center for NASA's scientific and technical information. The NASA STI Program Office provides access to the NASA STI Database, the largest collection of aeronautical and space science STI in the world. The Program Office is also NASA's institutional mechanism for disseminating the results of its research and development activities. These results are published by NASA in the NASA STI Report Series, which includes the following report types:

- TECHNICAL PUBLICATION. Reports of completed research or a major significant phase of research that present the results of NASA programs and include extensive data or theoretical analysis. Includes compilations of significant scientific and technical data and information deemed to be of continuing reference value. NASA counterpart of peer-reviewed formal professional papers, but having less stringent limitations on manuscript length and extent of graphic presentations.

- TECHNICAL MEMORANDUM. Scientific and technical findings that are preliminary or of specialized interest, e.g., quick release reports, working papers, and bibliographies that contain minimal annotation. Does not contain extensive analysis.

- CONTRACTOR REPORT. Scientific and technical findings by NASA-sponsored contractors and grantees.

- CONFERENCE PUBLICATION. Collected papers from scientific and technical conferences, symposia, seminars, or other meetings sponsored or co-sponsored by NASA.

- SPECIAL PUBLICATION. Scientific, technical, or historical information from NASA programs, projects, and missions, often concerned with subjects having substantial public interest.

- TECHNICAL TRANSLATION. English-language translations of foreign scientific and technical material pertinent to NASA's mission.

Specialized services that complement the STI Program Office's diverse offerings include creating custom thesauri, building customized databases, organizing and publishing research results ... even providing videos.

For more information about the NASA STI Program Office, see the following:

- Access the NASA STI Program Home Page at ***http://www.sti.nasa.gov***

- E-mail your question via the Internet to help@sti.nasa.gov

- Fax your question to the NASA STI Help Desk at (301) 621-0134

- Telephone the NASA STI Help Desk at (301) 621-0390

- Write to:
  NASA STI Help Desk
  NASA Center for AeroSpace Information
  7115 Standard Drive
  Hanover, MD 21076-1320

NASA/TM-2007-214894

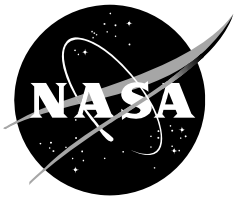

Overview of Supersonic Aerodynamics Measurement Techniques in the NASA Langley Unitary Plan Wind Tunnel

Gary E. Erickson
Langley Research Center, Hampton, Virginia

National Aeronautics and
Space Administration

Langley Research Center
Hampton, Virginia 23681-2199

August 2007

Acknowledgments

The following individuals at NASA Langley Research Center and NASA Ames Research Center are acknowledged for their helpful discussions and contributions to this paper: James E. Bartlett, Adolphus B. Blair, Stephen E. Borg, Alpheus W. Burner, James E. Byrd, Stanley R. Cole, Bradley L. Crawford, Richard DeLoach, A. T. Ferris, Tom D. Finley, Gary A. Fleming, Joel L. Everhart, Robert M. Hall, James B. Hallissy, Michael J. Hemsch, Robert A. Kennelly, M. Trent Kite, William B. Krieger, Darrell G. Livingston, James F. Meyers, John R. Micol, Clifford J. Obara, Naresh Patel, Ray D. Rhew, William I. Scallion, Richard J. Schwartz, David S. Shaw, Leonard M. Weinstein, Floyd J. Wilcox, and Mark J. Won.

Available from:

NASA Center for AeroSpace Information
7115 Standard Drive
Hanover, MD 21076-1320
301-621-0390

National Technical Information Service
5285 Port Royal Road
Springfield, VA 22161
703-605-6000

Table of Contents

Abstract

An overview is given of selected measurement techniques used in the NASA Langley Research Center (NASA LaRC) Unitary Plan Wind Tunnel (UPWT) to determine the aerodynamic characteristics of aerospace vehicles operating at supersonic speeds. A broad definition of a measurement technique is adopted in this paper and is any qualitative or quantitative experimental approach that provides information leading to the improved understanding of the supersonic aerodynamic characteristics. On-surface and off-surface measurement techniques used to obtain discrete (point) and global (field) measurements and planar and global flow visualizations are described, and examples of all methods are included. The discussion is limited to recent experiences in the UPWT and is, therefore, not an exhaustive review of existing experimental techniques. The diversity and high quality of the measurement techniques and the resultant data illustrate the capabilities of a ground-based experimental facility and the key role that it plays in the advancement of our understanding, prediction, and control of supersonic aerodynamics.

Introduction

Wind tunnel experimental techniques to measure the aerodynamic characteristics of airplanes, missiles, and spacecraft that operate in the supersonic flight regime have experienced significant advancements in the past several years (reference 1). These advancements range from improvements to existing technologies such as strain-gage balances, model attitude sensors, and electronically-scanned pressure measurement systems to the emergence of new optical measurement techniques to acquire field measurements of surface pressures and temperatures, aeroelastic deformations, and off-surface flow-field velocities. Flow visualization methods based on well-established aerodynamic principles have also benefited from the advancements in digital imagers, illumination sources, and image acquisition/processing hardware and software. The ability to create computer models of the wind tunnel testing environment, including the installation of complex image acquisition systems, using virtual facilities is another available tool to optimize the test process and the performance of flow measurement techniques (reference 2). The quality of the overall wind tunnel testing process may be significantly improved by a design of experiments approach, a process-based measurement technique that randomizes the data acquisition and may dramatically reduce the systematic experimental errors (reference 3).

This report provides an overview of several measurement techniques that have been used in the NASA LaRC UPWT during the past decade. The discussions will emphasize their implementation at supersonic speeds, but the techniques, with few exceptions, are applicable to any speed regime and any wind tunnel facility. A description of the UPWT facility is given along with a detailed account of the test processes involving the preparation and use of strain-gage balance and electronic pressure-scanning instrumentation in this facility. Descriptions and examples are provided of on-surface and off-surface flow visualization and optical measurement methods, statistically-designed experiments, and techniques to quantify missile aerodynamics, stores carriage drag, flutter suppression, sonic boom signatures, dynamic stability derivatives, flow-field parameters, reaction control jet-induced effects, stage separation aerodynamics, and launch vehicle and reentry vehicle high angle-of-attack aerodynamics.

Nomenclature

alpha	angle of attack, degrees (deg)
AF	axial force, pounds (lbs)
AMS	angle measurement system
b or bw	reference span, inches (in.)
AC	alternating current
BDDU	balance dynamic display unit
BM	bending moment, inch-pounds (in-lbs)
BLMS	balance loads monitoring system
c or cw	reference length, in.
CA1	axial force coefficient, $\frac{AF}{q(sw)}$
C_D	drag force coefficient, $\frac{Drag}{q(sw)}$
C_{NF}	normal force coefficient, $\frac{NF}{q(sw)}$
C_{BM}	bending moment coefficient, $\frac{BM}{q(sw)cw}$
C_{TM}	torsional moment coefficient, $\frac{TM}{q(sw)bw}$
C_p	pressure coefficient, $\frac{p - p_\infty}{q(sw)}$
$C_{p,wall}$	test section ceiling static pressure coefficient
CAD	computer aided design
CCD	charge coupled device
CCU	camera control unit
CFD	computational fluid dynamics
CIHW	confidence interval half width
CPA	critical point analyzer
DAS	data analysis system
DC	direct current
Delta X	axial translation of orbiter model relative to booster model, in.
Delta Z	lateral translation of orbiter model relative to booster model, in.
DGV	doppler global velocimetry
DoD	Department of Defense
DQA	data quality assurance
DESL	data engineering scripting language
ESP	electronically-scanned pressure
FADS	flush air data sensing
F. S.	full scale
H_o	stagnation pressure, psfa
HSR	high-speed research
IFC	interface control
IR	infrared
KPG	known pressure generator
LaRCNET	Langley Research Center network
LEX	leading-edge extension
LGBB	Langley Glideback Booster
M or Mach	free stream Mach number
MDOE	modern design of experiments
MIIDAS	Multi-Instrument Integrated Data Acquisition System
MRC	moment reference center
M_∞	free stream Mach number
NF	normal force, pounds
NTF	National Transonic Facility
NTSC	National Television System Committee
OFAT	one-factor-at-a-time
p	local static pressure, psfa
p_{jet}	jet total pressure, psia
p_∞ *or* p_{inf}	free stream static pressure, psfa
psfa	pounds per square foot absolute
psia	pounds per square inch absolute
psid	pounds per square inch differential
PC	personal computer
PCU	pressure calibration unit
PM	pitching moment, in-lbs
PMI	projection moiré interferometry
PPG	portable pressure gage
PRT	platinum resistance temperature device
PSP	pressure sensitive paint
q or q_{inf}	free stream dynamic pressure, psfa
QFlex	gravity sensing servo accelerometer
Re or Re/ft	Reynolds number per foot, millions
RCS	reaction control system
RM	rolling moment, in-lbs
RP	remote processor
s	wing local semispan, in.
sw	reference area, square feet (sq. ft.)
SCSI	small computer systems interface
SDI	scanner digitizer interface

SDU	scanner digitizer unit
SP	system processor
SVS	single vector system
T_0	stagnation temperature, degrees Fahrenheit (^{o}F)
TSP	temperature sensitive paint
TSTO	two-stage to orbit
UPWT	Unitary Plan Wind Tunnel
UV	ultraviolet
V_x	output voltage from ESP sensors
ViDi	Virtual Diagnostics
VMD	video model deformation
x	distance along wing centerline measured from the apex, in.
y	distance along wing local semispan measured from wing centerline, in.
α	angle of attack, deg
β	angle of sideslip, deg
σ	standard deviation
η	nondimensional semispan location
Δ	denotes delta coefficient value; in data repeatability analysis, Δ's are obtained by interpolating in each run to the nominal values of the independent variable, then averaging and subtracting the averages from the interpolated data
$\Delta C_{nf,induced}$	RCS jet-induced normal force coefficient increment
$\Delta C_{pm,induced}$	RCS jet-induced pitching moment coefficient increment

Discussion

Facility and Data System Descriptions

The Unitary Plan Wind Tunnel (UPWT) (references 4 and 5) is a closed-circuit pressure tunnel with two test sections that are nominally 4 feet by 4 feet in cross section and 7 feet long. A photograph of the facility is shown in figure 1. The primary elements of UPWT are a 100,000-horsepower compressor drive system, a dry air supply and evacuating system, a cooling system, and the necessary interconnecting ducting to produce the proper air flow through either of the two test sections. The Mach number range is approximately 1.50 to 2.86 in Test Section 1 and 2.30 to 4.63 in Test Section 2. The stagnation pressure can be varied up to a maximum of approximately 50 psia in Test Section 1 and approximately 100 psia in Test Section 2. The nozzle throat-to-test section area ratio is varied by a lower asymmetric sliding nozzle block that provides continuous variation of the Mach number. Figures 2 and 3 illustrate the asymmetric sliding nozzle block and the general layout of the UPWT test sections, respectively. The second-minimum area is controlled by moving hinged sidewalls to provide the proper constriction to stabilize the normal shock downstream of the test section at the various operating Mach numbers. In order to cover the entire Mach number range for each test section, the tunnel duct configurations must be altered to provide the proper compression ratio. Six centrifugal compressors are used in five tunnel configurations or modes, and the tunnel operating modes are available for only one test section at a time. Test Section 1 has two modes within which the Mach number is varied from 1.50 to 2.16 and 2.36 to 2.86, respectively. Three modes exist in Test Section 2 within which the Mach number is varied from 2.30 to 2.96, 3.00 to 3.71, and 3.82 to 4.63, respectively. The tunnel stagnation temperatures are typically 125^o F and 150^o F, depending on the mode of operation. Typical Reynolds numbers for testing at UPWT are 2.0 to 4.0 million per foot, although a range of Reynolds numbers from 1.0 to 5.0 million per foot can be easily accommodated. A Reynolds number of 6.0 million per foot is possible on a selected basis only because of tunnel drive system operational limits. Several methods to support the model have been used, but the basic mechanism is a horizontal wall-mounted strut which is capable of forward and aft travel of over 3 feet in the streamwise direction. A main sting support is attached to the strut and has lateral traverse and sideslip motion of +/-20 inches and +/-12 degrees, respectively. Forward of the main sting support is the angle-of-attack mechanism which provides pitch motion from -15 degrees to +30 degrees. A roll mechanism can be installed ahead of the pitch mechanism to provide continuous roll motion with a range of 360 degrees. The model is mounted to the roll

mechanism or the pitch mechanism by means of a wide assortment of available stings. Recent upgrades to the facility include a Tunnel Flow Control System for automated control of the tunnel stagnation pressure, stagnation temperature, and dewpoint and Model Attitude Control Systems for Test Sections 1 and 2 providing automated test sequencing for pitch, yaw, and roll angles, axial and lateral positions, and data acquisition.

The test section stagnation pressure is derived from one of two pitot probes located in the tunnel settling chamber. A vacuum-referenced, Ruska Series 6000 quartz differential pressure transducer measures each settling chamber pressure. Tunnel humidity is monitored using a General Eastern SPECTRA L1 Hygrometer. An Instrulab 25 ohm platinum resistance thermometer (PRT) measures tunnel total temperature. No corrections for thermal transfer, flow losses or other dissipative effects are applied to these tunnel measurements.

Each test section has its own dedicated data acquisition system and instrumentation suite that is centered on a Modcomp 88100 Open Architecture System. Data acquisition and real time data reduction are performed utilizing a Modcomp 88100 computer complex that is interfaced to Neff 620 analog amplifier conditioning units and Pressure Systems Incorporated (PSI) 8400 System Processors (SP). Final data reduction and post-processing functions are accomplished on personal computer (PC) workstations using NASA Langley-developed Multi-Instrument Integrated Data Acquisition System (MIIDAS) software. The workstations are linked to the Langley Research Center network (LaRCNET).

The standard Modcomp data sampling rate for all Neff analog input channels is 15 frames per second (frames/sec), averaged over a 2 second interval for each data point (30 frames averaged per point). The standard electronically-scanned pressure (ESP) data sampling rate between the Modcomp and the PSI 8400 SP is 10 frames/sec, which is also averaged over a 2-second interval (20 frames averaged per point).

Force and Moment Measurement Techniques

Strain-gage balance instrumentation and pretest preparations

Strain-gage balance measurements are a critical element in the determination of the aerodynamic characteristics of a wind tunnel model. Measurements up to six degrees of freedom are made, ranging from a single-component balance to acquire hinge moments on a model control surface to a six-component balance for total forces and moments on a complete model. A recent technology assessment of balance design, fabrication, and calibration is provided in reference 6. The design, fabrication, and calibration phases are labor- and time-intensive and require several months or more to complete. This effort does not end upon delivery of the balance to the wind tunnel, since considerable work is necessary by the facility staff to ensure the proper installation and performance of the instrument during an experiment. The desire to measure forces and moments to sufficient accuracy to define the drag coefficient to within one count (+/-0.0001) at supersonic cruise conditions has imposed more stringent requirements on the installation and utilization of these instruments. The present section will summarize many of the procedures that are used at UPWT to ensure that the force and moment measurement requirements for a given test are met.

Six-component, internal strain gage balances that are most frequently used at UPWT are single-piece, direct-read instruments based on LaRC design practices discussed in reference 7. The balance-to-model attachments are two types, namely, diameter fit and expandable diameter fit secured and located by a dowel pin. A LaRC expander-type balance is shown in figure 4. This design provides the same cylindrical fit as the non-expandable balances but with increased adaptability by expanding a

sleeve on the balance tapered front end to fit the model bore.

The balance-to-sting attachment is a tapered fit augmented by a double nut or set screw. Relative movement in roll is controlled by a key inserted in slots cut into the balance and sting tapers. The balances are parallel-wired and the new standard is that the electrical connectors are an integral part of the balance instead of being attached at the end of a leadwire system. The input voltage is monitored on the balance. Consequently, span checks to adjust the primary sensitivities for voltage drop due to the tunnel wiring are no longer necessary. Standard practice is also to incorporate PRTs at three locations along the balance length (forward, middle, and aft sections) to monitor balance temperatures and thermal gradients. The measurement of the average balance temperature allows a first-order correction to the balance primary sensitivities, provided thermal calibration runs were included in the balance calibration process. Methods to correct for balance thermal gradients have not been established. Instead, thermal gradients are minimized by preheating the balance in wind-on conditions prior to acquiring data.

Wind tunnel model systems that have been approved for testing at UPWT are subject to a detailed, pretest inspection process to ensure a satisfactory assembly of the model, balance, and sting. Note that this process is essentially duplicated, since the procedures described next are performed for both the primary and backup balances for a given test. Quality Assurance (QA) inspections are made on a three-dimensional (3-D) validator table of the model interface to the balance, which might feature an integral bore and dowel hole or a separate balance strongback. These inspections identify anomalies such as bore and dowel hole out-of-roundness and taper, spatial and angular misalignments of the bore and dowel hole relative to the model reference axes, and surface finish irregularities. If warranted, remachining of the model interface to the balance is performed. Accurate determination of angular offsets between the model and balance is essential, since these offsets are included in the Euler angle rotation sequence to compute the angles of attack and sideslip in the wind tunnel data reduction program. Similar inspections are made of the strain-gage balance and sting. The balance and sting are fit to ring and plug gage and taper gage sets. The front expander is visually inspected to ensure proper movement of the expander on the forward taper and satisfactory engagement of the gear and pinion assembly. The percentage of surface contact between the balance and sting tapers is evaluated by applying a thin layer of fluorescent oil to one taper, assembling the components, and observing the mating surfaces under an ultraviolet light source after disassembly. Any discrepancies lead to a more detailed mapping of the tapers on a validator table to identify sections that may require remachining to achieve the desired minimum 90% surface contact. The balance and sting keyways and balance dowel hole are also mapped as a necessary step in the process of fabricating custom dowel pins and key for the model, balance, and sting assembly. Until recently, a standard dowel pin was typically a 0.0002-in. interference fit and was fabricated from Beryllium-Copper (Be-Cu). Nitronic-60 is now the material of choice, since it is robust but softer than the model and balance materials in which it is in contact. In addition, the desired interference fit is 0.0001 in. The pins frequently require a step to adapt from the model dowel hole to the balance dowel hole. Two dowel pins are fabricated (one as a spare) along with an aluminum alignment pin. The latter pin is sized to be a press fit and provides a preliminary alignment of the model to the balance before installing the final pin. A custom key is also fabricated and, like the dowel pins, is typically stepped to accommodate the different widths of the balance and sting keyways. A 0.0001-in. interference fit is specified for the key-to-balance, while a sliding (yet snug) fit to the sting is required to ensure that the balance will fully engage the sting taper. The balance and sting are assembled without and with the key, and respective measurements are recorded of the distance from the balance aft bulkhead to

the forward edge of a sting access hole after securing the draw nut or set screws (the measurements must be identical). These results are retained for future reference during the model, balance, and support system build-up in the wind tunnel test section.

Update recalibrations of the balance are routinely conducted. Independent temperature and humidity runs can be made to evaluate the existing temperature compensation and the integrity of the moisture protection coating. Until recently, the update recalibrations included only primary loadings, and the coefficient matrix from the primary updates were combined with the previous calibration to generate an updated matrix. The quoted balance accuracies were transferred unaltered from the previous full calibration without an independent verification. The primary update calibration is now treated as a calibration verification and includes an independent check of the accuracies by including three multi-component loadings in addition to the 17 primary loading sequences. A full calibration is recommended if an analysis reveals that the difference in errors between the updated calibration and the last full calibration exceed the component accuracies. Should this be the case, the remaining 64 loading sequences are performed. A total of 738 dead weight loads are applied in a full calibration (82 loading sequences with 9 loadings per sequence) and feature primary and secondary loadings over all six components to establish the balance sensitivity and interaction coefficients. It is noted that the calibration process at NASA LaRC is undergoing revolutionary changes as a result of the development of a Single-Vector Balance Calibration System (SVS) combined with formal experimental design, which is discussed in reference 8. The SVS has resulted in an order-of-magnitude reduction in the calibration turn-around time, improved calibration data quality, and new insights regarding balance interactions.

Build-up of the sting, balance, and model is generally done in the test section. The balance is installed to the sting, and verification of proper fit is ensured by matching the pre-test measurements cited earlier. The sting center bore is sealed after verification of the balance fit in order to prevent the transmittal of flow-induced (and non-repeatable) effects through the sting and into the model chamber. Response and channel assignment checks are performed of the balance and PRTs, which include simple hand loadings of all six balance components and the application of a heat gun to verify the status and locations of the temperature sensors. Balance-alone zeroes are acquired with the balance in the upright and inverted orientations, and the voltage outputs are compared to pretest zeroes acquired at the LaRC Balance Calibration Laboratory and to a computer listing of the balance zeroes history over the life of the instrument.

The amplified and buffered analog signals from the balance are input to a dynamic loads monitor, termed a Balance Dynamic Display Unit (BDDU) which is described in detail in reference 9. The BDDU normalizes and multiplexes these signals so that the displayed output on an oscilloscope denotes percent of full-scale (F. S.) design loads in six sequential horizontal locations. Two-level visual and audible alarms are incorporated to indicate when a signal exceeds 80% and 100% of the design load. The BDDU is frequently programmed with design load limits of model or support system hardware instead of the balance in order to satisfy LaRC model systems safety requirements. The observations from the BDDU include real-time static plus dynamic load, frequency content, and the relative load level from component to component. The BDDU monitoring system was originally designed to monitor the wind-on dynamic loads, but it is also very useful during the in-tunnel calibrations and the model build-up process to avoid overloading any balance components. The BDDU monitors individual components and does not indicate the maximum combined stress on the balance. Certain high-stress locations on the balance, called critical points, exist when all six design loads are applied simultaneously. A second instrument to monitor the dynamic loads

is a critical point analyzer (CPA) (reference 9), which scales and sums each normalized signal from the BDDU to obtain combined static and dynamic signals representative of the dynamic loads at pre-defined high-stress points. Simultaneous application of the design loads on all six channels is uncommon in UPWT testing and, consequently, the CPA is not typically used. The BDDU concept has recently been extended to a dedicated graphics-rich PC-based system and is referred to as the LaRC Balance Loads Monitoring System (BLMS).

A precision-machined calibration fixture is installed to the balance prior to initiating sting deflection calibrations, which are discussed in a later section on angle of attack measurement techniques. A hand-held force gage having a 55-lb load capacity and accurate to +/-0.1% of full-scale (F.S.) reading is used to apply check loads to all six balance components. The force gage is interfaced to the wind tunnel data acquisition system, and the applied loads are compared to the computed balance loads to verify proper balance output. The applied and computed forces and moments are easily observed on a large digital display mounted to a wall outside each test section. The sting deflection process provides additional verification of the balance and data reduction program status, since the computed forces and moments are monitored and compared to the loads applied using a 1000-lb hydraulic load cell apparatus accurate to within +/-0.03% F.S. or using calibrated weights suspended from a pan and double knife-edge assembly.

Installation of the model onto the balance is performed by first aligning the respective dowel holes with the alignment pin, applying a preliminary torque to the expander (if applicable), removing the alignment pin, installing the final pin, and applying a maximum prescribed torque to the expander. Final check of the expander fit is done by applying a near-maximum rolling moment in both directions and applying torque to the expander until no further movement is detected. Model build-up, as necessary, progresses after the model-to-balance interface is completed. A silicone-based sealant is applied to all mating surfaces that represent boundaries between the external flow and the model chamber to prevent “leakage” into the model, which would affect the chamber pressure measurements and the balance axial force output. Additional check loads are applied using the hand-held force gage. This procedure is particularly useful in verifying an interference-free model-to-balance assembly and confirming the model fuselage station of the balance moment center. A fiber optic borescope is also available to visually inspect the model chamber area. The normal force and pitching moment outputs of the balance caused by the weight of the complete model are also compared with measurements made outside the test section, where the model is weighed on a digital scale and the center of gravity is estimated by marking the balance point of the model. Final check loads that approximate the maximum forces and moments (and combinations thereof) to be expected during wind-on testing are applied using the hydraulic load cell with double knife-edge (and a buffer plate between the knife edge and model surface) or weights suspended from a pan and double knife-edge assembly. A fully-assembled model ready to run in UPWT Test Section 1 is shown in figure 5.

Neff data acquisition unit calibrations are performed daily as a standard practice, and amplifier drifts are negligible. The manufacturer’s quoted accuracy is +/-0.02% of range plus 2 microvolts (μV) over a 30-day period of time without interim calibrations (typical range is 10 millivolts (mV)). Additional checks of the strain-gage balance instrumentation are performed using a Wavetek Model 4800 multifunction analyzer and various Neff diagnostic programs, which include histograms of the balance component outputs.

Within-test procedures

A history of the balance wind-off zeroes with the model support system set to a level pitch attitude is maintained throughout the testing. The standard procedure at UPWT is to acquire wind-off zeroes at atmosphere and at pumpdown

conditions, where the test section is evacuated to a pressure that is typically 300 psfa to 400 psfa, before and after a run series. The pumpdown zeroes also allow evaluation of model chamber and/or base pressure measurements which are made using individual +/-5 psia Druck transducers. The manufacturer-specified uncertainty as a percent of full-scale is +/-0.1% for these transducers. The measurements are critical to the computation of the corrected axial force and should read within +/-0.5 psfa of the stagnation pressure reading from the tunnel Ruska Model DDR-6000 digital direct-reading pressure gage.

Several wind-off pump and purge cycles are performed in order to remove moist air from the tunnel circuit. This process involves repeated evacuation of the tunnel to low pressure, purging, and inbleed of dry air. Wind-on test data will not be acquired until the desired dewpoint has been achieved in order to avoid the adverse effects of humidity on the quantitative measurements.

Preliminary, or shakedown, runs are conducted at the outset of a test in order to assess the operational status of all instrumentation, to evaluate the on-line data reduction, including comparison to previous test data if available, and to observe the model, balance, and support system response over the desired ranges of pitch, roll, and yaw, as appropriate. Preliminary determination of the wind-on time required to minimize balance thermal gradients is also made. This initial run series is followed by the acquisition of hot wind-off zeroes in order to assess the stability of the balance zeroes. The goal during an aerodynamic performance (drag) test is to encounter no greater than +/-2 μV shift in the balance zeroes from beginning to end of a run series. This is not always achievable, however, because of nuances in the balance design, fabrication, temperature compensation, or moisture-proofing. Reference 7 indicates that the current accepted tolerance for balance zero shifts during a temperature compensation run as part of the calibration process is approximately +/-10 μV to +/-15 μV. For a typical drag test of a supersonic transport model at UPWT, this shift represents nearly +/-1 drag count, which is twice the value that is now considered acceptable for data repeatability. Although only a general guideline, zero shifts on the axial component of +/-5 μV, representing about 0.3 drag counts, are unacceptable, and facility resources are expended in order to minimize these shifts. Shakedown runs are conducted whenever it is deemed necessary in order to stabilize the balance zeroes over a given run series. In addition, production data will not be acquired until the wind-on balance thermal gradient is approximately 2 degrees or less. This measurement approach improves data quality but is in obvious conflict with reduced cycle time. Wind tunnel tests in which stability and control characteristics are the primary outcome are subject to similar concerns, but the constraints regarding balance zero shifts and thermal gradients may be more flexible.

The balance zeroes are acquired at prescribed time intervals overnight and during weekends using an automated data acquisition program. The data is processed and plotted to assess the time histories of the balance zeroes and to help plan a strategy, as necessary, for the next run series.

Data quality assurance

Repeat runs, typically of a baseline configuration, are made at selected test conditions at the beginning, middle, and end of a test entry in accordance with a Data Quality Assurance (DQA) program at LaRC (reference 10). Three upright runs and 1 inverted run are made in each of the two groups, and quick-look statistical quality control charts are prepared by a DQA team to illustrate the back-to-back polar repeatability and the reproducibility within a single test entry (reference 10). Diagnostic plots are also created from off-line analysis tools which interpolate the normal force, axial force, and pitching moment coefficient data to each nominal value of the angle of attack, average the data, and subtract the averages from the interpolated data. Figure 6 shows an example of

a scatter plot using data from a test of a supersonic transport model. These scatter plots provide a first-order assessment of the data repeatability and can flag problems or changes that might have been introduced within and between the repeat groups. Testing of several supersonic transport models at UPWT in recent years has indicated that the scatter in the normal force, axial force, and pitching moment coefficients (ΔC_N, ΔC_D, and ΔC_m, respectively) in the attached flow regime are typically +/-0.001, +/-0.00005, and +/-0.0001, respectively. At very low angles of attack where flow separation occurs along the lower surface, or at higher angles of attack where upper surface flow separation occurs, the data scatter increases because of model vibration and unsteady flow effects.

The within-test repeat runs are part of a much broader program at NASA LaRC to determine reproducibility of multiple entries in the same tunnel and tunnel-to-tunnel reproducibility (reference 10). A check standard model is used for this purpose and is a key element in determining the measurement uncertainty and to ensure that the measurement process is stable and meaningful in a statistical sense. The configuration illustrated in figure 7 was tested on a regular basis in UPWT Test Section 2 and served as an interim check standard. An existing general research fighter model was identified as a permanent check standard for UPWT. It has been tested in this capacity in both test sections twice a year since 2001.

Specialty balances

The measurement of loads on individual model surfaces is accomplished using single- and multiple-component strain-gage balances. Individual model surface loads were measured in UPWT testing of the X-33 technology demonstrator configuration. The X-33 was a suborbital flight-test vehicle and was tested as part of a larger program to develop a next-generation space transport vehicle. A 2%-scale model that was tested in UPWT Test Sections 1 and 2 is illustrated in figure 8. This model incorporated elevons, rudders, and body flaps instrumented with hinge moment gages, and canted and vertical fins featuring 3-component balances to measure the normal force, bending moment, and torsional moment. Photographs of the various gaged components are shown in figure 9. Single and dual flexures were designed as part of the control surfaces to measure the hinge moment, while providing a reasonable output of 1 to 2 millivolts per volt (mV/V). The balance accuracies expressed as 95% confidence limits about the mean response were typically +/-1% F.S. Single flexures were integrated into the fins to measure the 3-component forces and moments. Space constraints resulted in relatively short flexures, which increased the stiffness in the normal force and torsional moment directions. This compromised the accuracies of these components. The accuracies for the canted fin and vertical fin normal force and torsional moment ranged from +/-2% to +/-3.6% F.S., whereas the corresponding accuracies for the bending moment were approximately +/-0.3% F.S. The balance design load ranges were higher than would typically be recommended for testing at UPWT, since the design conditions were driven by higher loads in previous testing of the same model in the NASA LaRC 16-Foot Transonic Tunnel. This was of particular concern for testing at the higher Mach numbers in Test Section 2 (up to Mach = 4.6), where the component loads could be within the measurement accuracies of the balances. For this reason, testing was conducted at a higher Reynolds number to improve the resolution of the measured forces and moments. In order to test ranges of instrumented vertical fin rudder and canted fin elevon deflections, several gaged control surfaces were fabricated with integral deflections. In contrast, several angle brackets instrumented with hinge moment gages were built for a common body flap.

Although all balance bridges on the X-33 model were thermally compensated, operational experience in the wind tunnel revealed thermal-induced electrical zero shifts to various levels in all gaged components. These drifts were controlled by conducting shakedown runs in the same manner as previously described for the six-

component balance testing. The proximity of retaining fasteners to the gaged sections was a factor and, for consistency, the fasteners were always installed and torqued to prescribed values in the same sequence. Particular attention was paid to all metric breaks to ensure adequate clearance. In addition, the routing of the fine-gage wiring through the model required considerable pretest preparation and modifications to the instrumentation passageways in the model to avoid nicking or severing the wires during model changes. Check loads were applied using custom fixtures to verify the output from the instrumented control surfaces and fins on the fully-assembled model in the test section. A simple weight-hanger arrangement was used in the test section to apply a normal force to the calibration load points on the fins and control surfaces. The photograph in figure 10 shows an example of a check load application. The model pitch and roll support mechanisms allowed the model to be positioned so that the check loads could be applied in a vertical plane. The voltage output from any selected balance component was then verified against the full calibration results prior to every run series. The outputs from all gaged components were routed to BDDUs for continuous monitoring of the balance static and dynamic responses. Despite the concerns and limitations of the fin and control surface balances, a consistent and repeatable database was acquired. Figure 11 shows representative plots of the 2%-scale X-33 model right-hand canted fin normal force, bending moment, and torsional moment coefficients encompassing ranges of elevon, body flap, and rudder deflections at Mach = 2.16.

A problem specific to the fin balance design and installation arose during a purge cycle in Test Section 2 when the BDDU output from the vertical fin bending moment gauge went abruptly full-scale. Electrical resistance readings isolated the problem to the gaged section embedded in a silicone pocket at the base of the fin. Application of slight pressure to this pocket caused large changes in the resistance readings, and it was concluded that flexing of an air pocket within the silicone damaged a wire as a result of frequent pressure cycles in the 16-Foot Transonic Tunnel and UPWT. Removal of the silicone sealant revealed three damaged wires. Repairs were made off-site to all wires, and the silicone was reapplied while avoiding air entrapment during this process. Testing with the instrumented fin was resumed without further incident.

Model Attitude Measurement Techniques

Precision measurements of the model angle of attack are essential to the determination of drag to the levels of uncertainty required in current wind tunnel performance testing at transonic and supersonic cruise conditions. Reference 11 compares three model attitude systems featuring active target photogrammetry (Optotrak™), precision accelerometer, and laser interferometer. The extension of a videogrammetric model deformation system to angle of attack measurements is discussed in reference 12. The latter method has been used on a limited basis at UPWT as a secondary measurement, since its primary use has been to measure aeroelastic deformation. The goal in wind tunnel testing is to produce angle of attack uncertainties of less than +/-0.01 degrees (with 95% confidence level). The primary type of instrumentation currently in use at UPWT for attitude measurement is a gravity-sensing servo accelerometer (QFlex) (reference 13). Model attitude is determined in one of two measurement methods. The direct measurement uses an accelerometer mounted in the model. The indirect measurement features an accelerometer installed in a protective housing on the knuckle component of the model support system with corrections applied to account for aeroelastic or mechanical deflections of the model, balance, and sting assembly. In the latter case, the indicated support system angle is adjusted using a series of Eulerian rotations to determine the attitude of the model axes relative to the free-stream flow direction. Corrections for deflection of the model support system under aerodynamic loads are determined as functions of the measured aerodynamic forces and

moments through the process identified as sting deflection calibrations. The test requirements dictate which measurement is used and, on occasion, both methods will be applied to provide redundant attitude measurement capability. In general, however, the indirect method is used for performance testing to avoid bridging the balance with an on-board QFlex cable or its individual wires and possible bias errors of a model-mounted accelerometer caused by model dynamics. The latter phenomenon is referred to as sting whip and is discussed in reference 14. For static (unaccelerated) model conditions, the QFlex measures changes in angle relative to the horizontal by accounting for the differences in the component of the force due to gravity acting parallel to its sensitive axis. Although the instrument response to acceleration is linear, its response under unaccelerated conditions to changes in attitude relative to the local gravity vector is sinusoidal. For test conditions at which model dynamics are an issue, the instrument may start to act like an accelerometer and bias the attitude measurement. Normal small-amplitude model vibrations are not generally a problem in this respect because the acceleration is sinusoidal in nature and that portion of the signal resulting from these accelerations is removed by filtering circuits within the control unit. Sting whip, however, in either the horizontal or vertical plane, results in an acceleration increment which is of a sine-squared nature, and this increment does bias the accelerometer output. A prototype sting whip correction package consisting of miniature piezoelectric accelerometers and magnetodynamic rate sensors was tested in UPWT and 16-Foot Transonic Tunnel in order to quantify and correct for the effects of centrifugal accelerations (reference 14). Available internal volume and the routing of the instrumentation wires across the balance are issues that must be addressed early in the test program, particularly for any test where drag is of paramount importance. It is noted that models undergoing performance testing at UPWT typically exhibit small-amplitude vibrations in the vertical plane, and sting whip is not as significant an issue as it is at transonic speeds.

The development of the NASA LaRC Angle Measurement System (AMS) (reference 15) has brought significant improvements to the angular measurement capabilities at UPWT. The AMS is a self-contained package consisting of three orthogonally-mounted QFlex accelerometers mounted in a titanium housing with precision base and interfaced to a signal conditioning unit and a laptop computer system. The AMS is capable of measuring absolute pitch and roll angles to within +/-0.001 degrees. This system serves as the standard for calibrating knuckle- and model-mounted QFlex accelerometers, performing sting deflection and roll mechanism calibrations, and determining and verifying pitch and roll angular offsets between the model and balance. Selected balance calibration fixtures have been modified to include the AMS package mounting hole pattern for positive and repeatable attachment. The emerging model design standard is to transfer the AMS hole pattern to a reference surface machined into the model. Alternatively, a separate model leveling plate is fabricated that includes the AMS mounting hole pattern. QA inspections are performed to quantify any angular offsets of this reference surface relative to a model horizontal reference plane. The AMS packages at UPWT are interfaced with the wind tunnel host computer so that the pitch and roll angle measurements are acquired and recorded by the data acquisition system.

Sting deflection calibrations are performed in the test section with the AMS package installed to the balance calibration fixture and a load cell with double knife edge capable of applying a force up to 1000 lbs. or calibrated weighs suspended from a double knife edge and pan assembly. Deflections of the balance and sting assembly caused by the application of normal force, pitching moment, side force, and yawing moment to the expected levels during wind-on testing are determined by differencing the measurements obtained from the AMS package and the QFlex accelerometer installed in the

support system knuckle. Deflections due to applied rolling moments are measured directly from the AMS package. For performance testing, the differences between the curve fit and measured deflections at all load conditions, and the corresponding standard deviations, must not exceed a few thousandths of a degree. Note that the mechanized roll coupling is not used during performance testing because of the increased potential for support system mechanical misalignment and associated errors in the attitude measurements.

Flow angle measurements are made at all Mach numbers by conducting upright and inverted model runs. The design of the asymmetric sliding nozzle block in Test Section 1 typically results in higher flow angles in comparison to Test Section 2, and the computed flow angle can vary from a few tenths of a degree to as high as 1.5 degrees or more depending on the Mach number and mode of operation. Use of the mechanized roll coupling facilitates the flow angle measurements, since the upright and inverted runs can be made in the same series. In addition, on-line estimates of the flow angle can be made by processing and plotting data using Data Engineering and Scripting Language (DESL) scripts. The flow angle estimates are input to a lookup table in the online data acquisition setup file so that subsequent runs at a given Mach number are made with the appropriate flow angle values. For performance testing, the tunnel must be brought off-line in order to manually roll the model to the inverted or upright positions, resulting in less effective utilization of the facility occupancy time. A delta pitching moment coefficient correction due to nonuniformity of the flow angle across the test section is also estimated from the flow angle runs. This correction is only applied in the offline data reduction process.

Electronically-Scanned Pressure (ESP) Measurement Technique

System Description and Implementation

The System 8400 data acquisition instrumentation (reference 16) manufactured by PSI has been installed and in use at UPWT since 1991. The UPWT ESP system is interfaced with the wind tunnel data acquisition system, and can accommodate modules mounted internally to the model and external modules located outside the test section. The primary components include the system processor (SP), scanner-digitizer unit (SDU), remote processor (RP), local slave (LS), pressure calibration unit (PCU), interface control logic unit (IFC), internal and external ESP scanner modules, vaccum pumps, and known pressure generators. There are two complete System 8400 installations to accommodate both test sections. The primary chassis is the SP, which provides input unit control, data synchronization and processing, and an IEEE-488 interface to the wind tunnel Modcomp host computer. The SP houses one SDU, which is a high-speed (50 KHz) scanning analog-to-digital converter that converts the analog millivolt data from the ESP scanners and converts these signals to a digital format used by the SP to generate pressure data. The SDU has 16-bit resolution and can accommodate up to 1024 pressure measurements during each scan period. The distance between the host computer room (UPWT Data Room), where the SP is located, and the test area exceeds IEEE-488 distance constraints. This situation is addressed by the placement of the RP in the test area, which communicates with the SP via an RS-485 multi-drop serial link. The RP serves a dual purpose by physically extending the system and increasing the computing power since it contains its own processor. The RP houses up to four PCUs which provide calibration pressures to the ESP pressure scanners. The LS is an expansion rack used in conjunction with the RP to provide additional physical expansion of the system. The LS is interfaced to the RP via an RS-488 link and can also contain up to 4 PCUs. The 1 psia, 5 psia, 15 psia, and 30 psia PCUs in use at UPWT are digitally-controlled pneumatic

sources that provide valve control and generate calibration pressures for the ESP scanners. Calibration pressure accuracy is specified by the manufacturer as +/-0.02% F.S. The IFC has a direct link to the SP in the Data Room and can accommodate up to eight miniature ESP scanners that are installed inside the model and/or positioned outside the test section. The modules in use at UPWT are 32-port and 48-port configurations (slant- and straight-tube) with ranges of 10-inch water column (WC), 1 psid, 2.5 psid, 5 psid, 10 psid, 15 psid, and 30 psid. The manufacturer-specified uncertainty as a percent of full-scale is +/-0.1% for the 10-inch WC up to the 2.5 psid modules, and +/-0.05% for the 5 psid to 30 psid modules. The differential ESP modules are used almost exclusively as absolute gages at UPWT by evacuating the reference side of the modules using a common vacuum source. Turbo-molecular vacuum pumps are used to provide the reference pressure to all ESP modules and a vacuum supply to the 1 psia PCUs. Known pressure generators (KPGs) are units that generate and maintain a given pressure that is plumbed to specified module ports and used as system diagnostic tools for real-time accuracy checks. The units control the given pressure by the use of an MKS Instruments Type 250C pressure/flow controller that maintains the desired pressure automatically by continually admitting the correct gas flow to a vacuum system to compensate for gas being removed by the vacuum pumps. A Ruska Instrument Corp. Portable Pressure Gage (PPG) is connected to the supplied pressure leg of the circuit to monitor and transmit the known pressure value to the data acquisition system through the use of "smart cards", which electronically link the serial output of the PPGs to the digital input channels of the data acquisition system. Rotary vane vacuum pumps from several different manufacturers are used to supply a vacuum to the KPGs (two units per pump) which allows these units to set and maintain the low level check pressures applied to the ESP modules. For the internally-mounted ESP modules, the calibration pressures, reference pressure, scanner control pressures, and known pressures are routed to the area of the model support system inside the tunnel through a permanent flexible tubing arrangement to provide reliable, large volume connection points within 3 feet of a model. The signals generated by the scanner modules are transmitted via electronics cables to the IFC which is located immediately outside the test section.

Several scanner modules have been retrofit with a purge option, which involves a modification to the calibration valve to manifold purge pressure inputs to the measurement ports during calibration. With the valve placed in the calibrate position, the application of purge pressure will purge the measurement lines of any contamination such as moisture. The primary use of these purge modules at UPWT, however, is in conjunction with pressure-sensitive paint (PSP) testing. Purge air is applied to the scanners during the PSP application process to prevent contamination and clogging of the model pressure orifices. Slant tube configurations are not available with the purge option. In addition, the larger diameter purge air tubes, or "smokestacks," extend above the module measurement tubes. The model internal volume requirements to accommodate the larger envelope of the purge modules and the increased bend radii of the tubing to the module head covers are important considerations regarding the use of this modified instrumentation.

The standard ESP calibration consists of five points that are used to determine a quartic polynomial representation of the pressure-voltage signature of each transducer or sensor. Reference 17 has suggested that deficiencies exist in this calibration process, since it may not capture the low-pressure variation of the sensor and that any extrapolation beyond the calibration data range to either low or high pressures is tenuous because of a mathematical oscillation inherent in higher-order polynomials. The calibration pressure range is specified to encompass the expected pressures during the testing. The first, or lowest, calibration pressure supplied by the PCUs is constrained to approximately 0.1 psia for the 1 psia and 5 psia

PCUs and approximately 0.2 psia to 0.3 psia for the 15 psia unit. The calibration report provides guidelines for the interpretation of the results and flags those ports that do not meet the validity checks of the wind tunnel data acquisition system software. The typical procedure is to first scan the report listing to confirm that the calibration set pressures are the same as those selected in the software; check that no address line failures occurred (bad cable); examine the response and trend of the sensor voltages at the five set pressures; and then observe the listing of quartic polynomial coefficients for each sensor for progressively decreasing values from the initial to the final coefficients. The software flags are based on criteria developed for the NASA LaRC National Transonic Facility (NTF) and specify the offset (C_o) must be less than 25% of full-scale range (psia), the sensitivity or slope (C_1) must be between 1.0*F.S/5.0 and 1.5*F.S./5.0, and the combined linearity terms $C_2*V_x + C_3*V_x + C4*V_x$ must be less than 0.007*F.S, where V_x is the voltage output from each sensor. These criteria can be misleading if ESP scanner modules of different ranges are calibrated using the same PCU, as would occur if 10 psia and 5 psia modules were calibrated using a 5 psia PCU. In this case, the 10 psia module ports would erroneously be flagged for sensitivity and combined linearity errors. The manufacturer's recommended criteria based on operational experience is that the offset C_0 should be less than 10% of the full scale range of the scanner ($C_0 < C_1/2$), the slope should be two orders of magnitude greater than the psi per volt squared term ($C_1/C_2 > 100$), the slope should be three orders of magnitude greater than the psi per volt cubed term ($C_1/C_3 > 1000$), and the slope should be three and one-half orders of magnitude greater than the psi per volts to the fourth power term ($C_1/C_4 > 5000$).

Several system verification techniques are used during ESP testing at UPWT. Standard procedure requires that three known pressures be connected to each ESP module as a measure of system performance. Applied pressures of 50 psfa (0.347 psia), 200 psfa (1.389 psia), and 700 psfa (4.861 psia) are typical. The difference between the measured and applied pressures at these ports is displayed in real-time. The goal is to limit these differences to within +/-0.5 psfa (+/-0.0035 psia), but this is strictly a guideline and is test-dependent. One port on a given module falling outside this band is not necessarily a concern, but two ports warrant further investigation. This would include moving the module sliding blocks to the calibrate position and invoking a command from the front panel of the SP for the PCU to generate and send a set pressure to the modules. In general, if approximately 25% of the ports are reading more than +/-0.5 psf different than the set pressure, a full calibration is performed, which takes about 5 minutes to complete. Another opportunity for an ESP system check occurs during the acquisition of pumpdown wind-off zeroes, where the tunnel pressure is evacuated to a stable pressure of 200 psfa (1.389 psia) to 400 psfa (2.778 psia) for final instrumentation checks. Since the facility is large and pressure cannot be positively maintained during the pumpdown zeroes, this procedure provides more of a quick-look check of the ESP system rather than a full accuracy check. Thermocouple wires are often affixed to the outside surfaces of internal ESP modules, and the thermocouple output is routed to the data acquisition system for display and recording. This data provides an indication of the ESP module temperature stability during wind-on runs, but is strictly used for observation since the preceding diagnostic procedures provide a better evaluation of the system health.

The system verification techniques cited above are essential to the minimization of thermal-induced shifts of the ESP module output. If the internal volume of a wind tunnel model is sufficient, the ESP modules are mounted onto heat-insulating pads of bakelite to reduce the thermal conduction from the model. The thermal environment in which the ESP modules are located changes considerably from the initial wind-off conditions to actual operating conditions. Sufficient time must be allotted for the tunnel, support system, model,

balance, and ESP modules to achieve a stable thermal environment, at which time a full on-line calibration is performed (a zero-offset calibration option does not exist at UPWT because of the use of a hard vacuum as reference). The ability of the modules to transfer heat from its electronics package is subject to the widely varying conditions of which UPWT is capable, with static pressures ranging from nearly hard vacuum up to approximately 100 psia. Standard procedure is to perform a full on-line calibration whenever Mach number, Reynolds number, or stagnation temperature is changed, or within a long run series at constant test conditions based on the results of the system verification techniques. New-generation scanners are being developed by PSI that sense the temperature of each pressure sensor and apply a digital thermal compensation to reduce thermal errors by five-fold (reference 18). This new system features a miniature Scanner Digitizer Interface (SDI) module and a high speed fiber optic digital interface that may offer significant operational improvements over the pressure scanning system currently in use at UPWT. A system has been acquired for UPWT and will be implemented in late 2007.

A high vibration environment can also affect the performance of internal ESP modules. It is typical, however, that the tubing bundle inside the model is so tightly packed that it serves to positively secure the modules under all test conditions. The use of urethane tubing to connect the stainless steel tubing from the model to the corresponding tubes on the ESP module heads has reduced the overall volume, but experience indicates that the instrumentation bundle will also grow to whatever space is available inside the model. Double-back adhesive tape is used as a matter of practice to secure the modules to a mounting plate or directly to the inside surface of the model.

Leak-checking of all pressure tubes is accomplished by connecting the tube end to a pressure gage, providing a source of vacuum at the corresponding orifice, and sealing this vacuum at the orifice end. Vacuum is applied until the sensor output is reading below approximately 50 psfa, at which time a valve is closed in the vacuum supply line. A time history of the module sensor output is displayed at a computer workstation adjacent to the test section, and the real-time response is observed to ensure a leak rate of no greater than 2 psfa per minute. The on-line graphics help to identify plugged, obstructed or pinched tubes, leak rates, etc. The character of an “ideal” time history is quickly identified and features a fast response to vacuum input and equally rapid ramping to a constant pressure value. The response time of any pressure tubes that are connected to external modules is also useful in establishing a settling time for on-line data acquisition.

The internal ESP module electronics cables, scanner valve control pressure lines, calibration/reference/known pressure lines, and thermocouple wires bridge the internal strain-gage balance in a typical force and pressure model installation at UPWT. The effects of the hard nylon tubes that are used for the scanner valve control and reference pressure lines are particularly noticeable in the balance output. Consequently, the acquisition of credible force and moment data is deferred to a separate phase of the test during which the ESP instrumentation is removed from the model.

Applications

Three applications of the UPWT ESP system are now discussed. A 2%-scale X-33 model was tested to evaluate a Flush Air Data Sensing (FADS) system concept in which airdata are inferred from nonintrusive surface pressure measurements (reference 19). The airdata parameters provided by the FADS system include Mach number, angles of attack and sideslip, airspeed, and altitude. This system does not require probing of the local flow field to compute airdata parameters and extends the useful range of the airdata measurement system to the hypersonic flow regime since the extreme hypersonic heating caused by the small radius of a flow-sensing probe is avoided. For the preliminary design, there were three calibration

parameters that had to be evaluated for the FADS system from the 2%-scale X-33 model during wind tunnel testing. They were: the position error, the angle of attack flow correction angle, and the angle of sideslip flow correction angle. The wind tunnel model featured 21 static pressure orifices in an array on the nose cap, and the pressures were measured using an internal 32-port, 10 psid module (used in absolute mode). A close-up image of the instrumented nose cap on the model is shown is figure 12. The results from the UPWT testing spanning the Mach number range of 1.6 to 4.5 complemented a data base acquired at Mach = 0.25 to 1.20 in the 16-Foot Transonic Tunnel. Pressure measurements were obtained in small angle of attack increments over wide ranges of the angles of attack and sideslip and at model roll angles of 0^o, $+/-90^o$, and 180^o. It was essential in this test that the ESP system accuracy be maintained such that the measured pressures were within a band of approximately +/-0.5 psfa of the known pressure generators and the set pressures established by the PCU. This required continuous on-line observation of the ESP module status and numerous on-line calibrations to meet this test requirement.

A general research fighter model, referred to as the Modular Transonic Vortex Interaction (MTVI) model, involved extensive ESP measurements. The primary objectives of this test were to acquire detailed surface static pressure distributions, six component forces and moments, and off-surface flow visualizations on two chine forebody/wing/tail configurations for comparison to advanced computational fluid dynamics (CFD) solutions. The model is shown installed in Test Section 1 during the pressure measurement phase of the testing in figure 13. Seven ESP modules were required, 3 internal and 4 external, and an extensive instrumentation bundle extended from the base of the model to the sting support system. For obvious reasons, the pressure measurements were acquired independently of the force and moment measurements. Note that the flow visualization was also independently acquired, for reasons cited in a later section of this paper. Model attitude was measured directly with an onboard QFlex accelerometer, since the balance loads and, consequently, the computed sting deflections were compromised by the instrumentation bundle. The frequency of on-line ESP calibrations was driven by thermal effects on the internal modules, since the external modules were at ambient conditions and not subjected to large temperature variations. A settling time of 15 seconds was input to the data acquisition system and was based on the longer response time of the external modules, which featured a tubing length of approximately 15 feet from the model to the scanners outside the test section. This dwell time was conservative, however. The steady-state behavior of the flow field about the model and the small increments in angles of attack and sideslip within a run promoted small changes in the pressure field between each data point. The requirements for this test were somewhat unique in that the model change to a different chine body required a complete disassembly of the model from the balance. The pressure-instrumented wings and one internal ESP module were common to each model configuration, and these were subsequently transferred to the pressure-instrumented chine body and strongback of the new model configuration as it was installed on the balance. Figure 14 presents representative results from this test, which shows the effect of the chine forebody cross section on the spanwise pressure distributions obtained at seven measurement stations and a free-stream Mach number of 1.8.

The operation of a supersonic duct is dependent on the overall area ratio, and the blockage associated with a given model, support system, and instrumentation setup is a critical factor in determining the ranges of Mach number, angle of attack, and angle of sideslip within which successful tunnel operation will occur. Guidelines exist for estimating the allowable model size for a particular test (reference 4); however, there are uncertainties involved with the blockage effects of model size, method of mounting, and the model angle of attack. Additional factors are introduced

when the instrumentation bundles and protective metal conduits extending from the model are large and/or numerous, if video and still cameras with protective housings are installed in the test section, or if condensation is allowed to occur (as would be the case if a vapor screen flow visualization method is being used). Supersonic flow may be successfully established and maintained at low angles of attack for installations that broach the blockage guidelines. The flow will become unstable, however, if the angle of attack is sufficiently increased. The first signs of supersonic flow instability are marked by a change in the acoustic level in the test area surrounding the test section and an appearance of the normal shock in the rear portion of a real-time schlieren display. The forward advance of the normal shock into the test section may be sufficiently gradual that the model attitude can be quickly reduced to reestablish stable flow conditions. This is not always the case, however, as the next sign of flow instability is the abrupt forward movement of the shock to a position over or upstream of the model. This is a very dangerous condition as the resulting flow dynamics pose immediate safety hazards to the model, balance, and support system. For this reason, static pressure measurements along the tunnel ceiling centerline provide a quantitative indication of the normal shock position and its sensitivity to changes in the Mach number and model angle of attack and position in the test section. A single external 48-port ESP module was dedicated to measuring the ceiling pressures starting just upstream of the test section origin and extending a distance of over 34 feet downstream of this location. The real-time output of the ceiling pressures is displayed in bar chart form using the data acquisition system (DAS) on-line graphics software, and the shock location relative to the model location in the test section is observed and monitored. The graphical display is a key factor in determining the range of model angle of attack at a given Mach number that can be safely and consistently achieved for a particular test setup. The effect of Mach number on the ceiling centerline pressure signatures with the MTVI model set to an angle of attack of 14 degrees is shown in figure 15. The model base location in the test section is marked by the solid vertical line at a tunnel station of approximately –46 inches. The rapid pressure rise downstream of this location indicates the presence of the normal shock. The shock is stronger and closer to the model at the lowest Mach number of 1.60.

Optical Surface Measurement Techniques

Pressure-Sensitive Paint Technique

Global surface static pressure measurements are becoming more common in wind tunnel testing with the advent of the pressure-sensitive paint technique. A review of PSP applications for field measurements in aerodynamic testing is provided in references 20 and 21. The key elements of a PSP system include photoluminescent material in the form of a paint applied to the test article, illumination source to excite the paint, imaging device to document the paint in the excited state, and a data acquisition and processing system. A PSP system based on the work described in reference 20 has been in use at UPWT since 1996. Descriptions of the primary components and their practical applications at UPWT are described in this section.

The PSP method is based on the oxygen-quenching characteristics of certain luminescent materials. The emitted light intensity varies inversely with the local oxygen partial pressure and, therefore, the air pressure, since oxygen is a fixed mole fraction of air. A PSP formulation typically consists of three components. The luminescent material (luminophore) is the sensor component. For oxygen quenching to occur, the luminophore must be soluble in a suitable binder material. Finally, a compatible solvent is used for the application of the paint, via a spray gun, to the test article. Prior to the paint application, the model surface is primed with white paint. The white undercoat to the PSP coating serves a critical function in that it amplifies the PSP emission signal (reference 20). Certain characteristics of PSP coatings induce measurement error: photodegradation and temperature sensitivity. Specifically, the

emission response of the PSP decreases with time of exposure to the excitation radiation, and the luminescence intensity is sensitive to changes in the temperature. An earlier formulation successfully applied at UPWT is designated IEMA/PtT(PFP)P which uses a proprietary University of Washington copolymer. Laboratory calibrations at NASA LaRC indicated that the Stern-Volmer characteristics (reference 20) were very linear, and photodegradation was reduced compared to prior-generation paints used at UPWT. This formulation was not the most advanced in use at that time; however, it proved to be a robust and responsive formulation at the low static pressures typical of the supersonic testing at UPWT. Poly-2,2,2-trifluoroethylmethacrylate-co-isobutlymethacrylate (FEM) and platinum tetra (pentafluorphenyl) porphyrin, PtT(PFP)P, applied to a Prime'N Seal base coat was the most recent formulation used in UPWT. Reference 22 describes more recent PSP applications that include dual luminophores and uni-coat PSP chemistries that do not require the acquisition of wind-off reference images or the application of a base coat to the model surface.

The intensity of the light emitted by PSP is proportional to the excitation light that is absorbed. A stable illumination source must be used that is tailored to the absorption wavelength band of the PSP coating. Ultraviolet long wave (365 nanometer (nm)), 250-watt lamps connected to a regulated power supply are used in continuous mode to provide the illumination source in the UPWT system. The optical filters attached to these lamps allow passage of light at the absorption wavelength of the coating but prevent transmission of light at the luminescence wavelengths that could compromise the images acquired by the PSP cameras.

Electronic CCD imaging devices of two types are used: conventional video and scientific grade digital cameras. The original PSP system upon which the UPWT system was developed (reference 23) featured an 8-bit resolution image acquisition and processing system using standard NTSC format video cameras. These cameras continue to be used as monitoring devices only, since they have the advantage of providing real-time viewing of the PSP response to aerodynamic flow changes. Scientific-grade, thermoelectrically-cooled digital cameras connected to a regulated power source are used exclusively for PSP image acquisition because of their low noise, excellent linear response, and good signal-to-noise ratio. These cameras acquire an electronic snapshot only, and the exposure or integration time is set from the host computer. Cooled CCD digital cameras of 12-bit and 14-bit resolution and 1280 x 1024 and 1024 x 1024 pixel arrays have been used. Each camera can be commanded to acquire an image with the lens closed in order to acquire a “dark image”. A dark-level correction is applied to all wind-off and wind-on images to subtract out the CCD dark current and noise of the overall imaging system. Optical filters centered about 650 nm are installed on the conventional video and scientific-grade digital cameras to permit the passage of the luminescence emission wavelengths, while preventing the transmission of the excitation light source wavelengths to the acquisition cameras. The incursion of extraneous sources of light from the test cell area into the test section is prevented by sealing the sidewall access doors with coverings and enclosures.

Acquisition of the PSP images is controlled by UNIX- and PC-based workstations in the UPWT Data Room. The cable run length between the host computers and the cameras installed in the test cell is approximately 125 feet. The 12-bit, 1280 x 1028 pixel array digital camera and its electronic camera control unit (CCU) are interfaced to the UNIX workstation via a 200-foot fiber optic-based, Small Computer Systems Interface (SCSI) bus extender system. The 14-bit, 1024 x 1024 pixel array camera and its CCU are connected to a proprietary PCI-based image acquisition board installed in the PC via a custom electronics cable. Image acquisition on the UNIX system is performed using a NASA LaRC-developed program that allows user control of the camera integration time and camera gain, and

determines the minimum, maximum, and average pixel intensity values for the most recently-acquired image. The proprietary image acquisition software on the PC provides a more full-featured suite of utilities to evaluate the characteristics of an acquired image. However, the time-critical nature associated with the acquisition of production images during the testing typically precludes the use of anything but the most basic features. Images are stored on high-capacity disk arrays for off-line processing and archiving. Image processing is performed exclusively on a UNIX workstation using the software package described in reference 24 and referred to as PAINTCP. This software package is one of several PSP processing tools (see reference 25, for example) in use by the technical community, and it has been successfully applied at UPWT since 1996.

Optical access to both test sections of UPWT is provided by two doors that form the sidewalls of the test sections. Each of the test section doors has nine 5.5-in. by 48-in. windows, separated by 1.25-in solid webs. The windows are 1.5-in thick glass of optical quality to provide minimum distortion for schlieren and other flow visualization methods. There is no optical access to the test section from the ceiling. The test section can be isolated from extraneous light sources by the installation of a wooden panel on one door and a wooden enclosure on the other door, which provides sufficient volume to set up and access (during tunnel operation) a large array of cameras and lights. The test section layout offers both advantages and disadvantages to the implementation of the PSP technique. The primary advantages are the ease with which cameras and lights can be attached to the webbing. In addition, all instrumentation is located in ambient conditions, which eliminates the need for special pressure- and thermally-controlled enclosures for the imaging and illumination hardware. The test section and equipment are very accessible during tunnel operation, which allows regular system checks, close-up viewing of the paint status and its real-time response to pressure-field changes, and manual shuttering of the UV lights, as necessary. The primary disadvantages are the proximity of the cameras and lamps to the model and the optical quality glass, which affects the field of view, limits the positioning of cameras and lights relative to the model and to each other, increases the susceptibility to the adverse effects of reflections from the windows, raises concerns regarding thermal effects induced by the UV lamps on the glass, increases the effects of model dynamics on image quality, and amplifies the effects of small spatial differences between the wind-off and wind-on images. In addition, the sidewall optical access requires the model to be rolled 90 degrees to a wings-vertical position. The model angle of attack is then obtained by the twin-screw arrangement on the horizontal strut that is normally used to vary the yaw angle. As a result, the angle of attack is limited to a maximum of approximately +8 to +10 degrees, depending on the model size. The model support system is typically translated off-center (away from the camera) by about 4 inches to maintain field of view and focus at the higher angles of attack.

The installation of cameras and lights for a PSP test at UPWT is shown in figure 16. The initial application of PSP at this facility occurred in 1996 using a slender arrow wing-fuselage-nacelle model, which is shown in figure 17 with PSP and temperature-sensitive paint (TSP) applied to opposing wings. The PSP (pink color) is applied to the upper wing, while the TSP (yellow color) is applied to the lower wing. The camera locations, pointing angles, and lenses were chosen to maximize the viewing area of one wing (in this case, the PSP wing) while striving to avoid undesired reflections from the optical glass. The light sources were carefully selected and positioned to reduce the nonuniformity of illumination at the model. This procedure involved the activation of two to three lamps (depending on the model size) and a survey of the illumination source intensity at the model for a range of angle of attack. A hand-held digital long-wave radiometer was used to acquire local measurements and to guide the camera installation. A reading of approximately 300 microwatts per square centimeter ($\mu W/cm^2$)

at the model was used as a general guideline based on previous experience. Consistent readings in the 400 to 500 $\mu W/cm^2$ range were avoided due to concerns with more rapid and nonuniform photodegradation. The mutual proximity of the cameras and lamps raised the concern of electromagnetic interference that could damage the sensitive electronic components in the digital cameras. This might occur as the result of inadvertent power cycling of the UV lamps while the cameras were operational. The webbing of the test section door afforded some protection, but this was augmented by the placement of metal shields between the cameras and lamps.

The paint application and curing process requires one or more shifts to complete. This operation requires a skilled painter equipped with protective gear, including full face mask and a continuous air supply. The run schedule is designed, whenever possible, to conduct the painting after operating hours to avoid the resultant facility down time. The model is meticulously cleaned with solvents, and all model components except the region of interest are masked off. All models tested to date with PSP at UPWT have been instrumented with discrete surface static pressure orifices that are plumbed to internal ESP modules with purge air capability. The purge air pressure is applied and adjusted to provide adequate flow through all pressure lines to avoid contamination of the orifices during the paint application while avoiding local mounding around the holes caused by excessive, jet-like flow. This is the desired effect but rarely achievable. Approximately 4 hours are required for the curing of the base coat, and a comparable period of time is allotted after the PSP coating is applied. The PSP image registration process requires that reference marks, or control points, be placed on the model. The locations of these registration marks are defined by placing a Mylar transfer sheet containing a 1:1 scale drawing of the wing with pre-punched holes on the fully-cured PSP coating. After the hole centers are marked, the Mylar template is removed and black dots are drawn on the model using a plastic circle template and marker pen. Latex gloves are worn during this process to avoid contamination of the PSP coating. A final step prior to securing the test section for operation is to thoroughly clean the test section windows and to confirm that the transmission and absorption filters on the PSP light sources and cameras are free of contaminants. It has been found that operation in the higher modes in UPWT Test Section 2 is prone to the development of an oil film along the test section side walls as a result of a tunnel compressor seall leak. The presence of this oil film compromises the quality of the PSP images and the resultant quantitative pressure measurements..

Wind-off images are acquired at several angles of attack with the test section evacuated to low pressures, typically 200 psfa (1.389 psia) to 400 psfa (2.778 psia). This pumpdown condition is more representative of the static pressure levels that will exist on the painted wing during wind-on runs, and it provides an opportunity to define the digital camera integration times that will be used throughout the testing. In general, a range of integration time is determined from the wind-off run such that the maximum pixel intensity is approximately 60-70 percent of the saturation level of the camera. This approach provides a buffer against saturation during the wind-on runs where lower static pressures that occur locally on portions of the wing promote even higher pixel intensities at the same integration times. Integration times of 500 milliseconds (msec) to 1500 msec are typical. The longer integration time has not posed a problem since model dynamics have not been an issue in PSP testing at UPWT. Wind-off images are acquired in smaller angle-of-attack increments to provide a better range of reference images that are spatially aligned with the wind-on images. For example, depending on the aerodynamic loads on the model, a wind-off image acquired at $\alpha = 7.5^o$ will likely be more spatially aligned with a wind-on image acquired at $\alpha = 8.0^o$. This approach is similar to that used in applying wind-off corrections to video model deformation

system measurements, which are described in the next section of this paper.

Wind-on data acquisition consists of the discrete pressures measured from the ESP taps and the PSP images at the desired angles of attack. Full on-line calibrations of the ESP modules are performed to ensure they meet the previously-specified performance criteria, since the acquisition of high-quality ESP data is essential to the in-situ PSP calibration performed during the off-line image processing. The PSP illumination source is shielded during all transitional phases of tunnel operation (tunnel start-up and shutdown, Mach number changes, ESP calibrations) in order to reduce the overall exposure time of the PSP coating. To date, PSP image acquisition has been performed independently of the data acquisition performed by the wind tunnel host computer. The test conditions, ESP data, and other parameters are obtained off-line for use in input files required by the PSP image processing software. The wind-on, real-time response of the PSP is observed and recorded using the 8-bit video camera mounted in the test section door webbing. The signatures of particularly strong flow-field features such as shock waves and vortices are often clearly visible in the video display. A slight unsteadiness in the flow caused by model motion is manifested by a corresponding response in the shock and vortex pressure signatures. It is noted that PSP systems are being developed and applied that feature fast-response paint formulations to acquire unsteady global pressure distributions (reference 26). A repeat set of wind-off images and dark images are acquired after the wind-on runs. Comparisons of the initial and final wind-off pixel intensities at the same camera integration times provide an indication of the level of photodegradation that has occurred. In some cases, the final wind-off images are used in the image processing, since they may be acquired closer in time to the wind-on images that are being processed.

The image processing method features the subtraction of the dark image from the wind-off and wind-on images, identification of wind-off and wind-on control points, image registration, image ratioing, resection transform, and global calibration of the paint. Registration, or spatial alignment, of the two model images is performed to correct for nonalignment caused by model motion and/or deformation. A second-order biquadratic transform is used to align the wind-on image with the wind-off image. This process depends on finding the respective control points, or registration marks, which are used to determine the transform coefficients. The wind-off and wind-on intensity field images are ratioed, and the intensity field of the resultant image is proportional to pressure (Stern-Volmer relation). Note that the image ratioing process is effective in factoring out the effects of spatial nonuniformities in the light source intensity and PSP coating thickness. A resection transform based on photogrammetry techniques is performed next, which relates each point in the final intensity ratio image plane to a corresponding point on the model surface. The effectiveness of this transform depends on an accurate determination of the spatial locations of the model registration marks. To date, the image mapping performed in UPWT testing has been exclusively a two-dimensional (2-D) plane view representation of the wing. Quantification of the pressure field in the final intensity ratio image requires a calibration of the paint to determine the Stern-Volmer sensitivity coefficients. Evaluation of the response and photodegradation characteristics of various PSP formulations is routinely performed at LaRC in a pressure- and temperature-controlled chamber using painted coupons. However, this a priori method has not been used to calibrate the paint as applied to models at UPWT. Since all models used in PSP testing at UPWT to date have been instrumented with discrete pressure orifices, the in situ calibration method has been exclusively applied. In this method, paint intensity is calibrated from the pressure tap data at spatially corresponding locations. The distribution of discrete pressure taps on the wing is important, since the measurement of a wide range of pressures on the wing enhances the paint calibration. Ideally, the taps would be located

to completely span the range of expected pressures during wind-on testing, but this is not always practicable. The in-situ calibration process used at UPWT is iterative, since the first pass through the calibration rarely provides a completely satisfactory global match between the ESP and PSP pressure data. The paint cannot be calibrated at the exact location of the pressure orifice. This requires that the PSP image pixel locations used for calibration be slightly offset from the orifice. Additional offsets may be necessary if the purge air flow during the painting process was excessive and local mounding of the paint occurred about the orifice.

Figure 18 shows a result from a PSP test conducted in 1996 using the model shown previously in figure 17. The PSP image has undergone registration, ratioing, resection transform, and calibration, which is noted by the color-coded pressure coefficient bar in the lower right corner of the figure. The PSP image was acquired in UPWT Test Section 1 at Mach = 1.65, Re/ft = 3 million, and $\alpha = 6^{o}$. The angle of attack is sufficiently high at this Mach number that controlled leading-edge flow separation occurs along the main (inboard) wing and outboard wing panels, and the pressure signatures of these vortical flows are apparent in the image. The model installation image in figure 17 also showed the left-hand wing with TSP coating. TSP was applied in this test solely to ascertain if the metal wing of this model was characterized by thermal gradients during the PSP image acquisition. The TSP formulation responded to local temperature only, was excited by blue light, and emitted light in the near infrared (reference 27). As a result, the transmission and absorption filters were changed during the UPWT testing to enable the capture of the TSP images. Off-line processing of the results, which included only the registration, image ratioing, and resection transform, culminated in a uniform intensity image. This suggested that significant thermal gradients did not exist over the region of interest on this slender wing. A preferred alternative global surface temperature measurement technique is infrared (IR) thermography, which is discussed in a later section of this report.

A later application of PSP occurred in Test Section 1 in 1998 using a different slender wing, fuselage, and nacelle model. The upper surface of the right-hand wing and lower surface of the left-hand wing were instrumented with numerous discrete pressure taps distributed in chordwise rows at several span stations. PSP was applied to both wing surfaces during the same painting session; however, the upper and lower wings were independently imaged in back-to-back phases of the PSP testing. Consequently, the model was tested in the -90^{o} and $+90^{o}$ roll angle orientations, and this required slight adjustments to the installation of the PSP cameras and light sources in the test section side wall. The model featured a total of 4 internal ESP modules, three of which featured purge air capability (the entire UPWT inventory at that time). Since purge air could not be applied to all pressure orifices simultaneously, the pressure rows attached to the non-purge module were masked off with 0.06-in. wide tape during the paint application process. A region on the left-hand wing lower surface about the engine nacelles and nacelle diverters was of particular interest during this test, and figure 19 shows a collage of results obtained at Mach = 2.10, Re/ft = 4.0 million, and $\alpha = 3.5^{o}$. The false-colored PSP image shows the shock patterns created about the nacelle diverters. The shock signature extends across most of the wing span with strong mutual interactions between the nacelles. Note that the nacelle regions appear white in the image, since they were painted flat black to prevent reflected light from contaminating the wing surface images. In addition, the pressure rows that were masked during the painting process appear as stripes in the image. An in-situ global calibration of the paint was performed using the ESP tap data, and the PSP and ESP pressure coefficients are compared at all five span stations in figure 19. Note that the pressure distributions effectively capture the shock footprints at all measurement stations. The advantage of the PSP technique is that every pixel in the painted portion of the

image is effectively a pressure tap, so the pressure distributions can be resolved to much greater detail in all applicable regions on the wing. An example of the more detailed PSP pressure distributions derived from this test are shown in figure 20. The pressure coefficients are plotted at all available pixels from approximately the wing leading edge to the trailing edge in a selected chordwise row between the nacelles. The dual pressure signatures of the interacting shock waves emanating from the nacelle diverters are clearly shown in the figure.

A final example of PSP application at UPWT features the determination of the effects of surface porosity on the vortex-dominated flow about a general research fighter configuration shown in figure 21. The forward portion of the model was a flat-plate leading-edge extension (LEX) that could be configured as a "solid" surface or a porous surface having a 14.75% porosity level relative to the LEX exposed area. The LEX was mounted to a 65-degree cropped delta wing to which a centerline vertical tail or twin, wing-mounted vertical fins could be installed. The right-hand wing incorporated three spanwise rows of upper surface static pressure taps, which were used to perform in-situ calibrations of the PSP. Fully-processed images comparing the solid and porous LEX intensity field images are shown in figure 22, which corresponds to Mach = 1.6, Re/ft = 2.0 million, and $\alpha = 8^{o}$. The porous LEX configuration exhibits a single, broader vortex pressure signature, and the manner in which the wing vortex system interacts with shock waves from the wing-mounted vertical fins is also affected by the porosity. The corresponding PSP and ESP pressure distributions at the 60% chord station are compared in figure 23, which reveals a satisfactory global calibration of the paint. In addition, the pressure distributions effectively capture the effect of LEX porosity on the vortex-dominated flow at supersonic speeds.

Video Model Deformation Technique

Model deformation may be defined as the change in shape of a model, particularly the wings and control surfaces, under aerodynamic load in a wind tunnel (reference 28). The aerodynamic characteristics obtained in wind tunnel testing of a flexible model may differ from expected results or from CFD predictions based on rigid body assumptions. Reference 29 compares the current state-of-the-art of three optical techniques under study at NASA LaRC for measuring model deformation, which include video photogrammetry, projection moiré interferometry, and the commercially available Optotrak™ system. The fundamental technique used at UPWT to measure model deformation is photogrammetry, and developments at NASA LaRC in a video-based photogrammetry technique are summarized in reference 30. The basic hardware of a single-camera video model deformation (VMD) system includes a CCD camera, computer with frame grabber, diffuse light source, and array of retroreflective targets on the model. The VMD technique consists of a single camera, single view, photogrammetric solution from digital images of targets placed on the wing at known semispan locations, as shown in figure 24. The videogrammetric system determines the spatial coordinates of the targets from the target centroids in the images, and then computes the model twist and bending (deflection) produced by the aerodynamic loads. A VMD system was established at UPWT in 1996 as part of the optical measurement technique development program at NASA LaRC cited in reference 30. The primary application of the UPWT VMD system is to determine local wing twist, while secondary applications include wing deflections or bending and model angle of attack measurements. The use of the VMD technique to measure model angle of attack is described in detail in reference 29. In the UPWT system, a video signal from a standard RS-170 solid state camera with 752 horizontal by 240 vertical pixels per field is routed to a frame grabber controlled by a PC workstation which records a predetermined number of video fields into the frame grabber memory. The adjustable field integration time of the CCD video camera is set to 1/250 second or less in order to reduce the effects of dynamics on image recording. A 10 to 100 millimeter (mm) focal

length remote zoom lens is used for imaging. The focal length providing the desired field of view is established at the outset of the installation in the wind tunnel, and the lens remote control module is then powered down to prevent inadvertent focal length changes. The illumination source is a fiber optic-based ring light mounted to the front of the camera lens. The intensity of this diffuse white light is adjustable and is tailored to a particular model and test setup. The VMD system software described in reference 30 sets up the video capture hardware and reduces and analyzes the sequence of raw images automatically. Uncorrected values of the wing local angle of attack and vertical (Z) coordinates at all target rows are displayed real-time as each data point is acquired. The PC receives selected test conditions from the wind tunnel host computer via an RS-232 communications link. In addition, image acquisition is coordinated with the wind tunnel data acquisition via a contact closure activation system.

Retroreflective tape targets are placed on the wing upper surface at selected span locations and uniformly distributed within a chordwise row. The targets are typically 0.375-in. diameter except near the wing tip where 0.25-in diameter targets are used. The retrotargets are approximately 0.004-in. thickness and have excellent adhesion properties, provided the model surface has been thoroughly cleaned with alcohol prior to their application. An assessment of the possible intrusive effects of these targets is discussed in the Modern Design of Experiments (MDOE) section of this paper. The spanwise locations (Y) and chordwise locations (X) of the targets are known, either from QA validator table measurements or, more commonly, from reference locations on the wing such as the trailing edge, tip, flap breaks, pressure orifices, or fastener holes. A Mylar transfer sheet containing a 1:1 scale drawing of the wing with punched target locations provides an easy and repeatable means of locating and applying the targets onto the wing surface in the test section. To date, the Z positions of the targets have been ignored, since they are assumed to be in approximately the same plane. A typical array of targets applied to slender wings at UPWT is 5 chordwise rows beginning near the wing-fuselage junction (or on the fuselage), where the wing can be considered rigid, and 4 additional rows at roughly equidistant locations along the span extending to the wing tip region. The camera and light source are positioned somewhat above the model (resulting in an oblique view of the model) and clamped inside the webbing of the test section wall adjacent to the targeted wing. This provides excellent optical access to the model through the 1.5-inch thick optical-quality window. The proximity of the light source to the wing (about 1-2 feet depending on the target row) results in very high contrast images. Automatic target location is much faster and more reliable if the gray levels of the wing targets are significantly greater than the background. Glints from the highly-polished metal surface of the model can result in errors in the acquisition of target centroids. Regions of the wing that are susceptible to this undesired effect are identified, and a light application of flat paint is applied to eliminate the unwanted reflections. This causes the wing surface to appear dark after simple threshold removal, making it easier to automatically locate the retrotargets on the wing surface. The application of paint does not affect the aerodynamics of the wing at supersonic speeds, but this approach cannot be used at transonic speeds where the boundary layer and shock wave characteristics are more sensitive to the surface changes. The model is swept through a range of angle of attack, and adjustments are made to the variable focal length camera lens, as necessary, in order to bracket the targeted region through the desired range of angle of attack.

The pointing angles and location of the camera in the tunnel coordinate system are determined at the start of the test by photogrammetric resection on a target plate which is aligned to the X-Z plane of the tunnel. The target plate consists of a flat black plate with a 7x7 array of retrotargets with known locations. The target plate is translated a known

distance along an optical rail to several Y locations where resections are made. Figure 25 shows the calibration setup used at UPWT. During this process, a photogrammetric principal point (an effective camera focal length) is determined which causes the best agreement with the changing Y values of the target plate. A commercially-available software package (reference 31) is used in conjunction with the VMD software to derive the principal point. Having established the three pointing angles, the spatial (X, Y, Z) position of the camera, and the effective focal length of the camera, measurements are made on the target plate for an in situ check of the technique. Here, the plate is translated to different vertical positions of the plate at fixed Y locations, and the measured and known Z positions are compared. The calibration hardware is moved away from the model, and a final calibration step is conducted featuring the acquisition of model target images. An initial image is acquired with the model angle of attack set to 0^o (using an onboard accelerometer). The VMD-computed mean angles of attack (or local slope angle in the X-Z plane) and vertical displacements are recorded at each target row and inserted as zero-offset values to an input file that is read by the setup portion of the VMD software. Image acquisition is repeated with the modified input file to confirm that the computed mean angles of attack and Z displacements are essentially zero. This process is analogous to the acquisition of a set of balance wind-off zeroes. A static pitch sweep of the targeted model is conducted next, within which images are acquired over the same α–range as the wind-on runs. This static sweep is similar to the wind-on reference images that are required for PSP testing and to a model weight tare run, since the computed wind-off local angles of attack and displacements are applied as tares to the wind-on data. The static pitch sweep is repeated at the middle and end of the test as a check of the system stability.

VMD image acquisition and preliminary processing of the raw images is automated during the wind-on runs. The real-time display on the VMD PC workstation features the uncorrected local slopes and displacements at each target row, and this information is updated as each data point is acquired. The real-time data trends of local slopes and displacements with variations in independent variables such as the model angle of attack, Mach number, and Reynolds number can be determined during each run. Final reduction and plotting of the model deformation results occur off-line and involve a combination of software packages and computer platforms. The wind-off and wind-on image files created by the VMD software are processed on the PC using the computational software in reference 31. The image files contain the wind-off and wind-on target centroid locations, local slopes, and intercepts in the X-Z plane at each target row, which were determined using a process referred to as “blob analysis.” The local slopes with wind-on are corrected to first-order using the wind-off curve-fitted data. The procedure used at UPWT is designed to provide a better spatial mapping of the wind-on and wind-off images in a manner similar to the image registration process used in the PSP technique. The wind-off data are visualized graphically by plotting the difference between the VMD-measured local slope and the model angle of attack (measured directly using an onboard Q-flex) against the model angle of attack. Characteristic wind-off curves are generated for all target rows. The wind-on model angle of attack computed by the wind tunnel data system includes the tunnel flow angle and the effects of model, balance, and sting deflections caused by aerodynamic loads. To achieve the same angle of attack during wind-off conditions requires the support system to be driven to a higher pitch angle. The support system motion also promotes an axial displacement of the model, which causes a spatial misalignment relative to the wind-on case. Consequently, the wind-off tare that is applied is determined at an angle of attack that does not include the flow angle or sting deflection angles. The final wind-on VMD local alpha at each target row is then computed as the uncorrected wind-on angle of attack minus the static tare plus the flow angle at a given Mach number. The local twist is computed as the

difference between the VMD-measured angle of attack at a given target row and the model angle of attack computed by the wind tunnel data system. The resultant data file is then transferred to a UNIX workstation for conversion to binary format suitable for use in a Data Analysis System (DAS) software package for plotting (reference 32).

The first application of a dedicated UPWT VMD system occurred in 1997 using a model of a supersonic commercial transport configuration in Test Section 1 as shown in figure 26. This test was also performed in support of the NASA LaRC MDOE program, which is discussed in a later section of this paper. The right-hand wing incorporated a total of 19 retrotargets distributed in 5 chordwise rows. Representative results obtained from this experiment are shown in figure 27, which depicts the effects of the free-stream Mach number and the Reynolds number on the wing twist at the wing tip target row. Note that the Reynolds number effect is more correctly viewed as a dynamic pressure effect, since UPWT cannot provide Reynolds number variations at constant dynamic pressure.

A follow-on test was conducted in the same test section to investigate the model deformation characteristics of two supersonic transport models. The external lines of both models were identical. However, one model was instrumented with numerous pressure orifices (and corresponding pressure troughs in the wings) and incorporated segmented wing leading- and trailing-edge flaps. The second model was fabricated for force and moment testing only, and it did not include any flap components. These models are referred to as the "flapped" and "solid" wing configurations. The primary objective of the VMD testing was to quantify the differences in the wing aeroelastic deformation characteristics at supersonic speeds, which would assist in the verification of CFD predictions of the aerodynamic performance of this wing design. The model deformation measurements were coordinated with the scheduled test matrix, since the two models were tested in succession in the same entry. An identical array of retrotargets was installed on the right hand wing of each model, and a full camera calibration was conducted for each model change (for completeness and as a system stability check). Representative results obtained from this test are shown in figure 28, which clearly shows the more flexible behavior of the flapped wing relative to the solid wing.

Projection Moiré Interferometry Technique

Projection Moiré Interferometry (PMI) is an optically simple, nonintrusive measurement technique used since the 1970s for surface topology and shape characterization (reference 33). The fundamentals of PMI are well known, but only recently have PMI and similar systems been used to quantitatively measure wind tunnel model deformations while under aerodynamic load. PMI development for wind tunnel model deformation measurements is described in references 33-35. A PMI system was used at UPWT in 1998 as part of a wind tunnel test technique evaluation and unification experiment in Test Section 2 using the model shown in figure 29. The PMI system was used in conjunction with the discrete target-based VMD system and a Doppler Global Velocimetry (DGV) system in order to evaluate system implementation issues in larger-scale wind tunnels and the feasibility of simultaneous measurements from the three distinct techniques. The region of interest on the model was painted a flat rust color to eliminate unwanted reflections from the highly-polished model surface during the optical measurements.

The PMI system is characterized by optical simplicity since the only major components are a projector and a video camera. However, the image processing methods used to obtain quantitative deformation data are complex. Conventional PMI relies on the projection of a grid of equispaced, parallel lines onto the wind tunnel model surface. A raw PMI data image with perspective distortion removed is shown in figure 30. Any incoherent light source providing adequate illumination levels can be used for grid line projection. A pulsed laser diode bar emitting in the near infrared is often

used for wind tunnel testing because it allows lights-on tunnel operation without sacrificing grid line contrast and provides the high illumination levels required to measure large fields-of-view. The emission linewidth of most laser diode bars renders any speckle undetectable. This was the light source used in the UPWT testing. A Ronchi ruling (a binary grating of parallel lines having equal spacing and thickness – basically a piece of glass with lines etched in it) installed in the projector system is the physical element generating the projected grid lines. Surface preparation is generally not required for non-metallic models, but polished metal models typically require painting to obtain a diffuse scattering surface. A CCD camera with a narrow bandpass filter matched to the projector illumination wavelength is positioned to view the model off-axis. Images of the grid lines projected onto the model are acquired in reference (wind-off) and loaded (wind-on) conditions using a frame grabber installed in a PC-compatible computer. Image processing routines are then used to remove camera perspective distortion from the acquired images and to create interference patterns with respect to a computationally generated reference grid. This results in interferograms containing moiré fringes. These fringe patterns are further processed offline to obtain a quantitative, spatially continuous representation of the model surface shape or deformation (reference 33). The current PMI image processing software can process a single image in several seconds on a PC workstation. On-line data processing is not feasible at these rates, but key datasets can be processed overnight.

PMI system resolution is primarily dependent on the video camera field-of-view, optical modulation transfer function, and illumination and observation angles. The state of development at the time of the UPWT testing was such that VMD measurements generally had greater absolute accuracy than the PMI measurements, but PMI had the unique ability to resolve deformations occurring over the entire model surface within the field-of-view. PMI systems could therefore resolve deformations that were not detected by the VMD system, for example, deformations occurring in regions between the rows of VMD targets.

A PMI result showing global surface deformation characteristics obtained in the UPWT testing is shown in figure 31 for the test conditions corresponding to Mach = 2.4, Re/ft = 4.0 million, and $\alpha = 3.5^{o}$. The absolute shape of the wing, compared to a flat calibration plate, is indicated by the greyscale level (brightness/darkness) of each pixel. This is similar to a color contour map of surface elevation with a continuous contour interval. The image is scaled so that the color black (0) represents 0 mm of elevation, while the color white (255) represents 35 mm of elevation.

Infrared Thermography Technique

The IR thermography technique that has been used at UPWT features a video-based, non-contact system for global temperature measurements (reference 36). The technique provides instantaneous temperature and time history data over a large measurement area with a sensitivity of less than 0.2^{o} Celsius (0.2^{o} C) (32.36^{o} F) and a dynamic range of -20^{o} C (-4^{o} F) to 1500^{o} C (2192^{o} F). The IR thermography system consists of an infrared imager controlled by a PC workstation, which also serves as the platform for image processing and analysis. The applications that have been demonstrated in NASA LaRC wind tunnels to date include measurements of global temperatures, heat flux, location of boundary layer transition, and general flow visualization.

The application of IR thermography imposes several requirements of the wind tunnel facility and the test article (reference 36). Optical access to the test section must be provided, since the IR imager is situated outside the test section. An optical-quality, IR-transmissive window is typically required. Minimization of IR radiation sources in the test section prevents reflections on the model that can compromise the images. The flow, or test medium, must be suitable for the transmission of IR radiation. The model should

have high emittance and low thermal conductivity and specific heat characteristics. The latter two characteristics result in low thermal conduction losses and higher temperature changes on the test article. The imaging perspective should also be along the normal vector of the model surface area of interest in order to minimize directional emittance errors.

An alternate test section door that can accommodate an IR-transmissive window is used at UPWT for IR imaging tests. This assembly is shown in figure 32 and was used in conjunction with boundary layer transition detection experiments on a supersonic laminar flow wing in Test Section 1 in the 2002-2004 timeframe. The window is made of zinc-selenide with nominal 6.0-in. diameter and 0.40-in. thickness. A broadband (2.5-14 micron) antireflective coating is applied on the side of the window facing into the test section, which requires special precautions to prevent inadvertent damage to the window or oil film contamination during wind-on runs. Optical signal transmission in the 2.5-14 micron wavelength band is approximately 80%.

One approach to the use of the IR thermography technique to existing metal aircraft models is to apply a low thermal conductance skin to the upper surface of the wing to eliminate thermal conductance from within the model. Efforts have been made to apply this insulating layer to a representative aircraft model in order to identify and resolve any issues associated with the film application to a surface having compound curvature. The insulating layer is 50 micron-thick type "S" Upilex Polyimide film. The adhesive layer is 0.002"-thick acrylic contact adhesive film, and the goal was to reduce this thickness by approximately 50%. These materials and thicknesses were selected for hot-film instrumentation application and have been effectively used in IR imaging. The total thickness of the insulator and adhesive layers remains an issue, however, because of the resultant step and the effective change in the wing contour. Alternate approaches that have been used in recent UPWT tests include the application of a thermally-insulating powder coating having 0.004-to- 0.006-in. thickness to an existing model and the fabrication of a dedicated IR model that possesses the desired high emittance and low thermal conductivity properties.

An IR imaging system was one of several techniques used in reference 37 in UPWT Test Section 2 to detect boundary-layer transition on a generic flat-plate model at supersonic speeds. The IR imager used rotating mirrors for the scanning system, temperature sensitivity of 0.1^{o} Kelvin (0.1^{o} K), an 8-12 micron passband, and was cooled with liquid nitrogen. The model was an unpainted bakelite plate having a spatula-shaped flat upper surface and a lower surface fairing (support housing). The model was fabricated from a thermally-insulating material to reduce heat conduction from the lower fairing. This fabrication approach also eliminated the need for an insulating skin on the model surface. The fairing was found in an earlier phase of this test to induce larger temperature differences than those caused by transition from laminar to turbulent flow on an all-metal model having the identical dimensions of the bakelite model. Results obtained at Mach = 1.5 and selected Reynolds numbers are shown in figure 33. The heating resulting from a turbulent wedge is seen in the left-hand image by the red and orange colors representing the higher temperatures. Natural transition is shown in the right-hand image by the gradual heating of the plate, which is indicative of transition, as the colors change from the blues through the greens and up to the reds and oranges. Onset of transition was interpreted as the position where the surface temperature began to increase along the plate.

Optical Off-Surface Measurement Techniques

Doppler Global Velocimetry Technique

Doppler Global Velocimetry (DGV) is a nonintrusive flow diagnostic technique capable

of providing instantaneous 3-component, planar velocity measurements using the absorption characteristics of Iodine vapor as a Doppler shift-to-velocity converter (references 38 and 39). A requirement of DGV is the use of a single-frequency laser to produce green light that can be frequency tuned to match an Iodine absorption line. An injection-seeded, frequency-doubled Nd:YAG laser has been used to create a laser light sheet to illuminate very small (200 nm) particles entrained in the flow. An argon laser is used in a more current system at NASA LaRC. The laser light scattered by the particles as they pass through the light sheet is Doppler shifted. A portion of the scattered light is collected and passed through an Iodine vapor cell where the Iodine absorbs some of the light energy. The amount absorbed is related to the optical frequency of the scattered light. The value of the laser optical frequency is then subtracted to yield the Doppler frequency shift and, therefore, the velocity of the particles along the measured component. Two additional receiver systems are set to view the light sheet from other directions to provide measures of the remaining two velocity components. Each optical receiver consists of a polarization-insensitive beam splitter, an Iodine vapor cell, and two industry standard RS-170 CCD video cameras. The analog video signals are digitized using 10-bit frame grabbers installed in a network of PC workstations. Since DGV obtains velocity measurements from the absorption of scattered light, the resolution of each seeding particle is not required as with other laser velocimetry techniques. CCD video cameras can therefore be used to measure the scattered light energy pattern passing through the Iodine vapor and, ultimately, to define instantaneous 3-component flow-field velocity maps.

Figures 34 and 35 show DGV results from an investigation of the vortex-dominated flow about a 75-degree delta wing model in UPWT Test Section 2 (reference 38). The cross-flow pattern illuminated by the DGV laser system at Mach = 2.8 and $\alpha = 24^{o}$ is illustrated in figure 34. The flow pattern consists of three distinct scattered light intensity levels associated with the free stream, a cross flow shock, and the leading-edge vortex. The DGV velocity image in figure 35 is a contour plot of a single velocity component along the vector direction shown on the left side of the figure. The vector diagram shows this component to be slightly up and to the right of the streamwise direction. The system in use at the time of this experiment did not have the hardware to obtain simultaneous three-component velocity measurements. The general character of the flow is revealed in the contour plot but the expected changes in velocity at the intensity boundaries are not clearly defined. This anomaly was later traced to the inclusion of background light in both the signal and reference images, resulting in measurement errors. Sources of these errors, which were subsequently corrected, were the camera dark current, reflected laser radiation from surfaces, and ambient lights.

More recent DGV applications at UPWT have attempted to map the velocity field about a supersonic transport model, a flat-plate model with surface-mounted store, and a sonic boom model. Despite these efforts, however, DGV has yet to evolve as a turn-key, global velocity measurement system at UPWT.

Virtual Facilities

The use of optical measurement systems capable of acquiring global data in a wind tunnel testing environment requires detailed pretest planning to ensure the proper location of imagers, illumination sources, and other optical components. Wind tunnel experiments often require a unification of these image-based methods, whereby two or more systems are used simultaneously or sequentially. All optical methods in use at UPWT have a common requirement for cameras and light sources. However, each method demands its own imager and illumination system, and these systems often compete for the same mounting locations in the tunnel. Satisfactory field-of view and perspective of each camera within the desired ranges of the model attitude and position in the

test section are a challenge. Determination of the suitable imager and light source locations, and the resolution of conflicts with other systems, are still often performed in situ at UPWT. A technique referred to as Virtual Facilities (reference 40) has been developed at NASA LaRC that provides an accurate three-dimensional (3-D) computer representation of the wind tunnel testing environment. A Virtual Facilities rendering can include the wind tunnel test section and its surroundings, the test article (model), model support mechanism, articulation of the model and support mechanism assembly, components of the optical system(s), projection of light sources, and camera fields of view. The installation and performance of image-based measurement systems can therefore be simulated in advance of a test, and the data acquired by the optical instruments may be incorporated into the 3-D computer model. Figure 36 shows Virtual Facilities representations of a portion of the test section at UPWT and a rendering of a supersonic transport model with support mechanism in the test section.

Virtual Facilities incorporates three software categories which include computer-aided design (CAD), specialized scientific visualization programs, and computer animation programs (reference 40). Detailed modeling of the test article and the support mechanism is performed using CAD tools. This modeling can include all mechanical linkages and can define the safe limits of operation relative to the physical boundaries of the test section. Scientific visualization programs are used to map field data such as cross-plane velocities, global pressures, and surface deformation topographies to 3-D surfaces. Animation programs provide realistic simulation of cameras and lighting, including views of what the real cameras will see in the tunnel. Complex animations are possible which allow variations in the light levels, camera fields of view, and the angular/translational positions of the model in the test section.

Reference 40 discusses the 3-D modeling of a 3-component DGV system incorporated into the testing environment of UPWT. This modeling was done in support of a test techniques unification experiment conducted at UPWT in 1998. Three camera pairs were placed around the facility in order to measure the three components of velocity above the wings and into the wake. The vertical webs in the test section doors limit optical access, so direct viewing of the region of interest was difficult. Virtual Facilities was used to determine the feasibility of viewing the region of interest about the model and acquiring data using mirrors located outside the wind tunnel test section. Ray trace rendering was used to determine the placement of cameras to view the flow using mirrors. A ray trace rendering follows rays of light as they radiate from their source. The behavior of the light, including a coherent source from a laser, is computed as the rays are reflected from or transmitted through objects, the optical properties of which can be accurately simulated. A virtual reference plane representing the region of interest for flow field measurements was created in the computer simulation. The virtual cameras were directed at the mirrors, which were rotated to reflect the image of the simulated reference plane. The extent to which the region of interest could be viewed was determined in this manner. Cameras and mirrors were moved and rotated to optimize the field of view and perspective. Most of the DGV hardware was restricted to one side of the test section to allow access to the model during testing, and the virtual facilities technique was used to determine suitable instrumentation and hardware locations within this constraint. A complex support system was constructed to support the DGV components, including the laser and transmittal optics, as shown in figure 37. The test section side wall is obscured in the photograph by the DGV hardware. A physical reference plane was constructed to the same scale as represented in the virtual model in order to align the actual cameras and mirrors. As a physical analog to the Virtual Facilities simulation, the actual optics were positioned to view the maximum extent of the reference plane in the test section. The resultant field of view and perspective obtained in the final wind tunnel

setup were accurately predicted by the 3-D simulation.

More recent UPWT applications of this technique, which has evolved into the Virtual Diagnostics (ViDi) system at NASA LaRC, are summarized in reference 41. The focus of these experiments has been data visualization, including real-time 3-D renderings of the wind tunnel model with experimental surface static pressure distributions and flow visualization patterns and comparisons to CFD predictions on launch vehicle and reentry vehicle configurations.

Modern Design of Experiment

Conventional One Factor at a Time (OFAT) wind tunnel testing attempts to hold all variables constant while sequentially changing a single independent variable over the range of levels. A typical OFAT wind tunnel test to characterize the aerodynamic performance of a high speed civil transport model, for example, might feature angle-of-attack sweeps at constant Mach number, Reynolds number, and sideslip angle. This approach implicitly assumes a state of statistical control and, also, maximizes data acquisition rate and total data volume, which have been used in the past at NASA LaRC as productivity metrics. The OFAT approach is prone to superposition of systematic errors that might occur as a result of drifts in the tunnel operating condition set points (total pressure, temperature, dewpoint), strain-gage balance output, nozzle block and wall settings, sideslip angle, etc. Reference 42 demonstrates how the quality of an experimental result, in the presence of systematic error, can be influenced by the order in which the independent variables are set. An alternative approach, referred to as Modern Design of Experiments (MDOE) (references 42-44), has been used at NASA LaRC as a means of optimizing the independent variable sequence to improve the data quality while relaxing the requirements for high-volume data collection. MDOE features the processes of blocking, randomization, and replication to enhance the quality of data obtained in wind tunnel testing. Block effects arise in wind tunnel testing when the response variables such as the balance forces and moments, wing surface pressures, wing twist distributions, etc. measured in one block of time differ significantly from measurements made in another block of time under circumstances expected to yield identical results within experimental error. The method of blocking provides an effective defense against systematic variations by altering the run order to impose symmetry between the set of points acquired during one block of time and another. In this method, the independent variables are set in a manner that significantly departs from the sequence that would yield the highest data acquisition rate. An orthogonal blocking design (reference 43) referred to as the Box-Wilson or Central Composite Design has been used to fit second-order response surface models in NASA LaRC MDOE wind tunnel testing. A response surface can be viewed as a continuous representation of a dependent variable (the response) mapped in multi-dimensional space as a function of the independent variables. When plotted as a function of two independent variables, the dependent variable is visualized as a surface (first- or higher-order polynomial representation, for example) situated above a horizontal plane defined by the range of the independent variables. The Box-Wilson design is a symmetric distribution of independent variables that, for the case of three independent variables, can be viewed as a box with design points at the center and corner points. Additional data are acquired beyond the design space used to construct the model, and these confirmation, or star, points are used to confirm the predictive power of the model. Randomization is simply the act of setting the levels of the independent variables in random order to address within-block systematic variations. This method is used in MDOE to ensure that changes in response variables are related unambiguously to changes in the independent variables that influence them. In contrast to systematic errors, random errors tend to be distributed equally above and below some estimate of the true mean value, and their effects can be canceled by replication over periods of

time for which the mean is stable. Replication features the acquisition of repeated data points at random intervals throughout the test, with intervening changes in the independent variables having taken place.

The best MDOE test matrix is often not practicable because of wind tunnel facility operating constraints. In a hypothetical test at UPWT, for example, the desired response variable might be the yawing moment produced by vertical tail rudder deflection on a fighter model. Mach number, Reynolds number, angle of attack, angle of sideslip, and rudder deflection comprise the independent variables. It is assumed that control surface changes are manual. The time required to secure the test section for running, acquire pumpdown zeroes, start flow through the test section, and achieve stable operating condition set points may be an hour or more. Randomization on the rudder deflection would require frequent access to the test section and, therefore bring the facility to a wind-off condition, acquiring pumpdown and atmospheric zeroes, performing the model change, acquiring updated wind-off zeroes, initiating flow through the test section, and achieving stabilized flow conditions. This process would likely consume another hour or more of tunnel occupancy time. Although MDOE is a process-oriented technique and is not subject to the commonly-used productivity metrics, facility power costs and time required to effect model changes and resume wind-on testing are factors that must be weighed in the definition of the test matrix. Similarly, randomization on the Mach number is limited by UPWT operational procedures, since a mode change in Test Section 1 requires a return to a wind-off condition in order to change the tunnel duct configuration. In Test Section 2, mode changes can be done “on-the-fly” in increasing order, but it is not possible to return to a lower mode without returning to a wind-off condition to change the tunnel duct configuration. More complex experimental designs called split plot designs (reference 45) are available to account for these hard-to-change independent variables. Reynolds number, angle of attack, and angle of sideslip are more easily randomized. Overall wear and tear of facility equipment undergoing more frequent cycling is also a factor that cannot yet be assessed. It should be noted many of the operational constraints typical to a given wind tunnel facility may be adequately resolved by a suitable cultural shift, while others will have to be dealt with as effectively as possible (the UPWT mode changes, for example). The potential of MDOE to provide higher quality data, which is the product delivered by the wind tunnel, while requiring less total data points must be evaluated and exploited as best as possible. To accomplish this, more researchers and test facility personnel must become familiar with statistical methods and the design, implementation, and analysis phases of MDOE.

The first MDOE wind tunnel experiment at NASA LaRC was conducted in UPWT Test Section 1 in 1997 in which model deformation (wing twist and deflection) was quantified as a function of the independent variables angle of attack, Mach number, and Reynolds number using the supersonic transport model previously shown in figure 26. This test was conducted in both the classical OFAT tradition and using MDOE methods. The OFAT design featured 330 data points. The corresponding MDOE design required only 20 data points to obtain information of comparable or higher quality, in terms of 95% confidence interval half-widths (CIHW). Representative results from this test are shown in figure 38, which illustrates the effect of the angle of attack on wing twist at the 54% span station at a free-stream Mach number of 1.60 and Reynolds number of 3.0 million per foot. The OFAT points are shown with error bars along with the upper and lower limits of the 95% prediction interval for the MDOE response surface at the same Mach number and Reynolds number. Two-dimensional cuts through the response surface parallel to the angle of attack axis at constant Mach number and Reynolds number yielded MDOE equivalents of wing twist versus angle of attack sweeps. None of the 20 points defining the response surface for wing twist as a function of Mach number, Reynolds number, and angle of attack corresponded to any

of the measured OFAT data points in figure 38. In this test, the substantial reduction in the number of required data points resulted in approximately 60% fewer wind-on minutes in the MDOE version in comparison to the OFAT method. This initial success was the first of a on-going program at NASA LaRC to exploit the benefits of MDOE.

Another application of MDOE was conducted in 1999 in UPWT Test Section 2 to identify any intrusive aerodynamic effects caused by the independent application of pressure-sensitive paint and model deformation retroreflective targets to the wing upper surface. The slender arrow wing-fuselage model used in this test is shown in figure 39. The independent variables were angle of attack, paint state (on/off), and target state (on/off), while the response variables included the balance six-component forces and moments. Mach number and Reynolds number were fixed at 2.4 and 4.0 million per foot, respectively. Issues arose during the pretest planning phase regarding the desired randomization of the PSP application and, also, PSP applied to a wing featuring existing boundary layer transition trip dots (epoxy discs) near the leading edge. The paint process required a full operational shift to complete, which rendered the paint state as a difficult-to-change variable. Application of the paint over previously-applied trip dots would affect the local geometry of the dots and degrade their ability to promote boundary layer transition. Retaining an unpainted region along the wing leading edge was considered, since this would require only one application of the trip dots. However, the transition to a painted section downstream of the dots might introduce an aerodynamic effect that would mask the effect to be measured. It was decided to apply the dots after each paint application, thereby extending the model change time by 1-2 hours (the trip dot application is slow and time-consuming). The adherence properties of the dots to the PSP were poor, however, and a compromise solution was reached where a narrow strip along the leading edge was buffed after the paint application to enable a row of dots to be satisfactorily installed on the right wing of interest. Emphasis was placed on minimizing the thickness and nonuniformities of the base coat and PSP, and measurements were taken after paint application to ensure thicknesses of approximately 0.003 inches or less and surface roughness of 10 microns or less. The instrument used to measure the combined thickness of the primer and PSP coating was an ETG-2 Combo Gauge. Surface roughness was measured using a Mitutoyo Suftest-211. The internal strain-gage balance was the same instrument used in supersonic aerodynamic performance testing of high-speed research (HSR) models at UPWT, where the test requirements were to measure drag at the cruise condition to within +/-0.0001 (one count) with 95% confidence.

The results in figure 40 are based on four replicates of the model with paint on and paint off. The paint effect on the drag coefficient is not resolvable, that is, the effect is not distinguishable from zero with 95% confidence. Similar results were observed in the lift and pitching moment coefficients (not shown). The data were acquired and analyzed using a split-plot design (reference 45). In this experiment, it was hard to change the independent variable, paint state (paint on, paint off). The angle of attack was randomized while holding paint state constant. The paint state was then changed, and the process was repeated. Similar situations exist in NTF, for example, where temperature, analogous to the paint state, is a hard-to-change variable, and split-plot designs are used to accommodate such circumstances.

The model deformation target effects are shown in figure 41. There is no resolvable effect of the targets on the drag coefficient to within the 95% percent confidence intervals. A total of 19 retroreflective targets were applied to the left-hand wing in 5 chordwise rows, and the target diameter was 0.375 in. in all rows except the tip, where 0.25-in diameter targets were used. Target thickness was approximately 0.004 inches. The targets are likely embedded in the boundary layer at the supersonic speeds. This would not be expected at subsonic and transonic speeds, as noted previously on page 24, where

the thickness of the targets can be of the same order of magnitude as the boundary layer thickness. In this case, the presence of the targets could have a significant effect on the flow field (see references 30 and 46, for example).

On-Surface Flow Visualization Techniques

Sublimating Chemical Technique

The chemical sublimation technique was developed over 50 years ago for indicating boundary layer transition in low-speed wind tunnel testing (reference 47). This technique involves coating the surface to be observed with a very thin film of a volatile chemical solid. Wind-on conditions cause the development of areas on the model surface where the chemical film sublimates more rapidly due to the greater local shear stress within the boundary layer. Greater rates of sublimation will occur in regions of high shear stress or skin friction such as that found in turbulent flow. It is the stress-induced heating that produces the rates of sublimation. Consequently, this surface flow visualization technique is based on the same principle as the IR thermography boundary layer transition detection system.

The sublimating chemical coating must have high melting point, moisture resistance, low vapor pressure, solubility in a fast evaporating carrier, compatibility with model surface finishes, and manageable health hazards. The compound in use at UPWT is fluorene (solute). Fluorene is dissolved in Genesolve, a highly volatile solvent, in a 1 part solute to 8 parts solvent solution. Application of the sublimating chemical to the untreated surface of the model involves a "dry-spraying" technique, whereby the solvent is almost completely evaporated before the spray solution has time to wet the surface, leaving the sublimating chemical coating on the surface. The spraying via a compressed air gun is found to be the most effective when applied to a warm model in several light coatings. A number of white lights are distributed about the UPWT test section, and images are acquired during wind-on conditions using still cameras mounted to the test section sidewalls. An example of a sublimation pattern obtained in UPWT testing of a slender wing model in Test Section 2 is shown in figure 42. In this case, turbulent wedges can be seen emanating from boundary layer transition trip dots along the outer wing panel, and transition appears to occur slightly downstream of the trip dots along the inboard section of the wing.

Surface Oil Flow Visualization Technique

Implicit in the name of the technique, a picture of the flow pattern near the surface of a model can be obtained by applying an oil of suitable viscosity that incorporates a color pigment or fluorescent/phosphorescent dye. Proper consistency of the mixture results in streaky deposits (streaklines) indicating the direction of flow near the surface. Oil flow visualization is very useful in observing lines of separation and reattachment associated with separated flows, recirculation regions, footprints of shock waves and vortices and, given suitable oil mixture properties, boundary layer transition. In general, this technique is strictly qualitative, since questions arise regarding the possible intrusive effects of the oil film and whether the oil patterns are true indicators of the surface flow direction. It has been found, however, that if an oil of proper viscosity with respect to the surface shear stress is used, the oil will not always flow as a sheet but will often flow in streaks in the direction of the surface skin-friction lines (reference 48). This is the basis of the surface oil film interferometry technique, from which quantitative values of shear stress can be derived. A derivative of the oil flow visualization technique that has been occasionally used at UPWT is the oil dot method, which features the application of discrete oil dots of different colors (reference 49).

An ultraviolet (UV) oil technique is used in UPWT Test Sections 1 and 2 to visualize the surface patterns about wings, bodies, and other aerodynamic shapes at supersonic speeds. A

uniform coating of a mixture of 140W gear oil and Dayglo fluorescent yellow dye is painted onto the bare-metal model surface. The model roll angle orientation is upright or +/-90°, depending on the region of interest. The base of the model is typically plugged with tissue and tape to prevent oil from migrating into the fuselage cavity and contaminating the internal instrumentation. The UV oil is excited by several continuous UV light sources (the same units that are used in PSP testing at UPWT) and by 2000 Watt flash units. The surface flow patterns are documented with an array of externally-mounted still and video cameras that are positioned inside the webbing of the test section side walls. The UV oil will remain on the model surface in sufficient quantity at the desired test condition to allow several images to be acquired at 3 to 4 angles of attack. Imaging is accomplished with appropriate filters on 70mm Hasselblad still cameras and high-resolution color and gray-scale digital cameras. Video streams are acquired from color and black-and-white cameras that are connected to video recorders and PC-based video frame-grabbers. The UPWT PSP system provides scientific-grade digital cameras connected to PC and UNIX workstations to acquire and process high-resolution UV oil images. An example of a digital image acquired and processed via the PSP system is shown in figure 43, corresponding to a slender wing model at Mach = 2.4 and $\alpha = 4.5^{o}$ in Test Section 2.

Oil Film Interferometry Technique

Oil film interferometry is a relatively non-intrusive technique for measuring skin friction on models (reference 50). Although this technique is quantitative in nature, it is included in this section as a subset of the surface oil flow technique. The flow of an oil film driven by the shearing stress acting on its free surface is the basis of this technique. A surface with suitable optical qualities for interferometry (e.g. a paint-backed Mylar) is applied to the area of interest on the model, and oil of very low vapor pressure and high transparency is applied in a dot or line pattern to the Mylar. Interference is formed by the combination of the two specular reflections from the air/oil and air/Mylar interfaces. (A specular reflection from a smooth surface maintains the integrity of the incident wavefront.) A monochromatic light source positioned slightly off the normal to the oil surface reveals fringe patterns that can be best viewed from the same angular position. Optical interferometry is used to measure the slope of the oil surface at the leading edge of the oil, which is related to the component of local skin friction normal to the edge.

Oil film interferometry images were acquired on a supersonic transport model in UPWT Test Section 2 at a free-stream Mach number of 2.4 and Reynolds number of 4.0 million per foot in cooperation with the authors of reference 51. A result from this experiment is presented in figure 44, which shows the interference fringes that have formed downstream of three spanwise oil lines. Transparent silicone oil (Dow Corning DC-200) was used in combination with black "MonoKote" film (Top Flite Models, Inc.) of 0.04 mm (0.0016 inch) thickness applied to sections of the inboard and outboard wing regions. Wind tunnel run times were long enough to render negligible the effects of startup and shutdown transients. The oil viscosity (kinematic viscosity was nominally 10,000 centistokes (cSt)) was chosen to produce a convenient fringe spacing in that length of time. Run lengths with tunnel operating conditions established were typically 30 minutes, with startup and shutdown each taking about 5 to 10 minutes. The resulting fringe spacings were on the order of 1.8 mm (laminar) and 3.0 mm (turbulent), and could be measured from a photograph to within a few percent using a caliper. The illumination sources were 160-Watt, self-ballasted, high-intensity discharge mercury-type lamps with a strong spectral peak at a wavelength of 546.1 nm (green). A uniform diffuse illumination of the model was provided by reflecting the lighting from the lamps off a large white card. Photographic imaging was performed using a 35mm single lens reflex (SLR) camera and green filter.

Colored Water Flow Visualization Technique

The colored water surface flow visualization technique (reference 52) involves injecting colored water through the pressure measurement orifice tubes installed in a wind tunnel model. The apparatus used in this technique consists of three components: 1) a pressure-instrumented wind tunnel model, 2) a set of control valves, and 3) containers of colored water. An illustration of the system is presented in figure 45.

The model pressure tubes are routed outside of the tunnel and attached to a series of metering, shutoff, and switching valves and then routed to the containers of colored water. The water is tinted with ordinary food coloring. The natural pressure difference between the model surface pressure and atmospheric pressure draws the colored water from the containers and through the pressure tubes. The colored water then exits the pressure orifices on the model and flows along the surface to produce streaklines of the model surface flow. The wind tunnel model is painted white for good contrast with the colored water and is illuminated with flood lamps while either video or still photographs are obtained. This test technique has been successfully applied to investigate the flow fields in rectangular box cavities mounted in a flat plate and the flow field around missile fins mounted on a flat plate from subsonic to supersonic speeds.

Off-Surface Flow Visualization Techniques

Three off-surface flow visualization methods are currently in use at UPWT that are sensitive to variations in the optical index of refraction of the test gas and, consequently, the gas density: (1) conventional schlieren, (2) shadowgraphy, and (3) focusing schlieren.

Conventional Schlieren

Conventional schlieren provides a two-dimensional image of the density gradients in a three-dimensional flow field, since this method is related to light refraction along the entire optical path. Each test section at UPWT is equipped with a single-pass, off-axis schlieren system in a Z-layout similar to that described in reference 53. The light source passes through the test gas only once (hence, single-pass), and large spherical mirrors are used in this system in order to provide a 49-inch field of view. A schematic of the system is shown in figure 46. The complete system consists of a light source, two spherical mirrors, knife-edge, optical beam splitter, still camera, flat mirror, video camera, and image screen.

The entire system is supported from a beam as a unit and can be positioned along the longitudinal axis of the test section to provide schlieren images of any part of the test section. The light source is provided by a xenon vapor arc lamp that is operated continuously. An optical beam splitter is located just behind the knife edge and is used to provide a schlieren image for both the still and video cameras. The still photographic images are acquired using a 70mm Hasselblad camera with a digital back that is interfaced with a personal computer located in the UPWT Data Room. Representative photographs are shown in figure 47. Note that the vertical black lines in the photograph are the test section window support bars. Output from the video camera is supplied to a DVD recorder and is annotated on a real-time basis using a title generator with any desired on-line test parameters. The schlieren system is operated continuously on a nonintrusive basis unless the testing requirements preclude its use (for example, installation of an optical measurement system such as PSP or VMD). The real-time video output is an essential tool for model observation and model/facility safety as it provides constant feedback on the model flow-field response to changes in test conditions. The shock waves originating from the model and reflecting from the test section walls are observed to ensure that reflected shock impingement on the model is not a factor. Observation of model dynamics and its qualitative correlation with the real-time output from the BDDU or BLMS provide key information affecting decisions to continue or

terminate a given run sequence. In addition, the schlieren imaging is used to confirm the passage of the normal shock during flow start-up and shutdown procedures. The schlieren display provides an early warning regarding the forward advance of the normal shock into the test section, which might occur as a result of model and support system blockage at high angles of attack.

Dedicated schlieren flow visualization sequences are frequently included in the test matrix in order to acquire digital movies of the model flow field. These sequences often feature a continuous angle of attack sweep to observe the development of the flow field from a low to high-α condition. The schlieren system clearly reveals the shock waves generated from wings, bodies, tails, and control surfaces. The vortex flows shed from these same surfaces can induce sufficiently large density gradients that the vortex paths are also visible. Schlieren imaging will often reveal the tip vortices shed from wings, tails, and deflected control surfaces, the leading-edge vortices generated by highly-swept wings, and vortices shed from slender smooth-sided or chine-like forebodies. It is, at times, difficult to discern the specific origin of certain flow field features, since the images are integrated across the entire test section. However, the schlieren flow visualization can provide insights regarding the aerodynamic data, for example, the trends in the longitudinal and lateral/directional stability and the surface static pressure distributions.

The quality of the schlieren imagery is typically high, but it can be adversely affected by the mode in which a given test section is operated. The six centrifugal compressors at UPWT are used in five different operating modes, and certain modes are more prone to introducing oil into the test section due to compressor seal leaks, and this can obscure the flow visualization results. In addition, since the entire schlieren system is supported from a beam that spans approximately 63 feet from one side of the test section to the other, the schlieren output can be subject to the effect of system vibration.

Shadowgraphy

The shadowgraph method is a less complex optical flow visualization method and can be considered a subset of the schlieren system. Whereas the schlieren method is sensitive to changes in the first derivative of the gas density, the shadowgraph method visualizes details of flow fields in which the second derivative of the gas density is not uniform. In its simplest form, the only optical equipment that is required is one of the two spherical mirrors to make the light source parallel. Shadowgraphs are obtained with the same schlieren system described in the previous section, except the light source is operated in flash rather than in continuous mode. A film holder is placed between the test section window support bars at the location of interest. The lights in the test cell surrounding the test section are turned off, and the film is exposed by flashing the light source. An area approximately 4.5 in. by 3.5 in., corresponding to the film size, is captured in the shadowgraph. A sample result is presented in figure 48. The photograph is subsequently scanned using a high-resolution digital scanner for further analysis and documentation. This method is used on a selected basis at UPWT because of the detailed information provided by the relatively high-resolution, large-field schlieren system. However, shadowgraphy provides clear and rapid observation and documentation of regions of interest in the model flow field. In addition, this technique can readily be applied in facilities that may not be able to accommodate the more complex and costly schlieren system.

Focusing Schlieren

Conventional schlieren and shadowgraph techniques do not allow examination of the flow in selected thin slices, or planes, across the model or test section. As a result, the images from these techniques include the effects of thermal currents in the surrounding test cell, flow features along the test section windows associated with the tunnel boundary layer and/or reflected shock waves, flaws in the optical

windows, and undesired flow patterns superimposed on the region of interest. Another optical method is being evaluated at UPWT to examine flow density variations and features a focusing schlieren system capable of focusing in a relatively narrow portion of the optical path (reference 54). This so-called sharp-focusing schlieren system was first described in 1950 (see reference 54), but the system complexity at that time precluded universal acceptance in the wind tunnel testing community. This situation has changed as a result of more recent developments described in reference 55 that overcome limitations such as low brightness, small field of view, large depth of focus, or difficulty of use. A prototype focusing schlieren system at UPWT features a source grid to emit light which is passed through the test medium to a lens and blocking grid arrangement, where refracted light resulting from density changes in the flow can be imaged. The resulting image can be focused at different planes within the test medium by moving the image plane. A Fresnel lens with a diffuser plate is used at the image plane to increase the amount of light directed from the image toward the camera aperture. The prototype at UPWT is a dual-pass focusing schlieren system. and a sketch depicting the key components is shown in figure 49. The main lens, cut-off grid, Fresnel lens, diffuser, camera, and extended light source are contained in a single housing that is affixed to the test section side wall. Remote positioning of the cut off grid and image plane is accomplished using electric motors within the housing, which are controlled via a remote PC. The system is termed dual pass since the fiber optic-based, strobe light source is directed through the test section to a retro-reflective source grid with a dot array attached to the inside surface of the opposite wall and then back to the optics contained within the housing. Image acquisition using a mega-resolution black and white video camera is also controlled from the remote PC. A result from using a focusing schlieren system in reference 55 is shown in figure 50.

The capability for a two-camera system exists, which will extend the field of view from approximately 18 inches to 27 inches. The realizable field of view and depth of sharp focus (design goal of 0.4 inches) are subject to physical constraints that include the test section size and window layout, source grid size, available space outside the test section, access door arrangement, and the model positioning during testing. The focusing schlieren system will not replace the conventional schlieren apparatus at UPWT, but it does offer an additional flow diagnostic capability to address the specific requirements of a test.

Laser Vapor Screen Technique

The vapor screen technique is applied in UPWT Test Sections 1 and 2 to visualize the cross-flow patterns about airplane, missile, and spacecraft models at supersonic speeds. This technique has been used at UPWT for many years (references 56 and 57), and figure 51 shows a sketch of a typical system.

Water is injected into the tunnel circuit in a controlled manner and in sufficient quantity to promote condensation and the formation of a thin, uniformly distributed fog in the test section. The cross-flow patterns are illuminated by an intense sheet of light that, in earlier versions of the UPWT system, was produced by 1000-Watt mercury-vapor lamps, but is now produced by an argon-ion laser. The presence of the model in the flow field alters the uniform distribution of fog and, consequently, the degree of illumination. Several flow features are manifested in laser vapor screen images. The change in flow density through oblique shock waves results in a similar change in fog density so that shock positions and shapes are often clearly defined. Separated flows such as wakes, vortex feeding sheets, and vortex core regions appear dark or transparent, since condensate does not appear to be convected across the shear lines. Examples of laser vapor screen flow visualization images obtained at UPWT in recent years are shown in the photographs in figure 52.

The laser system consists of a laser head and power supply and fiber optic components that

refocus and direct the laser beam to an optics package to generate a thin sheet of light of controllable thickness and spread angle (reference 58). The light sheet optical package is secured to the test section side wall and remains fixed during the flow visualization runs. The flow patterns at different model longitudinal stations are observed by forward and aft traversal of the model support mechanism (horizontal blade strut). A flat paint is uniformly applied to the model and sting to reduce the flare when the laser light impinges on the metal surfaces. Observation and documentation of the flow patterns are accomplished with a 70mm Hasselblad film camera and a miniature color or black-and-white video camera, which are mounted in the test section in protective enclosures. Figure 53 shows a close-up view of the installed cameras, with the rear section of the Hasselblad camera housing partially removed. Alternatively, mirrors may be installed in the webbing of the test section side wall (see figure 51) to allow viewing and recording of the vapor screen patterns using an externally-positioned video camera. Proper control of the water injection allows extended vapor screen runs for ranges of angle of attack, sideslip, and Mach number.

The results from the vapor screen method as applied at UPWT are considered qualitative, although relative positions, sizes, and shapes of vortices and shock waves can be extracted from the vapor screen images, as desired. The appearance of condensation in the test section will affect the free-stream flow characteristics and the quantitative measurements of the model surface pressures and forces and moments. Condensation at supersonic speeds is accompanied by a stagnation pressure loss and a decrease in Mach number at the condensation shock (reference 57). At Mach = 2.0 in Test Section 1, for example, it is estimated that stagnation pressure is reduced 5 percent, Mach number is reduced by 0.05, and static pressure is increased by 4 percent. Static pressure measurements acquired from a loop of surface pressure orifices near the test section origin are routinely used to compute the Mach number as a check of the Mach number derived from the tunnel calibrations cited in reference 4. The presence of condensation during vapor screen flow visualization runs on a generic fighter model caused a Mach number decrease of approximately 0.05-0.06 in comparison to the nominal Mach = 2.16 value established during the condensation-free conditions for dedicated force and moment measurements. Reference 57 also cites a variation of about 5% in the normal force coefficients obtained during dry and humid tunnel conditions. Consequently, data acquired during the flow visualization phase of a test is recorded but used solely for monitoring and documentation purposes. Interpretations of the vapor screen images are still valid, however, and effective correlations can be made with the trends observed in quantitative model measurements such as surface static pressure distributions and six-component forces and moments. An example of such a correlation is included in figure 54, which compares the vapor screen cross-flow patterns about a model with solid and porous LEX (discussed previously in the PSP section) and the corresponding wing upper surface static pressure distributions. The lateral broadening of the vortex cross section caused by LEX porosity is consistent with the expansion of the wing vortex pressure signature.

The use of a Class IV laser system requires the implementation of special operating procedures, hardware setup, and safety precautions that must be approved by the NASA LaRC Nonionizing Radiation Safety Committee. In addition to the laser precautions, certain tunnel operating considerations arise whenever the vapor screen system is used. The effective reduction in the Mach number caused by condensation effects also reduces the maximum angle of attack at which stable supersonic flow can be maintained. For example, consistent and safe operation to a maximum angle of attack of 15 degrees in condensation-free conditions does not guarantee that the same angle of attack will be safely achieved during vapor screen runs, even though the nozzle block setting is the same and the stagnation pressure for the desired Mach number is maintained. The addition of a still

camera and housing assembly to the test section ceiling and a video camera and housing to the knuckle support system increases the blockage, which will also limit the maximum angle of attack for stable flow conditions during vapor screen runs. Finally, the forward and aft traversal of the horizontal blade strut can cause an alignment of these sources of blockage that can also promote instability of the supersonic flow in the test section. The use of the schlieren system to view the position of the normal shock is not possible during vapor screen runs, since the test section side walls are shielded during laser operations. The video camera mounted to the support system provides evidence of the normal shock only after the shock has entered the test section. Consequently, the tunnel ceiling centerline pressure distributions are the sole quantitative indicator of the shock location to define the angle of attack range that can be reasonably explored during vapor screen runs.

The real-time output from the miniature camera mounted to the support system is routed to video capture cards in PC workstations. One system is used to acquire digital movies for flow-field documentation and analysis. A second system is dedicated to routing the streaming video to several display monitors strategically located within the wind tunnel building for public observation during unclassified, nonproprietary tests.

Missile Aerodynamics Measurement Techniques

Remote Control Missile Apparatus with Multiple Fin Balances

Tests have been conducted on missiles to measure both overall forces and moments and fin loads. Unique UPWT test hardware known as the remote control missile apparatus is used to allow remote roll positioning of the main body and remote deflection of up to eight fins. Each fin can be mounted on its own 3-component strain-gage balance to measure normal force, bending moment, and hinge moment. The missile model is constructed as a shell which fits over the remote control missile test apparatus thus allowing any missile shape to be tested. All of the model roll and fin deflection movements are controlled by a computer which can be programmed to automatically step through a designated matrix of model roll and fin positions. The primary advantage of this apparatus is that no model changes are necessary to deflect any of the missile fins thereby significantly improving productivity. A generic missile instrumented with multiple fin balances is shown installed in UPWT Test Section 2 in figure 55. A more detailed description of this system and results obtained from its use at UPWT are provided in reference 59.

Rolling Tail with Braking System

Missile configurations utilizing forward surfaces, or canards, to provide control encounter induced rolling moments at supersonic Mach numbers (reference 60). Canard yaw control results in an adverse flow-field interaction with a fixed tail-fin afterbody and induces nonlinear rolling moments and roll control reversal. These induced effects are significantly reduced by a free-rolling tail, which uncouples the tail from the missile airframe. A more simplistic and modular design of the missile, featuring a single cruciform canard control system, is afforded by the rolling tail concept (reference 60).

The canard-generated flow field can cause the free-rolling tail to spin at undesirable high rates, and the experimental data base was insufficient to evaluate the effectiveness of a rolling tail at spin rates that bridged the fixed tail (zero spin rate) and unconstrained spin rate of the free-rolling tail. A free-rolling tail afterbody incorporating an electronic/electromagnetic braking system was developed in reference 60 for use with a generic cruciform missile configuration at UPWT. The braking system provided selectable tail-fin brake torques with continuous measurements of tail-to-mainframe torque using a one-component strain-gage torque balance and tail-roll rate measured by a photospeed transducer. This mechanism was combined with the UPWT remote control missile apparatus to provide a unique capability

for supersonic wind tunnel testing. The model installed in UPWT Test Section 1 is shown in the time lapse photograph in figure 56. The braking system was successfully implemented, and the test results in reference 60 showed that satisfactory control of the flow-field interactions could be achieved at lower spin rates of the rolling tail.

Store Carriage Drag Measurement Technique

One of the most important aspects of tangential and semisubmerged store carriage is the ability to place stores in various arrays to take advantage of favorable interference to minimize installed drag (reference 61). These arrays consist of lateral, tandem, and staggered arrangements. Typically, carriage drag increments for these types of arrangements are determined from wind tunnel tests of entirely metric models by subtracting the clean aircraft drag from the stores-installed aircraft drag. Because the balance must be sized to measure the entire aircraft drag, the accuracy of the store drag measurements is sometimes compromised. In addition, the interference effects between stores cannot be determined from the total drag increment.

In order to eliminate some of these problems, a technique was developed for application at UPWT that measures the drag of individual stores that are mounted in various arrays on a flat plate. The flat plate configuration, which is shown in figure 57, eliminates any interference effect caused by the complicated flow field of an aircraft and provides a uniform two-dimensional flow field for all of the store arrays. Since the drag of only one store is measured in an array, the interference effects between stores can be easily determined. In addition, by using a one-component balance which is sized to measure the drag of a single store, improved accuracy can be obtained. This technique has also been applied to the measurement of engine nacelle drag for a supersonic cruise transport aircraft model (reference 62).

Flutter Suppression Measurement Technique

Panel flutter is a large-deflection limit-cycle motion excited by the airflow. The application of piezoelectric materials is a potentially effective means of suppressing this limit-cycle motion. This class of materials is characterized by their ability to produce an electrical charge when subjected to a mechanical strain. The converse piezoelectric effect can be utilized to actuate a panel by applying an electrical field. In this scheme, piezoelectric actuators are driven by feedback controllers to modulate the panel dynamics. Numerical results obtained in reference 63 demonstrate that piezoelectric materials are effective in panel flutter limit-cycle suppression, and that the flutter-free region can be further enlarged if the actuator is triggered before the critical dynamic pressure is reached.

A flutter panel fixture was specifically designed and fabricated for testing at UPWT in the early 1990's and was used in NASA and Department of Defense (DoD)-sponsored research to define flutter boundaries (reference 64). The flutter panel support fixture shown in figure 58 is a vertical splitter plate mounted to the sidewall of UPWT Test Section 1. This splitter plate contains an integral cavity and mechanisms for supporting relatively thin sheets of metal (15 in. by 30 in. by .060 in.) or composite test panels parallel to the centerline flow. The support of the thin panel during starting loads was an important consideration. A relatively small pressure differential across a thin panel can produce loads beyond yield stress or cause significant material deformation. To secure the test article during wind tunnel startup, a mechanism called a waffle plate restraint was engaged underneath the test article using a direct current (DC) electric motor. A vacuum was applied to the cavity underneath the test article to secure it to the waffle plate. After the establishment of stable supersonic flow in the test section, the suction pressure underneath the test article was relieved to the static pressure on the test fixture surface static orifice and the waffle plate restraint was subsequently lowered. This allows the test article to flutter freely when

dynamic pressure values greater than critical dynamic pressure were encountered.

An experiment was conducted in UPWT Test Section 1 to determine the flutter suppression effectiveness of piezoelectric actuators applied to thin carbon composite panels at Mach = 2.0. Five different panels were tested with ranges of panel thickness, orientation of strain gages, and piezoelectric stiffness control strips. The experimental results indicated that suitable application of alternating current (AC) signals to the piezoelectric actuator extended the natural flutter boundary by approximately 1.3 times the freestream dynamic pressure at supersonic speeds. The flutter suppression control system used in this testing was triggered by a center-mounted trailing-edge strain gage. The test article flutter frequency and amplitude were taken as input to a control law equation which altered the phase and amplitude of the flutter input signal. The modified signal was amplified and applied as a control signal to the piezoelectric strain actuators on the test article as a means of suppressing panel flutter. A dynamic closed-loop control system was not used in this test since the constants for the control law equation that led to satisfactory flutter suppression were determined in situ.

Sonic Boom Measurement Technique

The sonic boom measurement test technique used at UPWT consists of surveying the flow field underneath an aircraft model with a static pressure probe to determine the shape of the aircraft sonic boom pressure signature. A photograph of a model installed in UPWT Test Section 1 for sonic boom pressure signature measurements is shown in figure 59, and a schlieren image illustrating the model shock wave pattern is provided in figure 60. References 65 and 66 discuss results obtained using this technique in UPWT. A solid test section door insert replaces the standard test section door that contains the multiple optical-quality windows. Two static pressure probes are attached to the tunnel side wall (that is, to the solid door insert). One static pressure probe is mounted so that it remains in the freestream flow at all times and is referred to as the reference probe. The second static pressure probe is mounted to a track that allows the probe to be moved approximately 6 inches longitudinally in the test section and is referred to as the survey probe. A 0.15 psid differential pressure transducer is used to measure the difference between the reference and survey probes. The model is mounted on a special angle of attack mechanism that varies the angle of attack in a horizontal plane. The model is then mounted with the wings vertical on the tunnel model support system, which has the capability to move the model longitudinally in the test section.

A typical run consists of adjusting the model angle of attack so that a given normal force is obtained and positioning the model a specified distance from the survey probe. Initially, the model is located so that the nose shock is downstream of the survey probe. The model is then moved forward in 0.125-inch increments while the model pressure signature data are obtained. The pressure signatures are obtained at various lateral separation distances and normal force loadings.

Dynamic Stability Testing Technique

Small-amplitude forced-oscillation tests are conducted at UPWT to determine the dynamic stability derivatives in the pitch, yaw, and roll axes. Figure 61 shows a 2.5%-scale model of the X-33 installed on a dynamic stability apparatus in UPWT Test Section 1. The NASA LaRC High-Speed Dynamic Stability system consisting of test hardware and data acquisition system is self-contained so that it can be used in any wind tunnel facility (references 67 and 68). The testing technique features mechanically forced oscillations of the model in the tunnel air-stream at a fixed amplitude and frequency. The model is forced to oscillate in either the pitch, yaw, or roll mode at an amplitude of about 1 degree for the pitch/yaw mode and about 2.5 degrees for the roll mode. For the pitch and yaw modes, the model is oscillated about a pivot

axis located on a custom dynamic stability balance. The oscillations are driven by a variable-speed motor located at the end of the model support sting. A shaft connects the motor to a rotary cam mechanism located in the balance and oscillates the balance and model in a sinusoidal motion over a variable frequency range of 3 to 30 Hz. The most accurate measurement of the damping coefficient is obtained at the frequency of velocity resonance, where the mechanical spring in the balance plus any aerodynamic spring contribution balances out model inertia. The only torque then required to oscillate the model at that particular frequency is the torque caused by the aerodynamic damping (reference 68). This torque is measured with strain-gaged beams located in the balance. In addition, the model angular displacement with respect to the sting is measured by a strain-gaged flexure plate. The roll oscillation tests are conducted in a manner essentially the same as the pitch and yaw tests except that the model is oscillated about the sting axis. The dynamic stability test hardware also has the capability to vary the model angle of attack.

Probe-Type Flow-Field Survey Measurement Techniques

Inlet flow-field survey

Achieving a successful propulsion/airframe design on a supersonic transport configuration is dependent on the flow conditions upstream of the engine inlet system (reference 69). Variations in pre-intake Mach number, total pressure recovery, and flow incidence occur throughout the aircraft's supersonic maneuverability envelope. Inlet stability margins and secondary inlet flow systems are defined around these flow disturbances to avoid engine surge and inlet unstart due to changes in local flow incidence and Mach number, as well as engine airflow.

Wind tunnel testing was conducted in UPWT Test Section 2 at a Mach number of 2.4 to survey the nacelle inlet flow field on the slender wing-body configuration shown in figure 62 (reference 69). Parameters of interest included Mach number, total pressure recovery and flow angles at the inboard and outboard nacelle wing stations. Multiple measurements were obtained using calibrated five-hole cone-probes mounted in place of the nacelles below the wing. Flow quantities were derived from cone-probe calibration data acquired in a previous UPWT test (reference 70). The surveyed inlet flow field contained sufficient detail for assessing nacelle design and integration for this configuration and for validating CFD computations.

Vortex flow-field survey

Measurements within the high angle-of-attack flow field about slender wing configurations at supersonic speeds are used to interpret the flow physics, understand the trends in surface static pressure distributions and force and moment characteristics, and to evaluate the ability of advanced computational methods to capture vortices and shock waves at supersonic speeds. Nonintrusive optical field measurement techniques such as DGV show promise in yielding details of flow fields dominated by vortices and shock waves. However, useful information can still be derived from instrumentation, albeit intrusive, designed to acquire discrete measurements in the flow field.

The UPWT Flow Field Survey Apparatus (FFSA) is a remotely-controlled device for surveying the characteristics of the flow in Test Sections 1 and 2 (reference 71). These characteristics are measured using a 5-hole probe and include Mach number, total pressure, upwash angle, and sidewash angle. The flow survey is conducted in the vertical plane with respect to the model support structure. Surveys of multiple vertical planes are accomplished by off-line adjustment of the longitudinal position of the probe support system. A typical survey is conducted of the right-hand upper quadrant with a maximum survey radius of 10 inches.

The FFSA is shown in figures 63 and 64 in combination with a flat-plate 75-degree delta wing and a supersonic transport model. The probe is capable of measuring the Mach number,

total pressure, and flow angles in a programmable fine grid. The probe is intrusive to the flow to be measured, so the resultant measurements must be interpreted with caution. At the supersonic speeds and angles of attack of interest, however, the presence of the probe does not promote premature vortex breakdown as it would at subsonic and transonic conditions.

Reaction Control System Technique

The high angles of attack that are encountered within the hypersonic and supersonic reentry envelopes of aerospace vehicles cause a loss of conventional control surface effectiveness because of a low-energy wake-blanketing effect (reference 72). As a result, the use of reaction control system (RCS) jets is necessary to control such vehicles during these phases of flight. Wind tunnel experiments to simulate RCS jets and to measure their direct (thrust) and induced (aerodynamic) effects are an important element in the development of next-generation space transport vehicles.

UPWT developed a high-pressure nitrogen delivery system for use in Test Sections 1 and 2 to provide a clean, dry test gas for RCS experiments. Figure 65 presents a photograph of the nitrogen delivery system, which features nitrogen bottles connected to a valving system to monitor and deliver the gas at a prescribed pressure to the test section via a high-pressure supply line. The latter is typically connected to the model sting, which serves a dual purpose of supporting the model and routing the high-pressure nitrogen to a plenum inside the model. This system requires special flow-through, strain-gage balances that allow passage of the nitrogen gas to the plenum and, subsequently, to the various supply line(s) that feed the jet nozzles. A modest inventory of 5-component flow-through balances exists at NASA LaRC that is used for RCS testing and is capable of measuring the typically small induced effects of the jets at supersonic and hypersonic speeds. The forces and moments induced by the RCS jet interactions are often on the same order of, or smaller than, the balance accuracies, as the balance must be sized for the loads of the complete model (reference 73). Figure 66 shows an exploded view of a 1%-scale X-33 RCS model with a 5-component flow-through balance (designated SS-12) that was used in an RCS test in UPWT Test Section 2. These balances are water-cooled (and instrumented with thermocouples) to control the thermal shifts caused by exposure to the heating environment of a hypersonic wind tunnel. This provision is typically not used at UPWT because of the comparatively benign thermal environment. Any thermal shifts that do occur in UPWT testing of these flow-through balances are typically addressed in a somewhat contrasting approach by preheating the model, balance, and support system assembly to a stable thermal condition by performing preliminary wind-on runs.

The 1%-scale X-33 RCS model is shown installed in the UPWT test section in figure 67. The model featured RCS jet nozzles with 0.011-inch throat diameters at four positions on the left side of the model and aft of the canted fin. These nozzles were positioned to simulate aft, side, up, and down thrusters. The jets were typically tested independently, or in combinations of two, while the inactive positions were plugged with nozzle blanks. The model accommodated a flow-through blade strut designed specifically for the SS-12 balance. The balance-to-sting, balance-to-model, and nozzle-to-model interfaces were sealed with O-rings. The plenum was located directly in front of the balance bore, and passageways drilled through the fuselage provided nitrogen to the RCS nozzles. A pressure transducer and a thermocouple gage were installed through two bores in the aft end of the model to measure the plenum total pressure and total temperature. A channel cut along the side of the sting allowed routing of the balance, pressure transducer, and thermocouple wires from the internal cavity of the model. The wires were routed in S-shaped loops within the model cavity to avoid bridging effects on the balance.

The integrity of the O-ring seals and interfaces along the nitrogen supply system was checked by installing all four nozzle plugs and pressurizing the system to the design limit of 1500 psia. The nitrogen source was then isolated to check the stability of the set pressure at the model. Static calibration of each nozzle was performed with the test section evacuated to a low pressure (200 psfa to 300 psfa) to better simulate the low static pressure environment into which the jets would exhaust during wind-on conditions. The calibrations were performed with the body-alone (all surfaces removed) to avoid jet-induced flow effects on the tail and control surfaces. The direct thrust effects on all five balance components were measured and compared to pretest thrust predictions. Equations were then derived for the data acquisition system so that the jet static thrust effects would be subtracted from the total wind-on balance forces and moments.

The X-33 RCS testing approach was to match the wind tunnel and flight jet momentum ratios (ratio of the jet momentum to the free-stream momentum based on the vehicle reference area) within the appropriate flight trajectory and, wherever possible, to match the calculated jet exit plume shapes. This was not always possible given the tunnel operating constraints, so a large range of momentum ratios was tested in the wind tunnel in an attempt to bound the problem. Figure 68 shows the normal force and pitching moment coefficient increments induced by a downward-firing nozzle for a range of jet total pressure. The largest effects occur at the highest angles of attack, where consistent trends with increasing jet total pressure are observed. Incremental coefficient levels expressed in terms of the balance calibration accuracies are plotted as darker horizontal lines in the figure. Repeat runs were made of all nozzle configurations throughout the testing, including removal of the nozzles and subsequent reinstallation, to determine levels of repeatability, since the induced effects and balance accuracies were frequently of similar magnitudes.

High Angle-of-Attack Aerodynamics Testing

A requirement for supersonic wind tunnel testing at high angles of attack up to 90 degrees or more, has existed for decades. For example, this capability was necessary in order to simulate the aerodynamics in the supersonic regime during the atmospheric reentry of manned capsules used during the Mercury, Gemini, and Apollo spaceflight programs. The importance of supersonic high angle-of-attack testing capability was demonstrated during the development of the Space Shuttle, which also operates at these extreme conditions during a portion of its atmospheric reentry profile (reference 72). Missiles often maneuver at supersonic, high angle-of-attack conditions. The development of advanced reusable launch vehicle concepts with fly-back, or return-to-launch site, capability, and the use of capsule designs for unmanned and manned planetary exploration underscores the continued need for high angle-of-attack wind tunnel testing at supersonic speeds.

The UPWT high angle-of-attack apparatus shown in figure 69 has been used for many years to conduct high-alpha testing of spacecraft and missile models. This articulated support system is capable of testing small winged-body and capsule models to angles of attack greater than 90 degrees using a series of available short stings. High angle-of-attack testing capability was required in an experiment featuring a small-scale generic wing-body configuration (approximately 13 inches long) designated as the Langley Glide-Back Booster 1 (LGBB-1) in support of a NASA reusable launch vehicle program (reference 74). A possible return-to-launch site scenario for this vehicle featured a high angle-of-attack maneuver at supersonic speeds. Figure 70 shows a photograph of the LGBB-1 model at a high angle of attack in UPWT Test Section 2 in which a stability and control database was established for this configuration.

Captive Carry and Stage Separation Aerodynamic Testing Techniques

The aerodynamics of captive-carry configurations are complex, and it has become common practice to apply wind tunnel testing techniques and CFD methods in tandem to understand and predict the aerodynamic interactions that occur in the subsonic through hypersonic Mach number regimes (reference 75). Captive-carry tests of a 6%-scale model of the NASA X-43A Hyper-X hypersonic research vehicle mounted to the nose of an Orbital Sciences Corporation Pegasus booster vehicle were performed in 2003 in UPWT Test Sections 1 and 2 to obtain overall six-component force and moment measurements and fin loads on the booster vehicle. Figure 71 shows a photograph of the combined Hyper-X and booster vehicle assembly (stack configuration) installed in Test Section 1. This test was indicative of the rapid response capabilities of UPWT to provide critical updates to the stability and control data base on the stack configuration in preparation for a return to flight in early 2004. The testing was a coordinated effort with the NASA LaRC 16-Foot Transonic Tunnel, in which the same model was tested at subsonic and transonic Mach numbers immediately prior to the UPWT supersonic experiments.

Two-stage-to-orbit (TSTO) vehicle designs that have been considered for future reusable launch vehicles (reference 74) must have an efficient and reliable means of recovering the booster while maintaining viable abort options. Stage separation and ascent aerodynamic environments must be accurately defined to establish the viability of proposed concepts and to support the design of abort scenarios. An experimental stage separation research program was undertaken in UPWT Test Section 2 beginning in 2002 to help develop and/or validate NASA's experimental and computational tools for assessing fully-reusable TSTO designs and for developing separation and abort aerodynamic databases. A fixed model support strut was designed and fabricated to enable the installation of a model on the side wall of the test section. The side wall-mounted strut was used in combination with the existing main support system to enable the simultaneous testing of two LGBB-1 models in which a bimese (belly-to-belly) launch configuration was simulated A photograph of the UPWT stage separation setup with both models in a test-ready, wings-vertical orientation is shown in figure 72. One model designated as the booster configuration was mounted to a fixed horizontal strut that was bolted to the test section sidewall. The second model designated as the orbiter configuration was installed on the main tunnel support system, which provided axial and lateral translation and pitch rotation capabilities. The multiple-exposure photograph in figure 72 shows the orbiter model in three positions relative to the fixed booster model, ranging from a captive bimese arrangement to two selected positions where the orbiter model was translated and rotated. Figure 73 shows a photograph of the models in a simulated captive arrangement. A spatial location and orientation that might be encountered during part of a supersonic separation trajectory is illustrated in the photograph in figure 74. Each model was instrumented with an internal six-component strain-gage balance and pressure tubes to measure the static pressure within the fuselage cavity.

The UPWT stage separation experiment was a unification of several technologies including Virtual Facilities, automated model control systems, and MDOE. The Virtual Facilities technique described earlier in this report was used to define limits to the relative position and orientation of the orbiter and booster models to ensure safe operation of the test articles and the model support system. A grid of spatial locations that bounded the range of projected supersonic trajectories and the estimated bow shock patterns at selected Mach numbers was superimposed on the Virtual Facilities rendering of the orbiter and booster models. An animation was created where the moment reference center (MRC) of the orbiter model was moved to selected locations in the grid pattern. A snapshot of the virtual facilities animation is shown in figure 75. Note that the booster model blade

strut was not modeled in this animation. Each dot in the image represents an orbiter model MRC spatial location during an initial phase of the testing in which an OFAT test technique was used. The simulated shock patterns corresponding to a free stream Mach number of 3.0 identified regions of potentially significant aerodynamic interactions. This simulation was useful in the statistically-designed experiment which was conducted in a separate phase of the UPWT entry. There were three independent variables, or factors, of interest, which included the axial separation distance between the orbiter and booster models, the vertical separation distance, and the angle of attack of the orbiter model. The ranges of these independent variables defined the experimental design space, or inference space (reference 76). Each point in the inference space corresponded to a unique combination of the three factors. There were twelve response variables corresponding to the six aerodynamic force and moment components measured on both models. A free-stream Mach number of 3.0 was selected as a representative condition for the designed experiment based on the OFAT test results obtained in the first phase of the experiment. The Virtual Facilities simulation was consistent with experience, which suggested that some of the forces and moments would behave differently in one region of the inference space than another because of different shock interaction patterns. As a result, the inference space was partitioned into smaller regions, or subspaces (reference 77), and separate response surfaces were fit in each region. Response surfaces were briefly discussed in the section on modern design of experiments. A response surface method (reference 78) is a family of analytical techniques by which the aerodynamic response variables can be represented as mathematical functions of the independent variables that influence them. In the present application, the Virtual Facilities output was useful in partitioning the inference space into several adjoining subspaces, within which a face-centered response surface design (reference 78) was defined. A response surface showing the orbiter model axial force coefficient (CA1) as a function of the axial and lateral positions (Delta X and Delta Z, respectively) within a selected subspace at $\alpha = 2.5^{o}$ is shown in figure 76.

Randomization is an important element in a designed experiment (reference 79). Accordingly, all factor combinations within a given subspace were run in random order, and the order in which the face-centered designs was run was also randomized. Manual translation and rotation of the orbiter model in a randomized fashion imposed a significant work load on a wind tunnel operator based on actual wind tunnel experience. The development of an automated model control system, referred to at UPWT as the Automated Test Sequence (ATS) system (reference 80), was essential to the successful implementation of modern design of experiments techniques in the stage separation experiment. Control system modifications tailored to MDOE operation were developed and validated that accommodated randomized test sequences, provided the flexibility to tailor the model translation and rotation rates, and incorporated software and hardware limits to ensure safe operation of the models within the entire inference space.

Planetary Entry Vehicle Aerodynamics Testing

Precision landing capability of planetary entry vehicles is of great importance to future generations of unmanned and manned exploration missions. The next-generation of Mars landers is being developed by NASA to provide an order of magnitude improvement in the accuracy associated with the targeted landing area (reference 81). A baseline configuration for a Mars “smart lander” was leveraged from Pathfinder and Mars Polar Lander designs which featured a 70^{o} spherically blunted cone with a conic afterbody. One concept to achieve aerodynamic trim during a lifting trajectory and therefore, landing precision, is a deployable body flap (reference 81). Figure 77 presents a photograph of a Mars lander model installed in UPWT Test Section 2 and details of three different body flap designs that were tested. The

insert at the top of figure 77 shows a 3-D rendering of the baseline configuration. The part lines that are visible in this rendering define where each body flap was installed to the model. The body flap and its mounting surface were an integral piece, and the flap protruded beyond the outer edge of the 70^{o} spherically blunted cone. Figure 78 shows schlieren images obtained on the baseline configuration at Mach = 2.7 and two selected angles of attack. This experiment was conducted in 2002 and contributed to the establishment of a database from subsonic through hypersonic speeds using the complex of wind tunnels at NASA LaRC.

Force and moment testing of capsules and other blunt bodies requires internal strain-gage balances that are specially designed to measure significant axial loads while maintaining the ability to accurately resolve the relatively small output of the other five force and moment components. A small inventory of water-cooled balances is available at NASA LaRC that is suitable for the testing of planetary entry vehicle models in UPWT and in the complex of hypersonic wind tunnels at LaRC (references 73 and 81). In some cases, the same model and balance combinations are tested through the supersonic and hypersonic Mach number ranges of these facilities. Water cooling is typically not used at UPWT because of the more benign thermal environment compared to hypersonic test conditions. Potential thermal effects on the balance output must still be considered in UPWT testing of this category of models, since the balance is often only partially embedded in the model. A nonmetric sting shroud is one means of safeguarding the exposed portion of the balance from the external flow. A sting shroud is illustrated in the model installation photograph previously shown in figure 77. However, the front and rear sections of the balance are subjected to different thermal environments. Consequently, wind-on preheat runs are often necessary to stabilize the balance temperature and to limit the potential effects of a thermal gradient on the balance electrical output.

The balance and sting combinations that are compatible with testing these blunt, axisymmetric shapes are often quite flexible and can be susceptible to undesired dynamics when a heavy model is subjected to an aerodynamic flow disturbance induced, for example, by shock wave development or boundary layer separation. Model weight reduction via material selection (aluminum versus stainless steel) and boring out any extraneous material allowed by the model design are two useful approaches to reducing the potential for model dynamics. It is noted, however, that an aluminum model is more susceptible to abrasion caused by exposure to airborne particulates, although this has not been an issue at the NASA LaRC UPWT.

Another model design consideration is to incorporate an air vent hole in the model or a slot in the model-to-balance sleeve to allow the escape of trapped air inside the model during balance installation. Failure to do so could prevent the installation of the balance.

Base pressures are typically measured on these blunt bodies using a rake of static pressure tubes that are run externally along the sting and terminate at selected radial positions near the surface of the model. These measurements are particularly important in monitoring changes in the wake flow that are caused by boundary layer separation and in making inferences about the potential effect of reflected shock waves on the wake closure.

Summary

An overview was given of selected measurement techniques for aerodynamic testing in a supersonic wind tunnel facility. Descriptions of the techniques and their applications to testing in the NASA LaRC UPWT facility were presented. The range of experimental techniques include conventional strain-gage balance force and moment measurements, model attitude sensing, electronically-scanned pressure measurements, and image-based systems designed to acquire global or field measurements of the surface

pressures and temperatures, wing aeroelastic response, and off-surface velocities. These optical measurement systems included pressure-sensitive paint, video model deformation, projection moiré interferometry, infrared thermography, and doppler global velocimetry. The application of Virtual Facilities to improve the setup and conduct of image-based measurement systems and to visualize experimental data was discussed. The significant advancements in the testing process that can arise from a modern design of experiments approach were summarized. On-surface flow visualization techniques featuring sublimating chemicals, oil flow and oil film interferometry, and colored water, and off-surface flow visualization tools such as conventional and focusing schlieren, shadowgraphy, and laser vapor screen were highlighted. Several additional techniques were reviewed that provide unique data sets encompassing high angle-of-attack missile flow-field control, stores carriage drag reduction, panel flutter suppression, sonic boom pressure signature measurement, dynamic stability characteristics, discrete (point) flow-field measurements, reaction control system jet-induced effects, high angle-of-attack testing, captive carry and stage separation experiments, and planetary entry vehicle aerodynamics. The diversity of the available measurement techniques and the corresponding range of high-quality data resulting from their application demonstrate the capabilities of ground-based testing facilities to advance the understanding, prediction, and control of the complex supersonic aerodynamics of modern aerospace vehicles.

References

1. Erickson, Gary E.: "Overview of Selected Measurement Techniques for Aerodynamics Testing in the NASA Langley Unitary Plan Wind Tunnel", AIAA Paper 2000-2396, June 2000.
2. Schwartz, Richard J.; Fleming, Gary A.: "Advanced Visualization of Experimental Data in Real Time Using LiveView3D", AIAA Paper 2006-3302, June 2006.
3. Deloach, Richard: "Tactical Defenses Against Systematic Variation in Wind Tunnel Testing", AIAA Paper 2002-0885, January 2002.
4. Jackson, Charlie M. Jr.; Corlett, William A.; Monta, William J.: *Description and Calibration of the Langley Unitary Plan Wind Tunnel*, NASA TP 1905, November 1981.
5. Wassum, Donald L.; Hyman, Curtis E., Jr.: *Procedures and Requirements for Testing in the Langley Research Center Unitary Plan Wind Tunnel*, NASA TM 100529, February 1988.
6. *First International Symposium on Strain Gauge Balances*, NASA/CP-1999-209101/PT1&PT2, March 1999.
7. Rhew, Ray D.: "NASA LaRC Strain Gage Balance Design Concepts", First International Symposium on Strain Gauge Balances, NASA/CP-1999-209101/PT2, March 1999, pp. 525-541.
8. Parker, Peter A.; Morton, M.; Draper, N.; Line, W.: "A Single-Vector Force Calibration Method Featuring the Modern Design of Experiments", AIAA Paper 2001-0170, January 2001.
9. Ferris, Alice T.; White, William C.: "Monitoring Dynamics Loads on Wind Tunnel Force Balances", ISA Paper No. 89-0021, 1989.
10. Hemsch, Michael J.; Grubb, John P.; Krieger, William B.; Cler, Daniel L.: "Langley Wind Tunnel Data Quality Assurance – Check Standard Results", AIAA Paper 2000-2201, June 2000.
11. Watslavik, Robert L.; Crowder, James P.; Wright, Frank L.: "Comparison of Model Attitude Systems: Active Target Photogrammetry, Precision Accelerometer, and Laser Interferometer", AIAA Paper 96-2252, June 1996.

12. Burner, Alpheus W.; Radeztsky, R. H.,;and Liu, T.: "Videometric Applications in Wind Tunnels", Videometrics V, Proceedings of the International Society for Optical Engineerings (SPIE), Vol. 3174, 1997, pp. 234-247.

13. Finley, Tom D.; Tcheng, Ping: "Model Attitude Measurements at NASA Langley Research Center", AIAA Paper 92-0763, January 1992.

14. Crawford, Bradley L.; Finley, Tom D.: "Improved Correction System for Vibration Sensitive Inertial Angle of Attack Measurement Devices", AIAA Paper 2000-0415, January 2000.

15. Ferris, Alice T.; Finley, Tom D.: *Angle Measurement System (AMS) Users Manual*, Langley Management System (LMS) document LMS-TD-0615, NASA Langley Research Center, 1999.

16. System 8400 Users Manual, Pressure Systems Incorporated, May 1996.

17. Everhart, Joel L.: "Calibration Improvements to Electronically-Scanned Pressure Systems and Preliminary Statistical Assessment", AIAA Paper 96-2217, June 1996.

18. Klaser, Harold N.; Juanarena, Douglas B.: "Using Digital Thermal Correction of Electronic Pressure Scanners to Improve Windtunnel Productivity", Pressure Systems Incorporated, 1999.

19. Cobleigh, Brent R.; Whitmore, Stephen A.; Haering, Edward A., Jr.; Borrer, Jerry; and Roback, V. Eric: *Flush Airdata Sensing (FADS) System Calibration Procedures and Results for Blunt Forebodies*, NASA/TP-1999-209012, November 1999.

20. McLachlan, Blair G.; Bell, James H.: "Pressure-Sensitive Paint in Aerodynamic Testing", Experimental Thermal and Fluid Science", Vol. 10, 1995, pp. 470-485.

21. Bell, James H.; Burner, Alpheus W.: "Data Fusion in Wind Tunnel Testing: Combined Pressure Paint and Model Deformation Measurements", AIAA Paper 98-2500, June 1998.

22. Gebbie, David A.; Reeder, Mark A.; Tyler, Charles; Fonor, Vladimir; Crafton, Jim: "PSP-Based Experimental Investigation of a Blended-Wing Body Aircraft", AIAA Paper 2005-4719, June 2005.

23. Erickson, Gary E.: *Wind Tunnel Application of a Pressure-Sensitive Paint Technique to a Faceted Missile Model at Subsonic and Transonic Speeds*, NASA TM-2004-212991, February 2004.

24. Trosin, Jeff; Hermstad, Dexter: "PAINTCP V2.3 User's Guide", TN-94-8006-000-48, Revision 1, NASA Ames Research Center, May 1995.

25. GreenBoot User's Guide, Version 2.10, Boeing Compary, November 1997.

26. Carroll, Bruce; Abbitt, John; Lukas, Erick; Winslow, Andy; Schanze, Kirk; Morris, Marty: "Pressure Sensitive Paint Time and Frequency Response", Workshop on Pressure, Temperature and Shear Sensitive Coatings, University of Florida, Gainesville, Florida, May 1995.

27. Obara, Clifford J.: "Pressure and Temperature Sensitive Paint", NASA Langley Research Center Wind Tunnel Enterprise Short Course on Wind Tunnel Test Techniques, January 2000.

28. Burner, Alpheus W.; Wahls, Richard A.; Goad, William K.: *Wing Twist Measurements at the National Transonic Facility*, NASA TM 110229, February 1996.

29. Burner, Alpheus W.; Fleming, Gary A.; Hoppe, John C.: "Comparison of Three Optical Methods for Measuring Model Deformation", AIAA Paper 2000-0835, January 2000.

30. Burner, Alpheus W.: "Model Deformation Measurements at NASA Langley Research Center", AGARD 81st Fluid Dynamics Panel Symposium on Advanced Aerodynamic Measurement Technology, September 1997.

31. *Using MATLAB - Version 5*, The MathWorks, Inc., December 1996.

32. Graham, A. Bruce: *The Data Analysis System, System Description and User's Guide*, NASA Langley Research Center, April 1993.

33. Fleming, Gary A.; Soto, Hector L.; South, Bruce W.; Bartram, Scott M.: "Advances in Projection Moiré Interferometry Development for Large Wind Tunnel Applications", Paper 1999-01-5598, 1999 World Aviation Congress and Exposition, October 1999.

34. Fleming. Gary A.; Gorton, Susan A.: "Measurement of Rotorcraft Blade Deformation using Projection Moire Interferometry", Third International Conference on Vibration Measurements by Laser Techniques, SPIE Vol. 3411, June 1998, pp. 514-527.

35. Fleming, Gary A.; Burner, Alpheus, W.: "Deformation Measurements of Smart Aerodynamic Surfaces", SPIE Paper No. 3783-25, July 1999.

36. Borg, Stephen E.: "Infrared Thermography for Wind Tunnel Applications", NASA Langley Research Center Wind Tunnel Enterprise Short Course on Wind Tunnel Test Techniques, January 2000.

37. Hall, Robert M.; Obara, Clifford J.; Carraway, D. L.; Johnson, C. B.; Wright, R. E.; Jr., Covell, Peter F.; Azzazy, M.: "Comparisons of Boundary-Layer Transition Measurement Techniques at Supersonic Mach Numbers", AIAA Journal, Vol. 29, No. 6, June 1991, pp. 865-871.

38. Meyers, James F.: "Development of Doppler Global Velocimetry as a Flow Diagnostics Tool", Measurements in Fluids and Combustion Engineering, Vol. 6, No. 6, June 1995, pp. 769-783.

39. Meyers, James F.; Fleming, Gary A.; Gorton, Susan A.; Berry, John D.: "Instantaneous Doppler Global Velocimetry Measurements of a Rotor Wake: Lessons Learned", 9th International Symposium on Applications of Laser Technologies to Fluid Mechanics, Lisbon, Portugal, July 1998.

40. Schwartz, Richard J.: "Virtual Facilities: A Tool for Wind Tunnel Instrumentation", AIAA Paper 98-2720, June 1998.

41. Schwartz, Richard J.; Fleming, Gary A.: "LiveView3D: Real Time Data Visualization for the Aerospace Testing Environment", AIAA Paper 2006-1388, January 2006.

42. DeLoach, Richard: "Applications of Modern Experimental Design to Wind Tunnel Testing", AIAA Paper 98-0713, January 1998.

43. DeLoach, Richard: "Improved Quality in Aerospace Testing Through the Modern Design of Experiments", AIAA Paper 2000-0825, January 2000.

44. DeLoach, Richard: "The Modern Design of Experiments: A Technical and Marketing Framework", AIAA Paper 2000-2691, June 2000.

45. Amer, Tahani R.; Liu, Tianshu; Oglesby, Donald M.: "Characterization of Pressure Sensitive Paint Instrusiveness on Aerodynamic Data", AIAA Paper 2001-0556, January 2001.

46. Schairer, E. T.; Mehta, R. D.; Olsen, M.E.; Hand, L. A.; Bell, J. H.; Whittaker, P. J.; Morgan, D. G.: "*The Effects of Thin Paint Coatings on the Aerodynamics of Semi-span Wings*", AIAA Paper 98-0587, January 1998.

47. Obara, Clifford J.: "Sublimating Chemical Technique for Boundary-Layer Flow Visualization in Flight Testing", Journal of Aircraft, Vol. 25, No. 6, June 1988, pp. 493-498.

48. Keener, Earl R.: *Flow-Separation Patterns on Symmetric Forebodies, NASA TM 86016, January 1986.*

49. Lamar, John E.: *Flow-Visualization Techniques Used at High Speed by Configuration Aerodynamics Wind-Tunnel-*

Test Team, NASA TM 2001-210848, April 2001.

50. Kennelly, Robert A.; Westphal, Russell V.; Mateer, George G.; Seelen, Julie: "Surface Oil Film Interferometry on a Swept Wing Model in Supersonic Flow", Flow Visualization VII – Proceedings of the Seventh International Symposium on Flow Visualization, Begell House, Inc., September 1995, pp. 302-307.
51. Kennelly, Robert A.; Goodsell, Aga: "Skin Friction and Transition Location Measurements on Supersonic Transport Models", Paper No. 160, to be presented at the 9th Millennium International Symposium on Flow Visualization, Edinburgh, Scotland, August 2000.
52. Wilcox, Floyd J.: "Use of Colored Water Flow Visualization in a Supersonic Wind Tunnel to Investigate Cavity Flow Fields", Flow Visualization VI – Proceedings of the Sixth International Symposium on Flow Visualization, Springer-Verlag, October 1992, pp. 41-45.
53. Merzkirch, Wolfgang: *Flow Visualization*, Academic Press, 1974.
54. Weinstein, Leonard M.: "An Improved Large-Field Focusing Schlieren System", AIAA Paper 91-0567, January 1991.
55. Weinstein, Leonard M.: "Large-Field High-Brightness Focusing Schlieren System", AIAA Journal, Vol. 31, No. 7, July 1993, pp. 1250-1255.
56. Snow, Walter L.; Morris, Odell A.: *Investigation of Light Source and Scattering Medium Related to Vapor-Screen Flow Visualization in a Supersonic Wind Tunnel*, NASA TM 86290, December 1984.
57. Morris, Odell A.; Corlett, William A.; Wassum, Donald L.; Babb, C. Donald: *Vapor-Screen Technique for Flow Visualization in the Langley Unitary Plan Wind Tunnel*, NASA TM 86384, July 1985.
58. Erickson, Gary E.; Inenaga, Andrew S.: *Fiber-Optic-Based Laser Vapor Screen Flow Visualization System for Aerodynamic Research in Larger Scale Subsonic and Transonic Wind Tunnels*, NASA TM 4514, January 1994.
59. Allen, Jerry M.; Shaw, David S.; Sawyer, Wallace C.: "Analysis of Selected Data from the Triservice Missile Data Base" AIAA Paper 89-0478, January 1989.
60. Blair, Adolphus B., Jr.: "Remote Control Canard Missile with a Free-Rolling Tail Brake Torque System", Journal of Spacecraft and Rockets, Vol. 18, No. 6, November-December 1981, pp. 550-555.
61. Wilcox, Floyd J.: "Tangential, Semisubmerged, and Internal Store Carriage and Separation at Supersonic Speeds", APAA Paper 91-0198, January 1991.
62. Flamm, Jeffery D.; Wilcox, Floyd J.: *Drag Measurements of an Axisymmetric Nacelle Mounted on a Flat Plate at Supersonic Speeds*, NASA TM-4660, June 1995.
63. Lai, Zhihong; Xue David Y.; Huang, Jen-Kuang; Mei, Chuh: "Panel Flutter Limit-Cycle Suppression with Piezoelectric Actuation", Journal of Intelligent Material Systems and Structures, Vol. 6, Issue 2, March 1995, pp. 274-282.
64. Cole, Stanley R.; Florance, James R.; Thomason, Lee B., Spain, Charles V.; Bullock, Ellen P.: "Supersonic Aeroelastic Instability Results for a NASP-Like Wing Model", unpublished.
65. Mack, Robert J.; Needleman, Kathy E.: "The Design of Two Sonic Boom Wind Tunnel Models from Conceptual Aircraft Which Cruise at Mach Numbers of 2.0 and 3.0", AIAA Paper 90-4026.
66. Dollyhigh, Samuel M.; Mack, Robert J.; Shrout, B. L.: *A Wind Tunnel Investigation of Sonic-Boom Pressure Distributions of Bodies of Revolution at Mach 2.96, 3.83, and 4.63*, NASA TN-D 6195, April 1971.
67. Dress, David A.; Boyden, Richmond P.; Cruz, Christopher I.: "Supersonic Dynamic Stability Characteristics of the Test

Technique Demonstrator NASP Configuration", AIAA Paper 92-5009, December 1992.

68. Tomek, Deborah M.; Boyden, Richmond P.: "Subsonic and Transonic Dynamic Stability Characteristics of the X-33", AIAA Paper 2000-0266, January 2000.
69. Won, Mark J.: *Experimental Inlet Flow Field Survey for the BaselineTechnology Concept Airplane*, NASA TM-CD-1999-208770, 1999.
70. Won, Mark J.: *Cone Probe Rake Design and Calibration for Supersonic Wind Tunnels*, NASA/TM-1999-208764, March 1999.
71. Byrd, James E.; McMillin, S. Naomi: *A Description of the Flow Field Survey Apparatus for the Unitary Plan Wind Tunnel, Volumes I-IV*, unpublished.
72. Erickson, Gary E.: *High Angle-of-Attack Aerodynamics*, Annual Review of Fluid Mechanics, Vol. 27, Annual Reviews Inc., 1995, pp. 45-88.
73. Miller, Charles G.: "Development of X-33/X-34 Aerothermodynamic Data Bases: Lessons Learned and Future Enhancements", NATO-AVT Symposium on Aerodynamic Design and Optimization of Flight Vehicles in a Concurrent Multi-Disciplinary Environment, Ottawa, Canada, October 1999.
74. Pamadi, Bandu N.; Brauckmann, Gregory J.; Ruth, Michael, J.; Furhmann, Henri D.: "Aerodynamic Characteristics, Database Development and Flight Simulation of the X-34 Vehicle," AIAA-200-0900, January 2000.
75. Buning, Peiter G.; Wong, Tin-Chee; Dilley, Arthur D.; Pao, Jenn L.: "Prediction of Hyper-X Stage Separation Aerodynamics Using CFD," AIAA-2000-4009, August 2000.
76. Deloach, Richard: "Applications of Modern Experiment Design to Wind Tunnel Testing at NASA Langley Research Center," AIAA-1998-0713, January 1998.
77. Deloach, Richard; Erickson, Gary E.: "Response Surface Modeling of Wind Tunnel Data Over Truncated Inference Subspaces," AIAA-2003-0456, January 2003.
78. Myers, Raymond H.; Montgomery, Douglas C.: *Response Surface Methodology: Process and Product Optimization Using Design Experiment*, 2nd edition, John Wiley & Sons, Inc., 2002.
79. Montgomery, Douglas C.: *Design and Analysis of Experiments*, 6th edition, John Wiley & Sons, Inc. 2005.
80. Micol, John R.: "Langley Research Center's Unitary Plan Wind Tunnel: Testing Capabilities and Recent Modernization Activities,"AIAA-2001-0456, January 2001.
81. Horvath, Thomas J.; O'Connell, Tod F.; Cheatwood, F. Neil; Alter, Stephen J.; Prabhu, Ramadas K.: "Experimental Hypersonic Aerodynamic Characteristics of the 2001 Mars Surveyor Precision Lander with Flap," AIAA-2002-4408, August 2002.

Figure 1. Aerial photograph of the NASA LaRC UPWT.

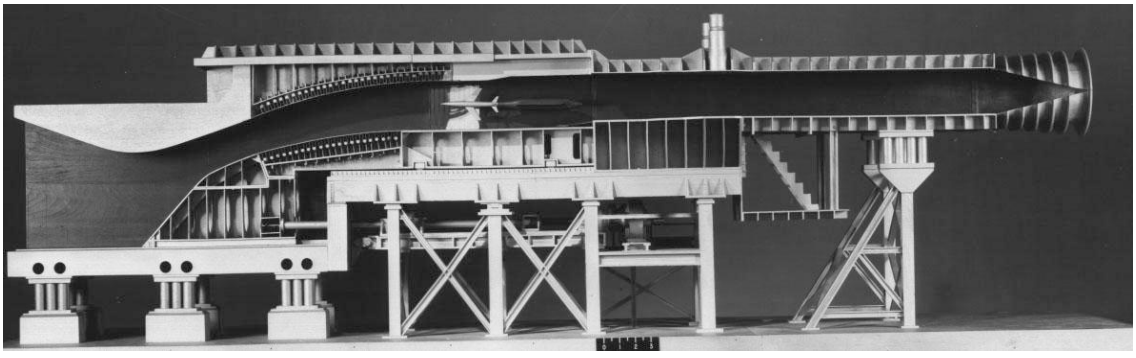

Figure 2. Illustration of UPWT asymmetric sliding nozzle block arrangement.

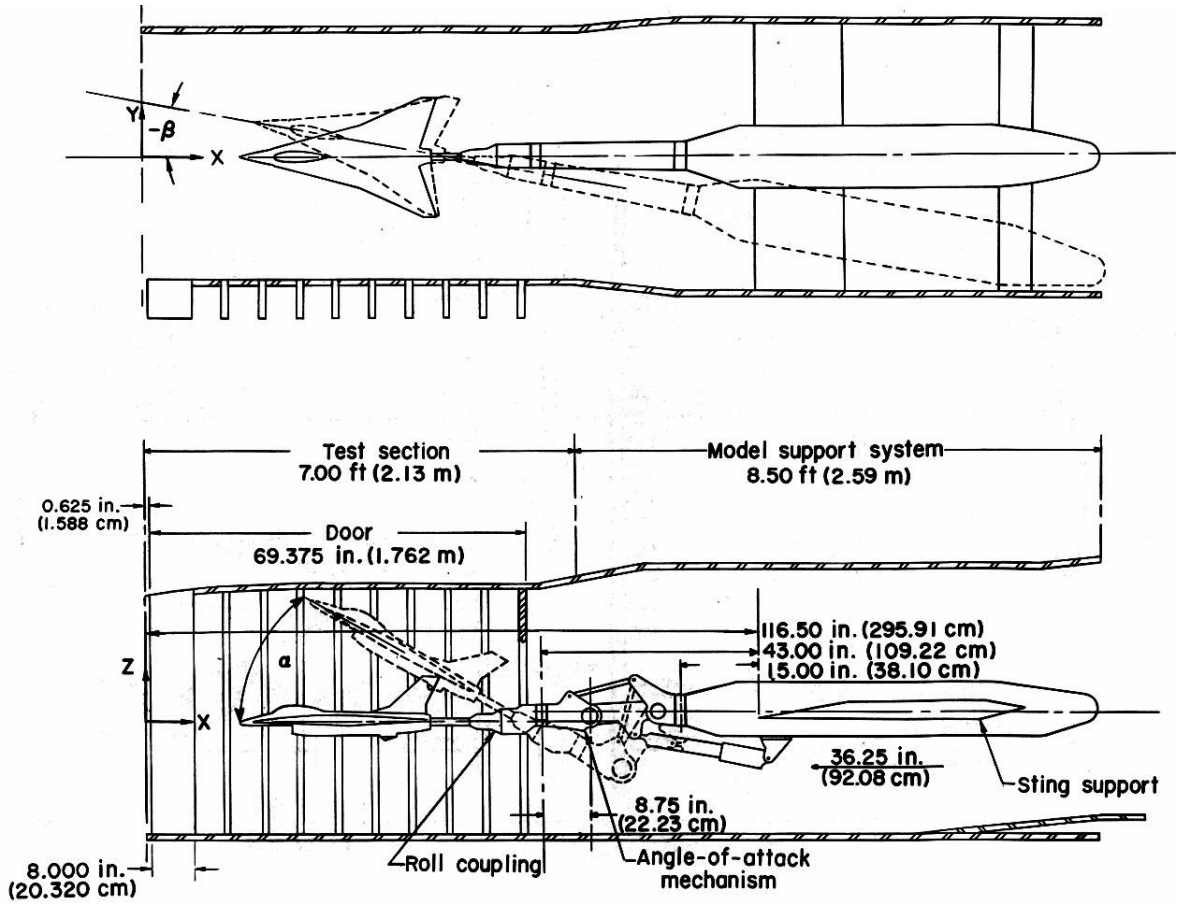

Figure 3. Overall UPWT test section layout.

Figure 4. NASA LaRC expander-type balance.

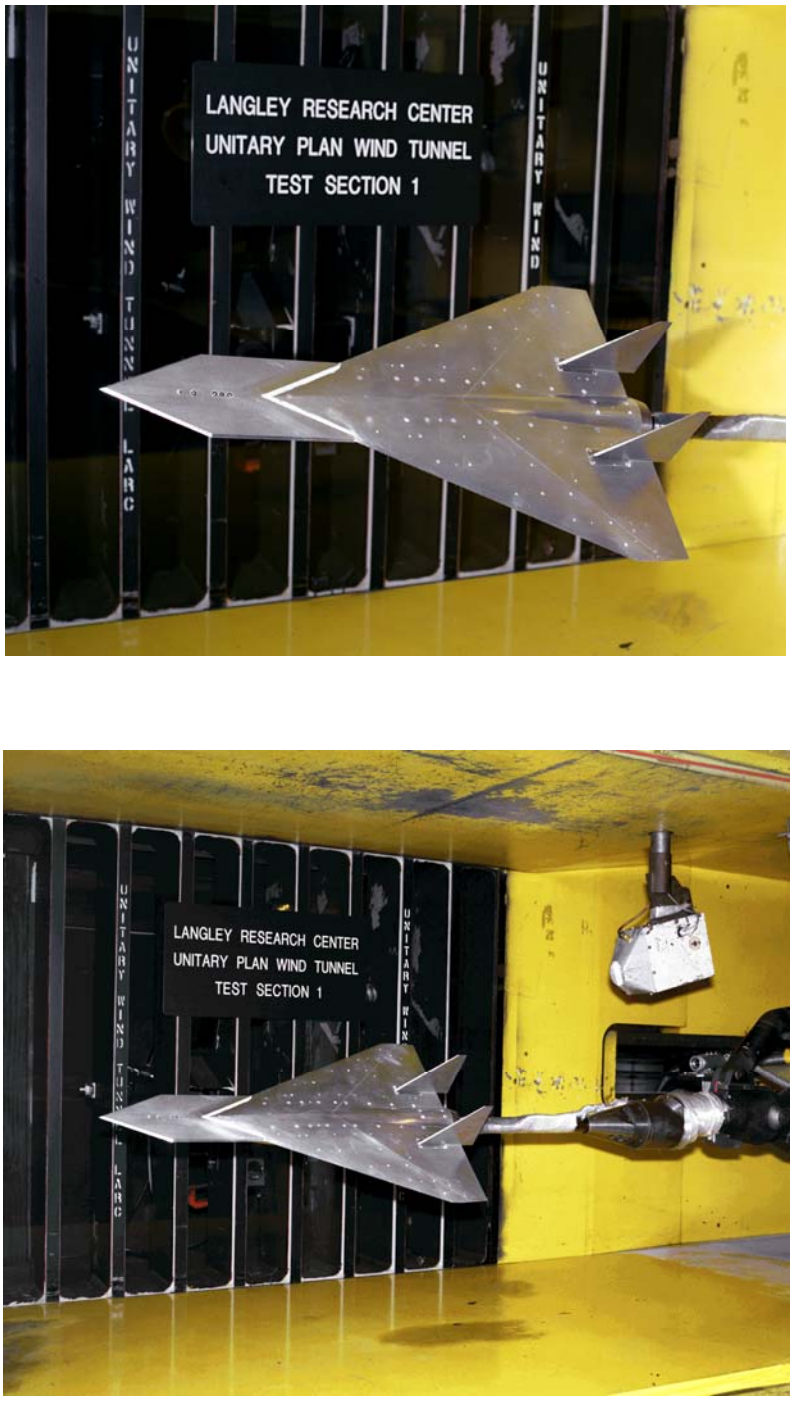

Figure 5. Test-ready general research fighter model.

	Test	Run	M_∞	PSP	Targets
○	1721.	73.	2.40	Off	On
□	1721.	74.	2.40	Off	On
◇	1721.	75.	2.40	Off	On
△	1721.	100.	2.40	Off	On
◺	1721.	101.	2.40	Off	On
◺	1721.	102.	2.40	Off	On

Δ's are obtained by interpolating in each polar to the nominal values of the independent variable, averaging, and subtracting the averages from the interpolated data.

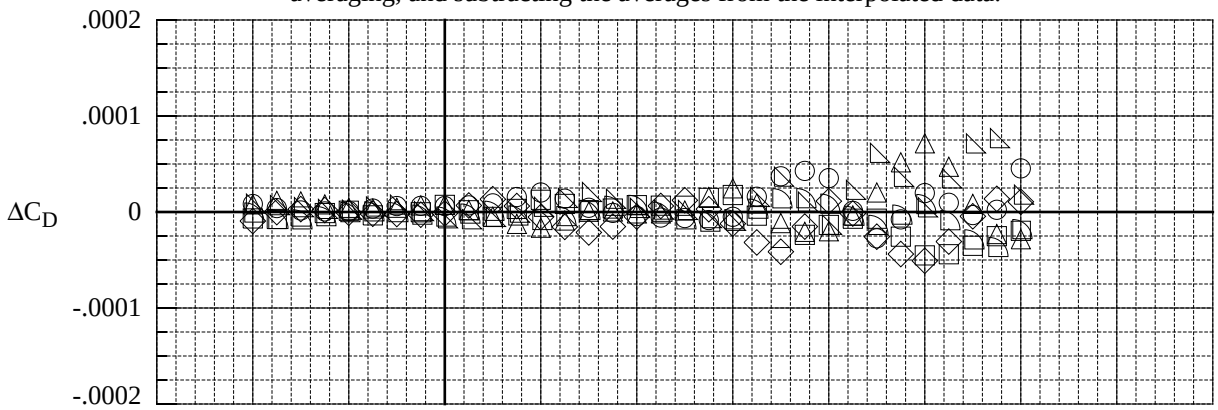

Solid line is a spline fit to the averages at the nominal values of the independent variable.

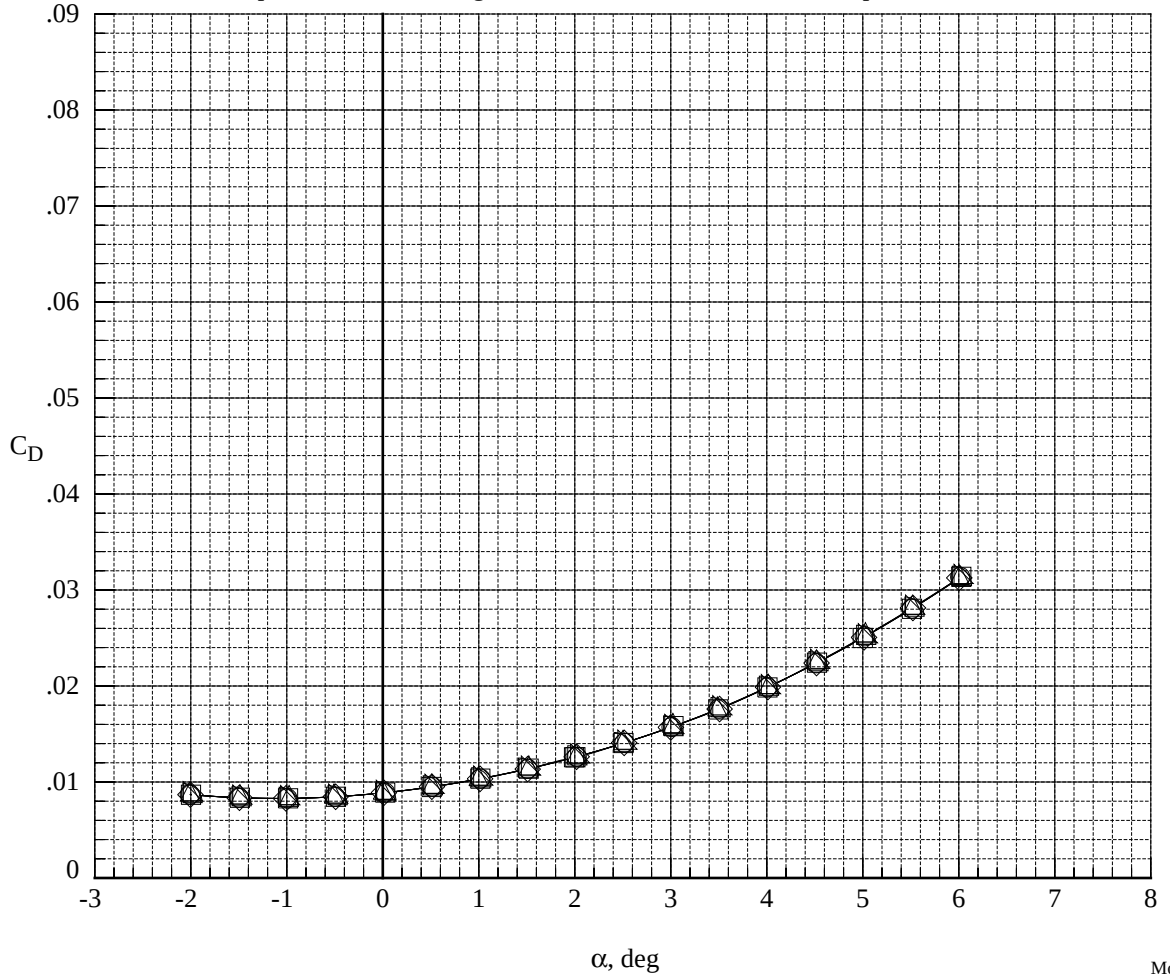

Mon Jul 16 14:00:13 2007

Figure 6. Data scatter plot for drag coefficient at Mach = 2.40.

Figure 7. Interim check standard model for UPWT.

Figure 8. 2%-scale X-33 loads model installed in UPWT Test Section 2.

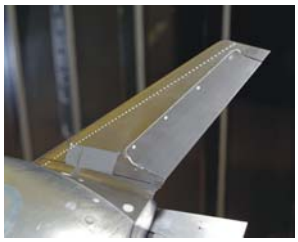

Canted Fin

Vertical Fin

Rudder

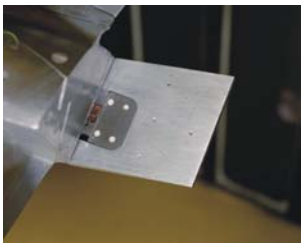

Body Flap

Elevons

Figure 9. Strain-gaged components on the 2%-scale X-33 loads model.

Figure 10. Check load application to instrumented canted fin using weight pan hanger.

	Run	Mach	β, deg	Canted Fins	Vert. Fins	LH/RH Inbd. Elev.	LH/RH Outbd. Elev.	LH/RH Body Flaps	LH/RH Rud.
○	55.	2.16	0.00	On	On	0/0	0/0	0/0	0/0
□	104.	2.16	0.01	On	On	-30/-30	-30/-30	0/-10	0/0
◇	121.	2.16	0.01	On	On	-10/-10	-10/-10	0/+10	0/0
△	137.	2.16	0.00	On	On	10/10	10/10	0/+30	0/0
◺	153.	2.16	0.00	On	On	30/30	30/30	0/0	-30/-30

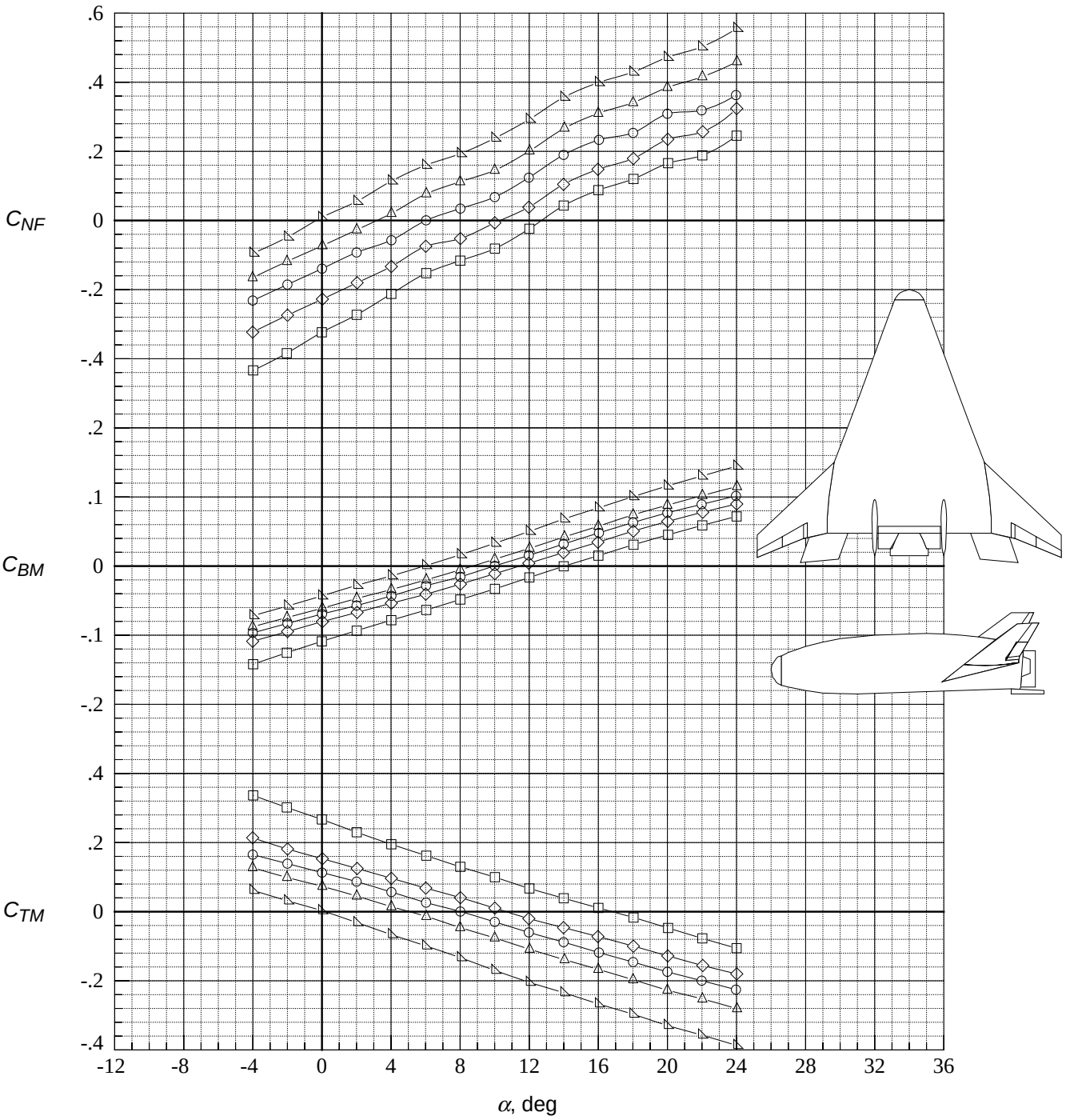

Figure 11. 2%-scale X-33 canted fin 3-component force and moment data.

Figure 12. Close-up photograph of pressure-instrumented nose cap for FADS calibration on a 2%-scale X-33 model in UPWT.

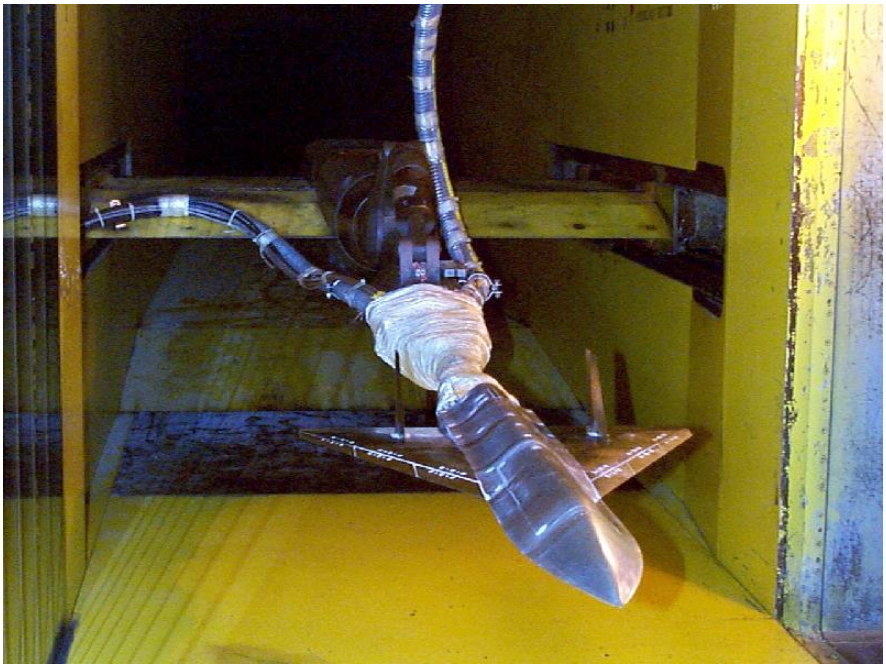

Figure 13. MTVI model configured for dedicated surface static pressure measurements in UPWT Test Section 1.

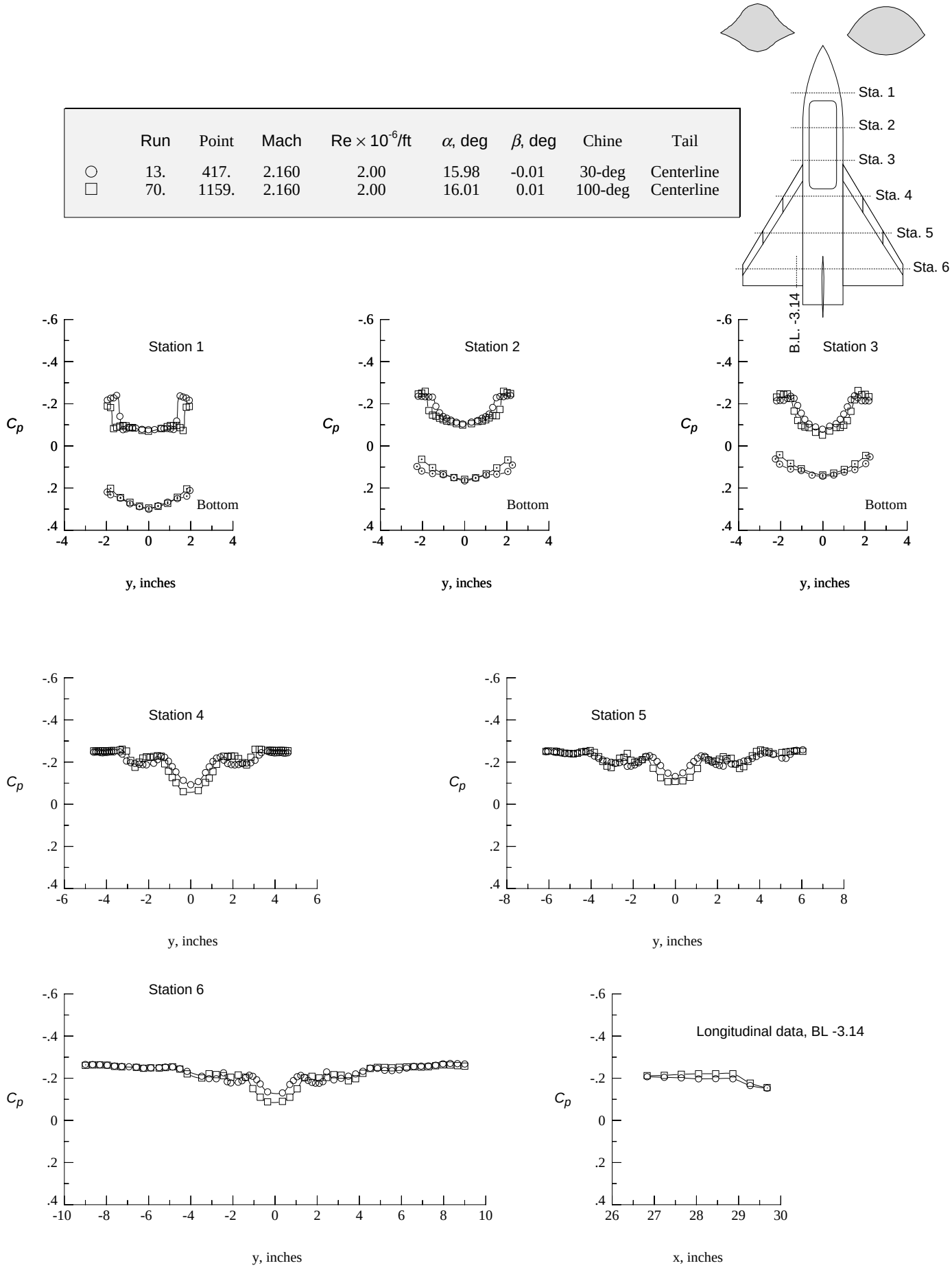

Figure 14. Forebody cross section effect on MTVI model pressure distributions at Mach = 1.80.

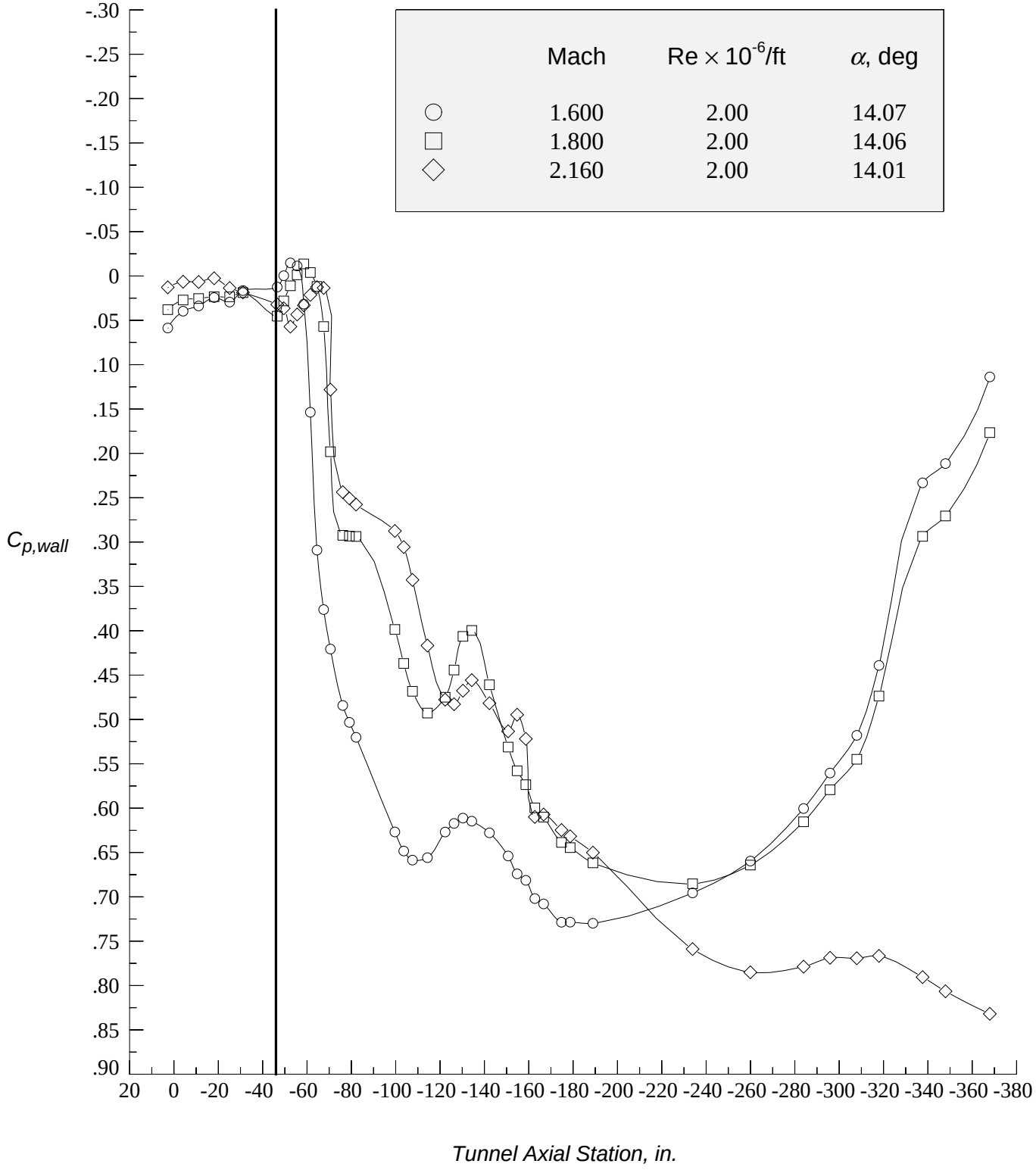

Figure 15. Mach number effect on UPWT Test Section 1 ceiling centerline static pressure distributions.

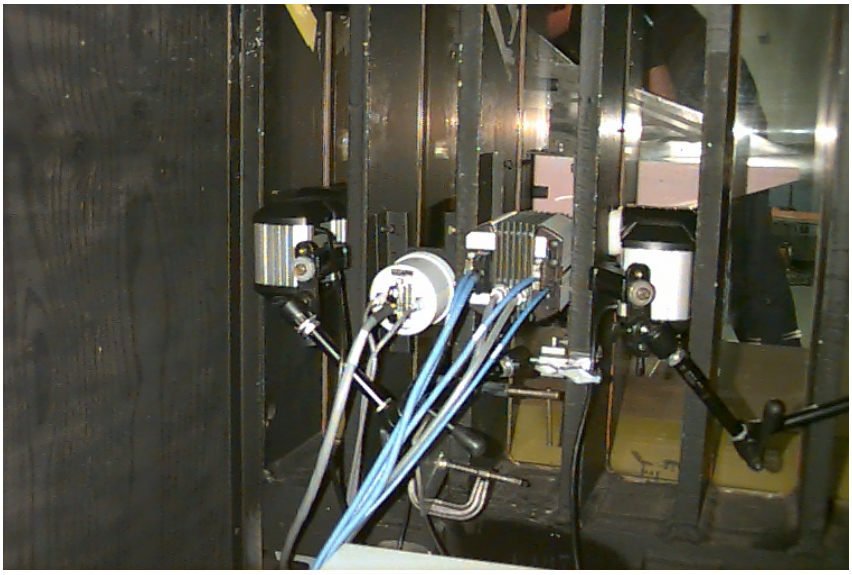

Figure 16. Installation of pressure-sensitive paint (PSP) cameras and ultraviolet (UV) lights at UPWT.

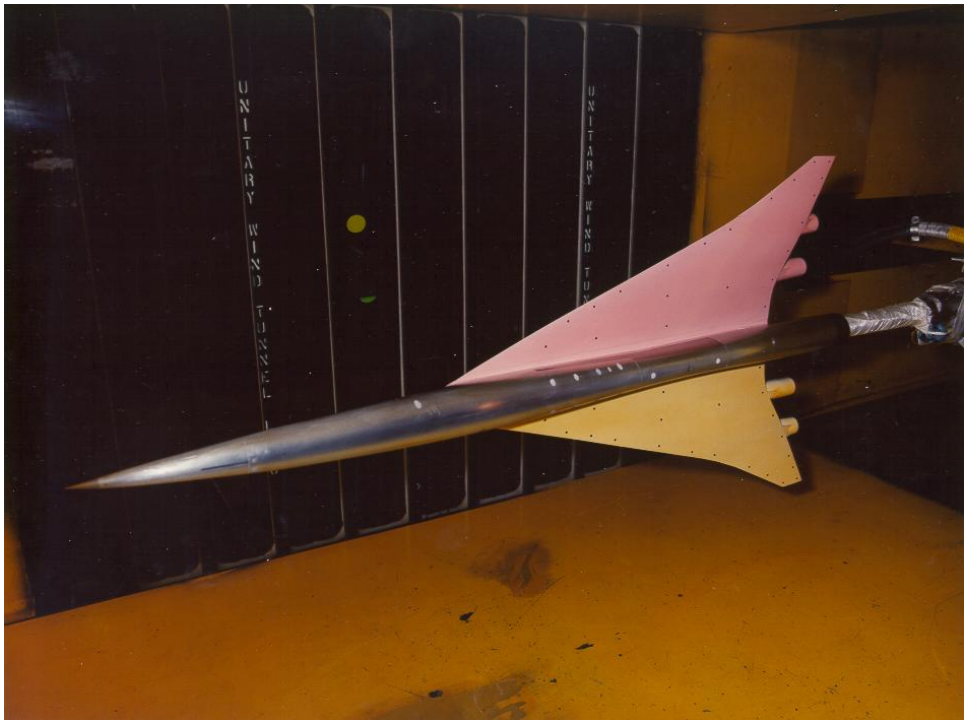

Figure 17. Arrow wing model installed in UPWT Test Section 1 with PSP (upper wing) and TSP (lower wing) coatings.

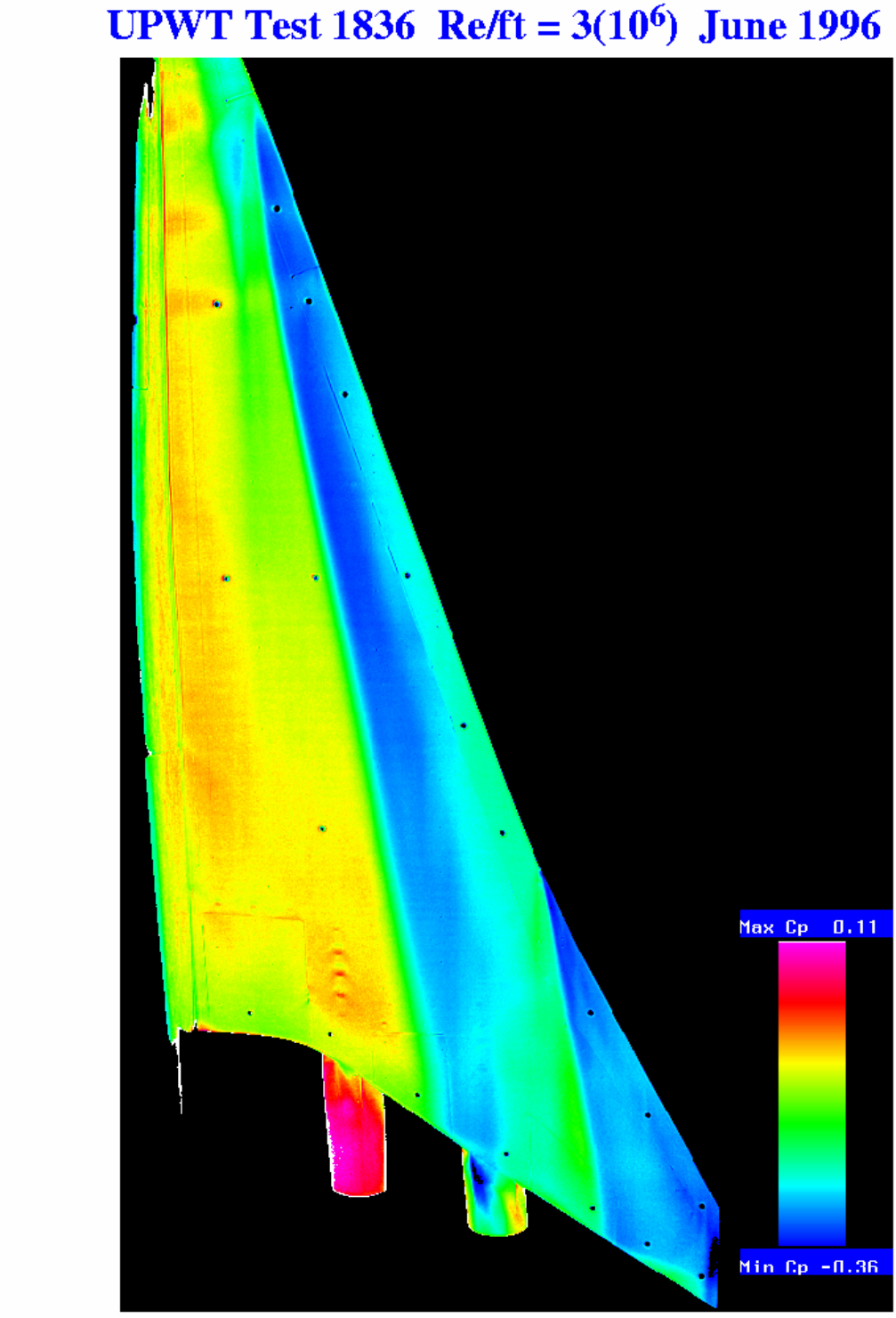

Figure 18. PSP image of arrow wing model in UPWT Test Section 1.

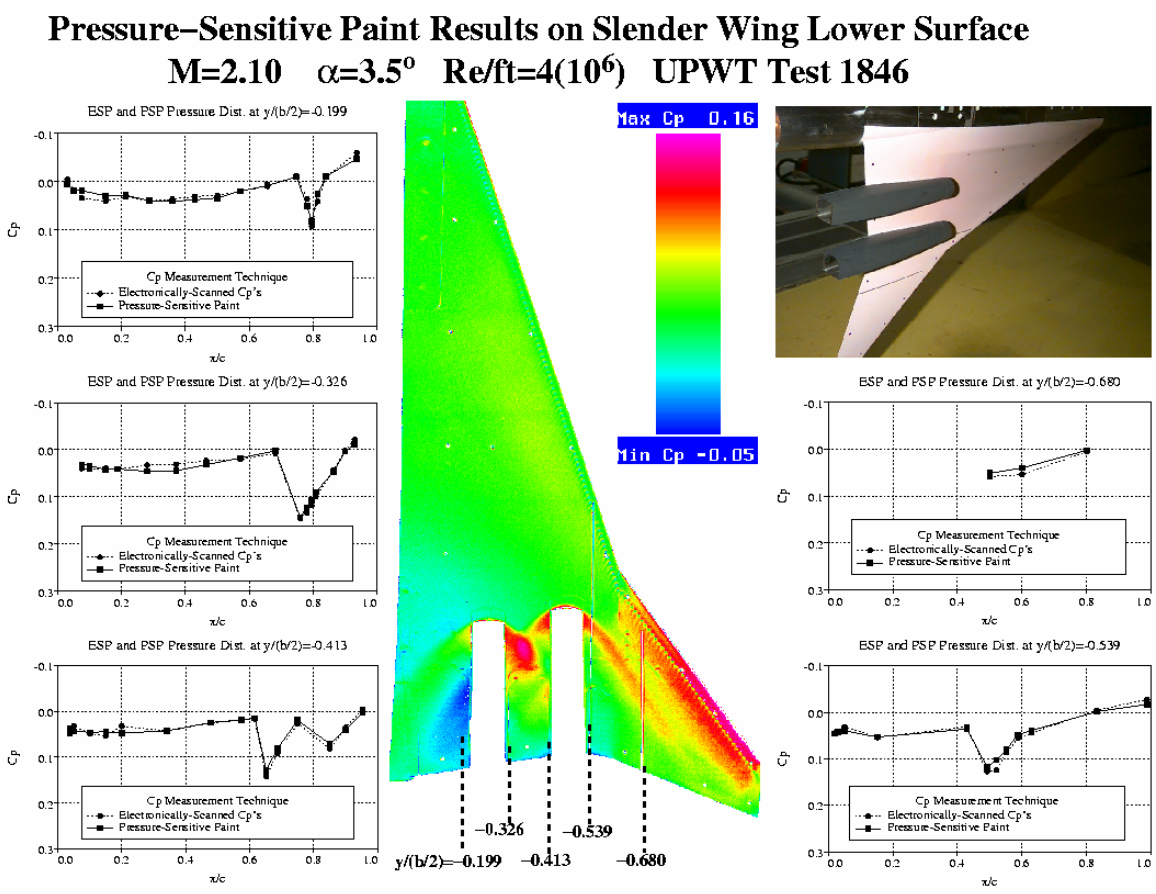

Figure 19. PSP results obtained on slender wing model in UPWT Test Section 1.

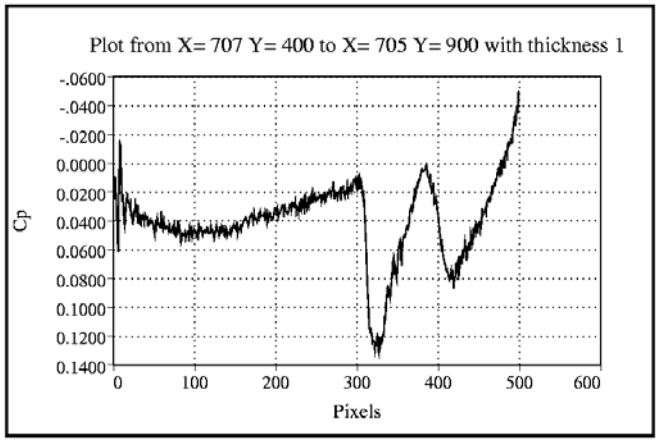

Figure 20. PSP pressure coefficients at all available pixels in a selected chordwise row between the engine nacelles from approximately the wing leading edge to the trailing edge.

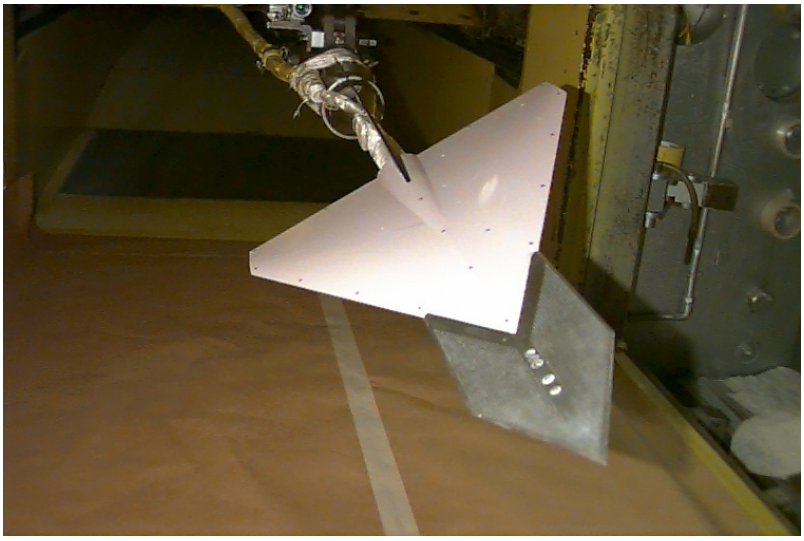

Figure 21. Cropped delta wing-LEX model installed in UPWT Test Section 1 with PSP coating on wing upper surface.

SOLID LEX **POROUS LEX**

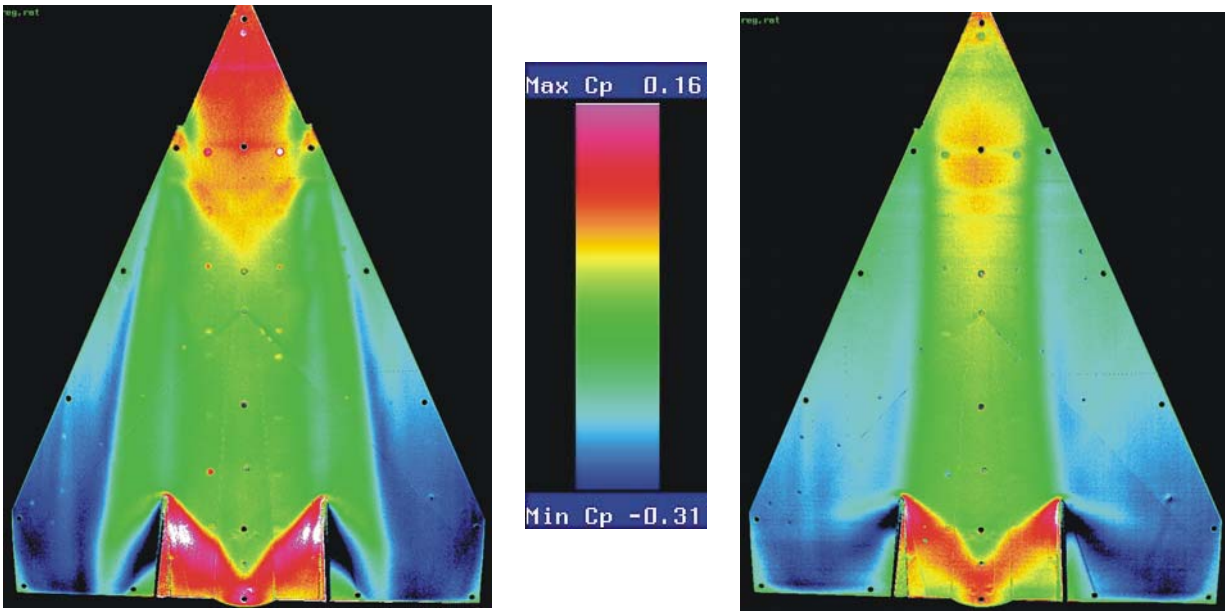

Figure 22. Effect of LEX porosity on PSP images at Mach = 1.6, α = 8 degrees with wing-mounted vertical fins.

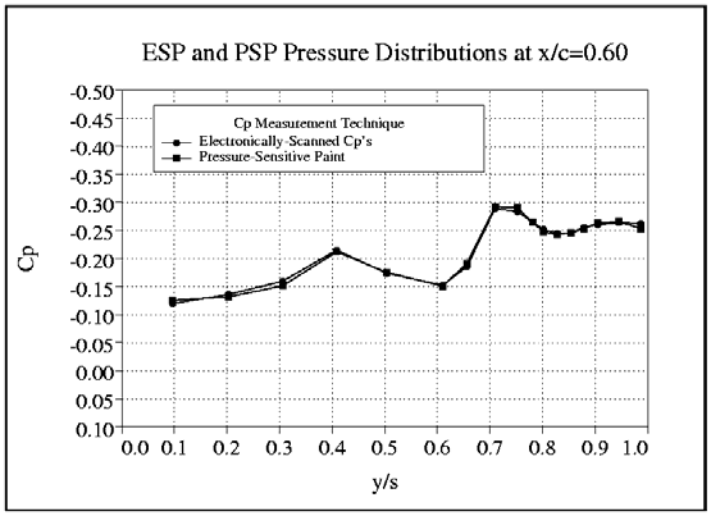

(a) Solid LEX

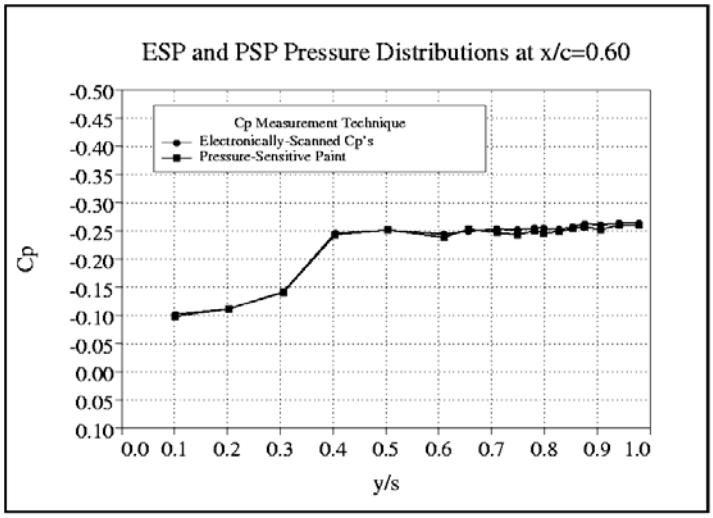

(b) Porous LEX

Figure 23. Comparison of PSP and ESP pressure distributions with solid LEX and porous LEX at Mach = 1.6 and α = 8 degrees.

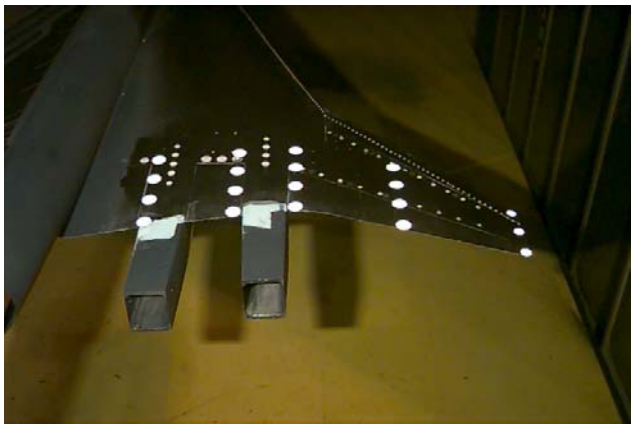

Figure 24. Retroreflective targets applied to the right wing of a supersonic transport model in UPWT Test Section 1.

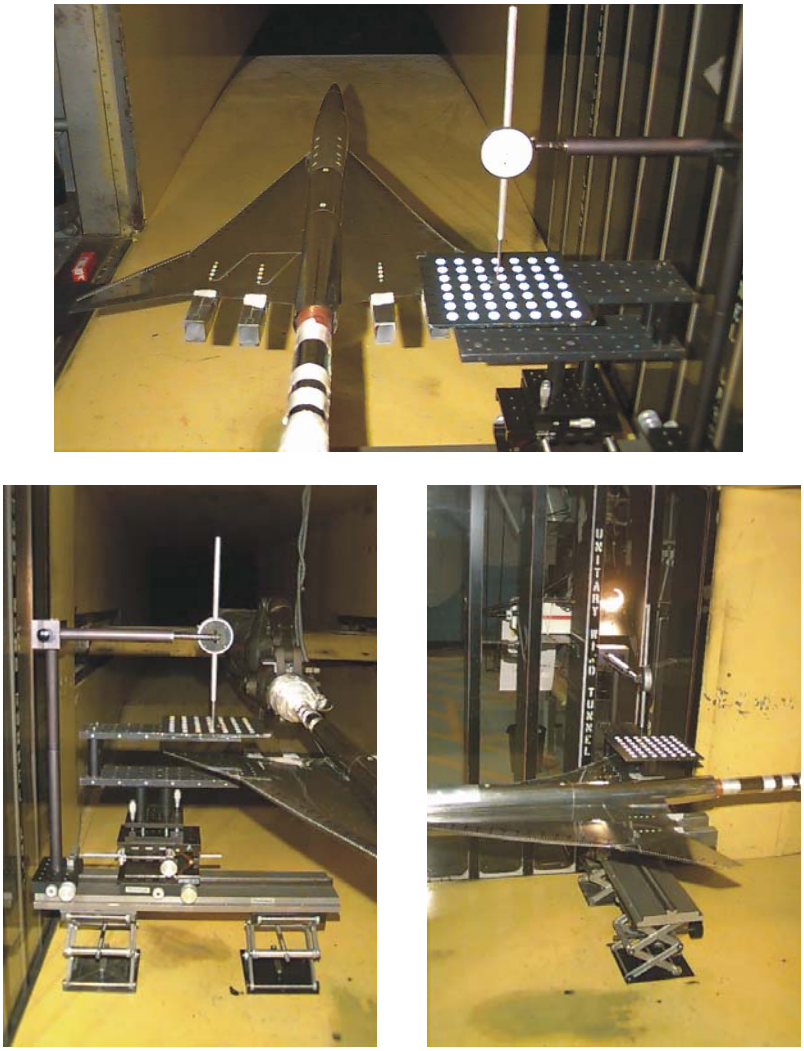

Figure 25. Video model deformation system calibration setup in UPWT Test Section 1.

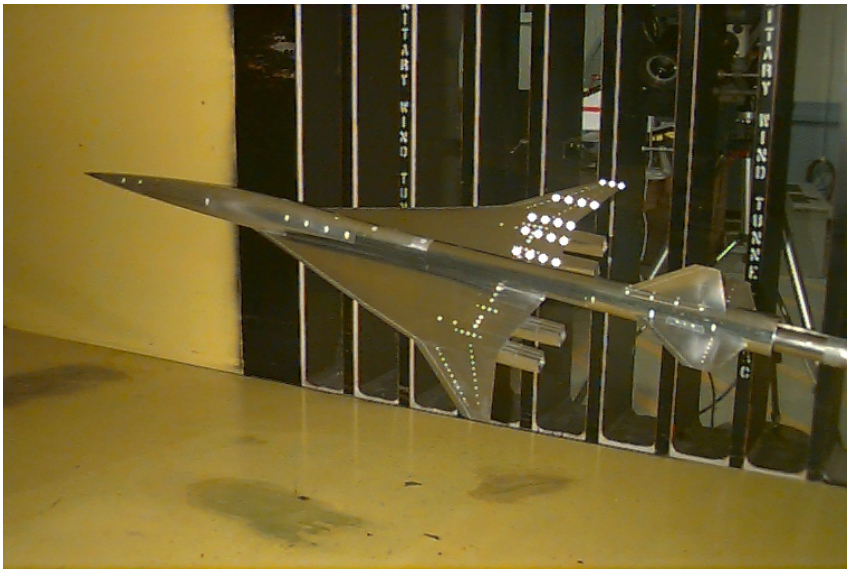

Figure 26. Supersonic transport model installed in UPWT Test Section 1 for wing deformation measurements.

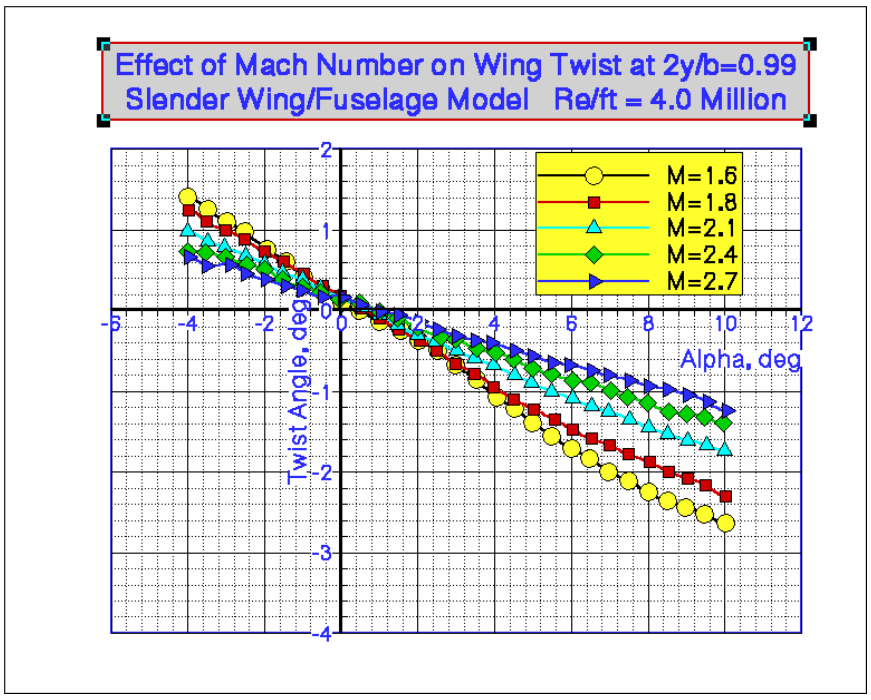

(a) Mach number effect

Figure 27. Mach number and Reynolds number effects on wing twist at $\eta = 0.99$ (wing tip target row).

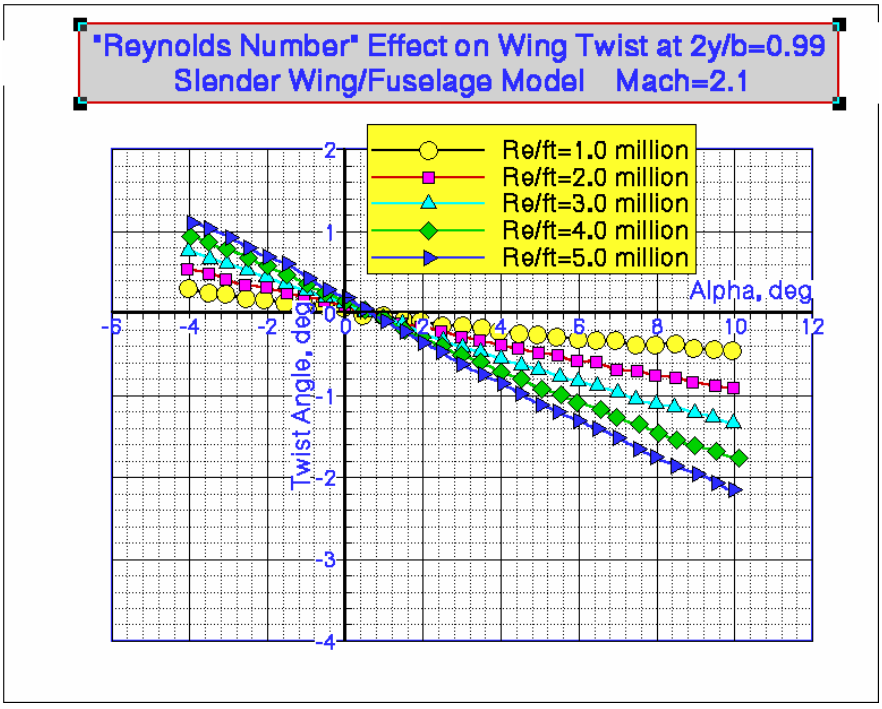

(b) Reynolds number effect.

Figure 27. Concluded.

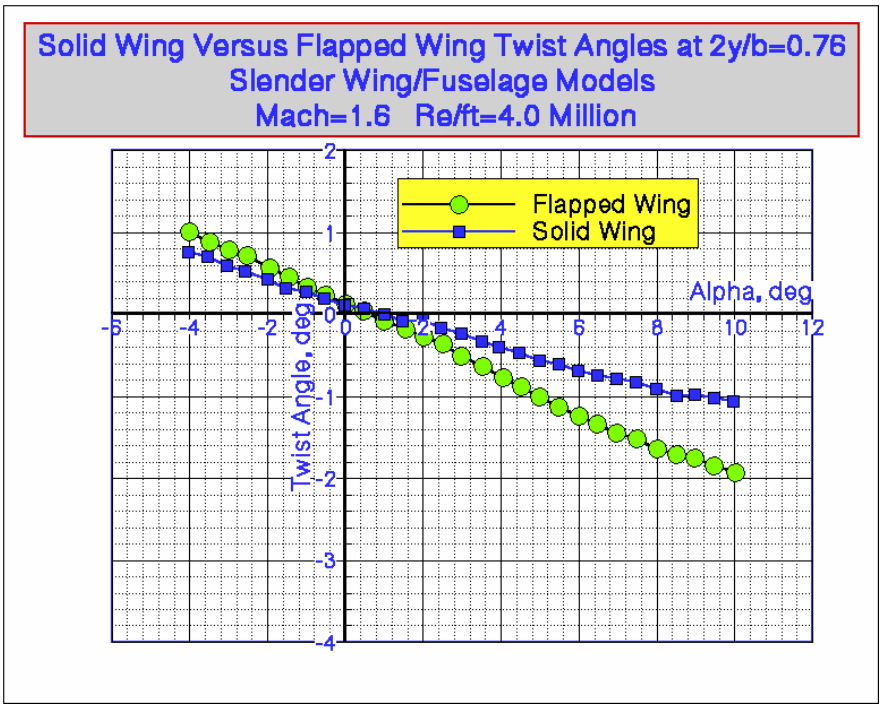

Figure 28. Comparison of solid and flapped wing twist at Mach = 2.1 and η = 0.76.

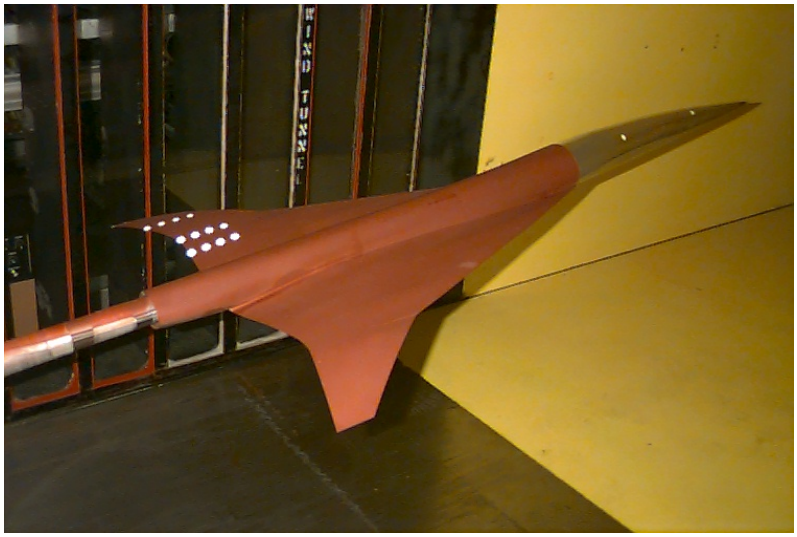

Figure 29. Wind tunnel model installed in UPWT Test Section 2 for test techniques unification experiment.

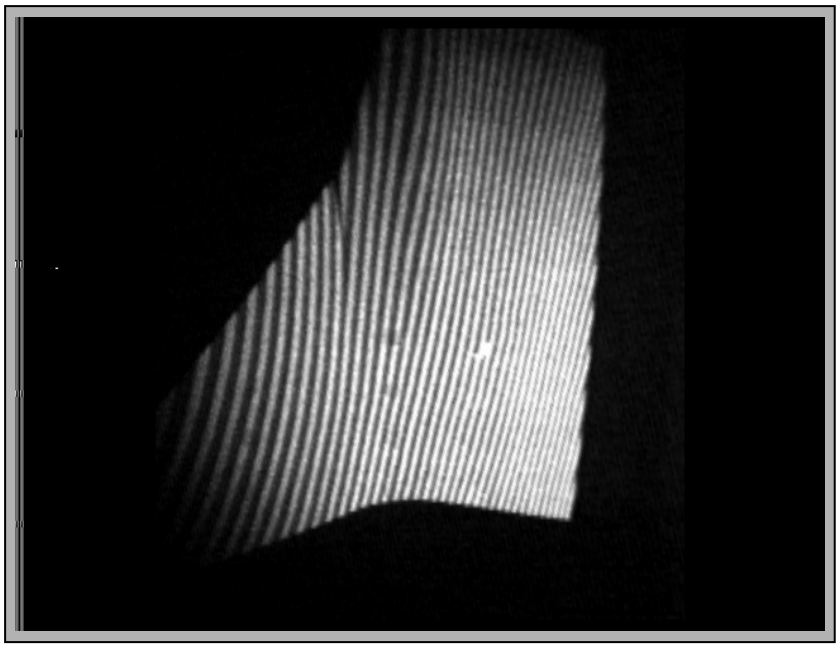

Figure 30. PMI projected grid lines on the left-hand wing upper surface.

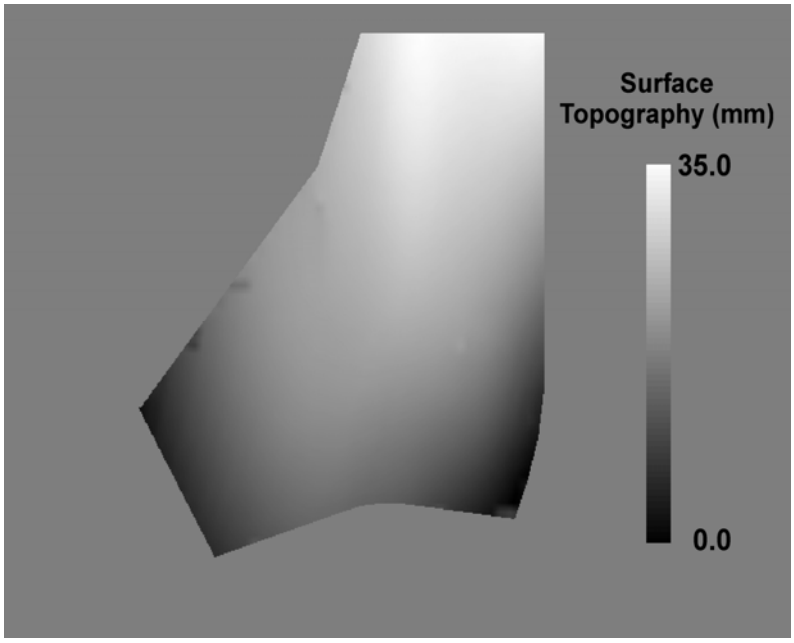

Figure 31. Finalized PMI image showing surface deformation topography.

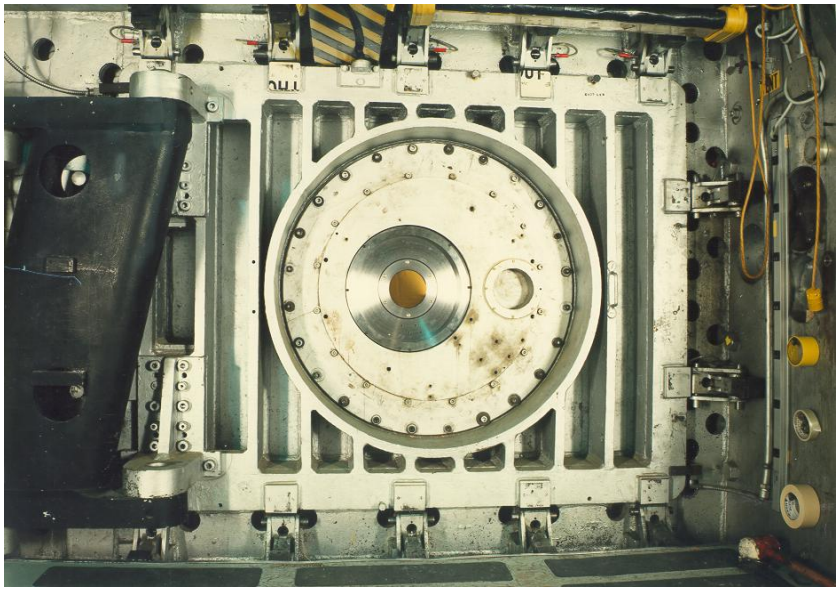

Figure 32. IR window installed in UPWT alternate test section door.

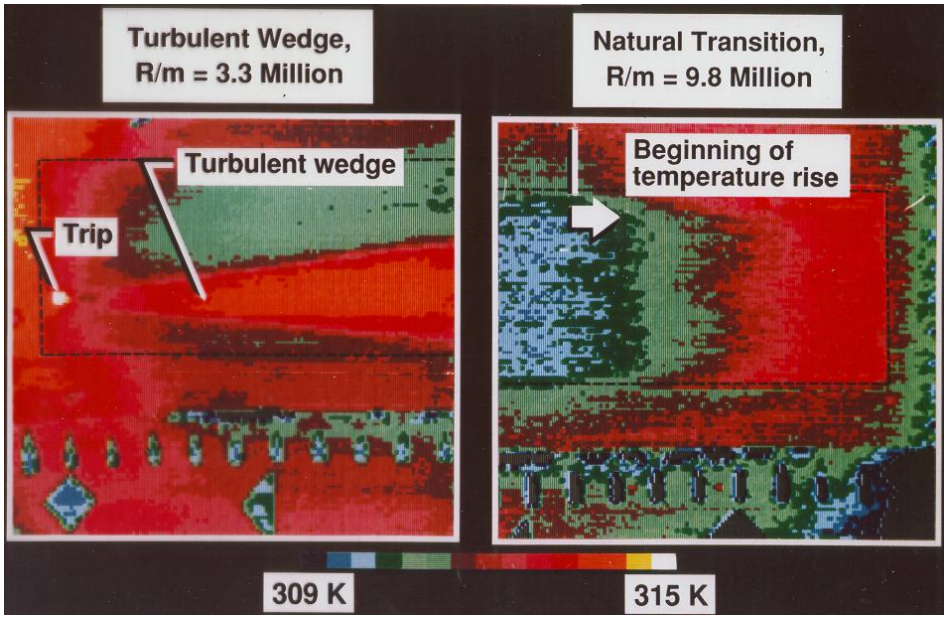

Figure 33. Examples of infrared imaging in UPWT Test Section 1.

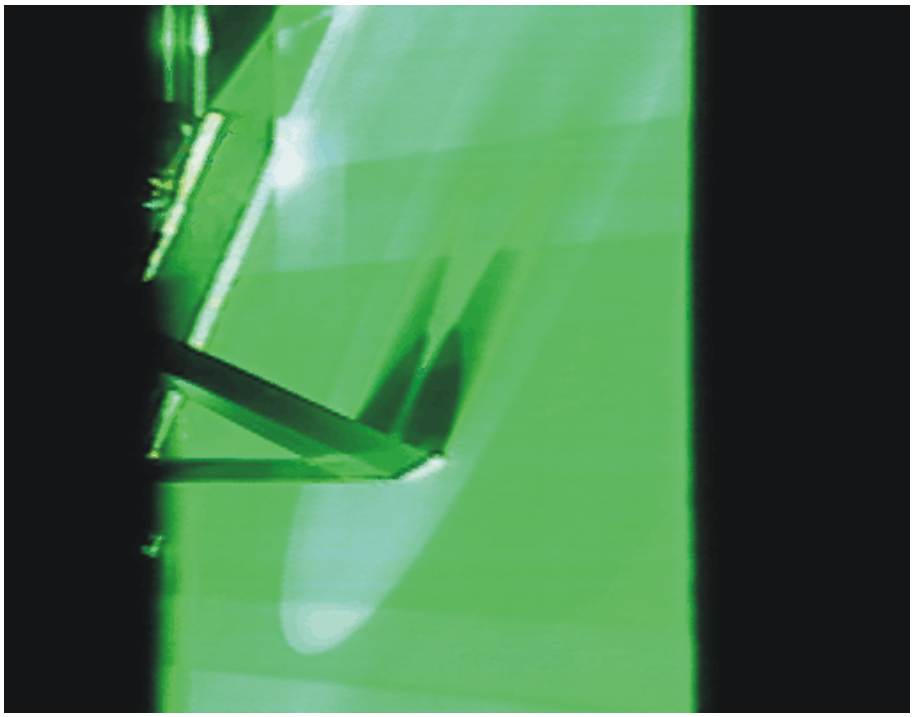

Figure 34. DGV laser light illumination of a delta wing cross flow in UPWT Test Section 2 at Mach = 2.8 and α = 28 degrees.

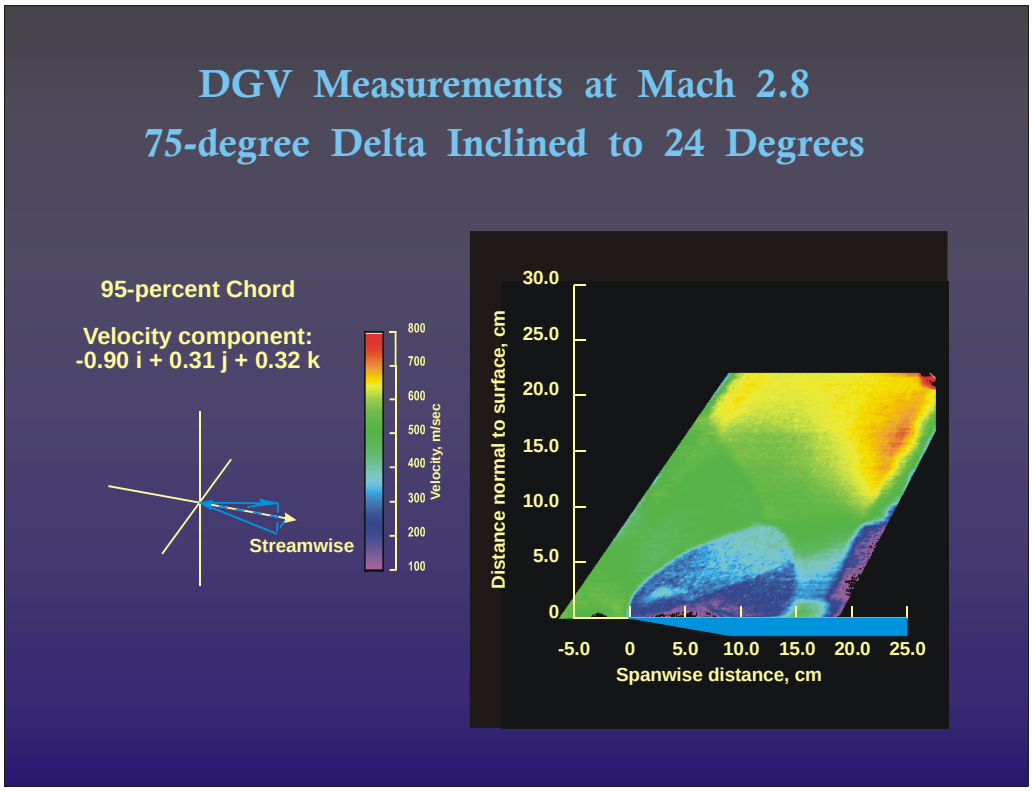

Figure 35. DGV velocity measurements in the delta wing flow field.

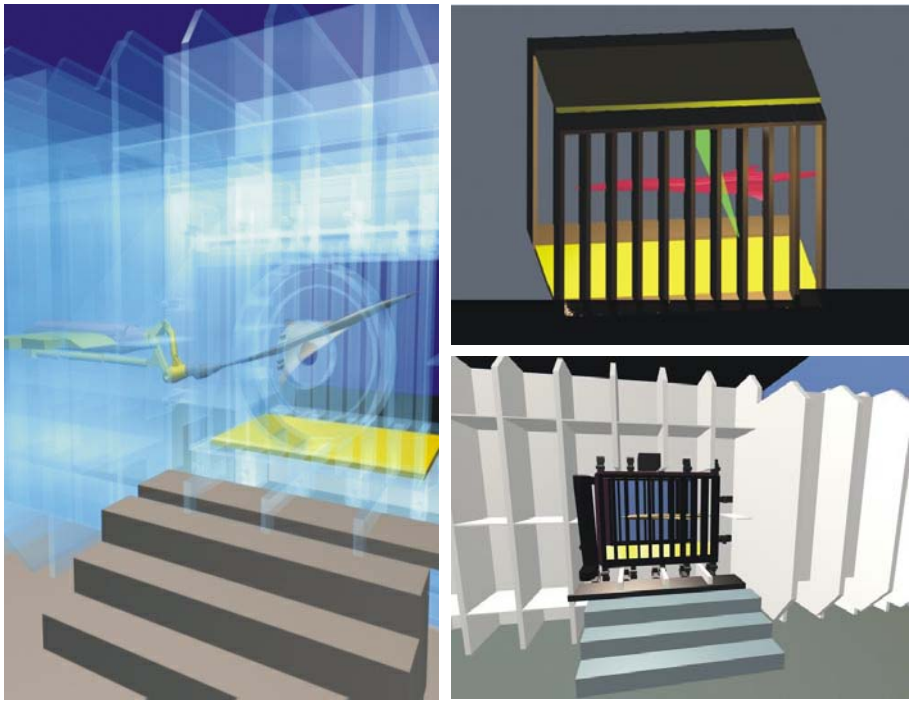

Figure 36. Virtual Facilities modeling of the UPWT testing environment.

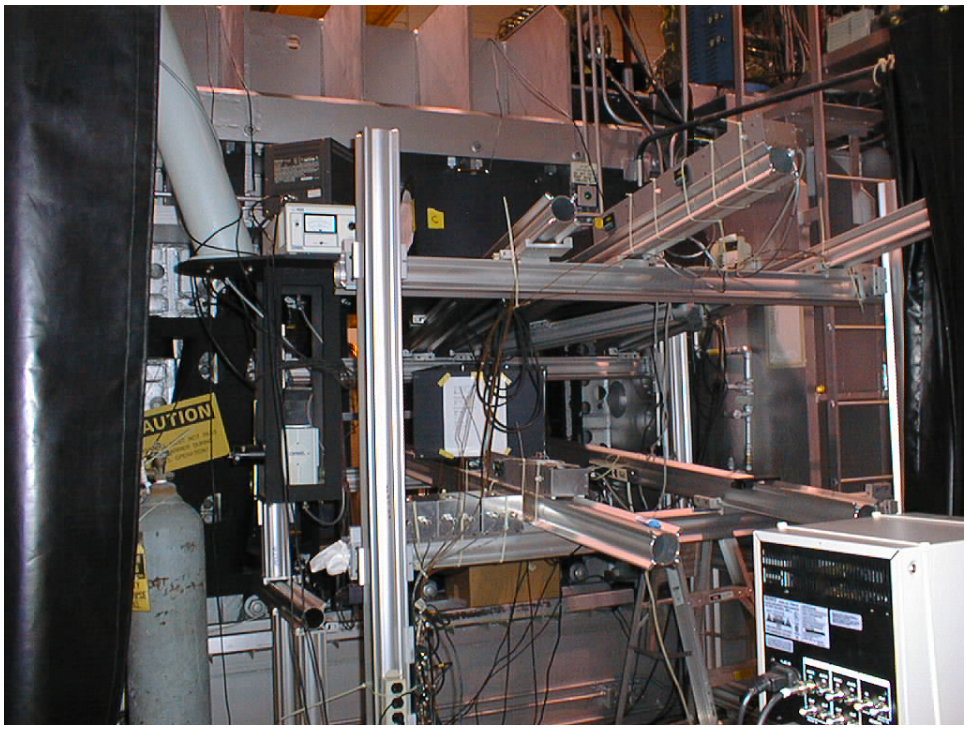

Figure 37. Setup of DGV system at UPWT based on Virtual Facilities analysis.

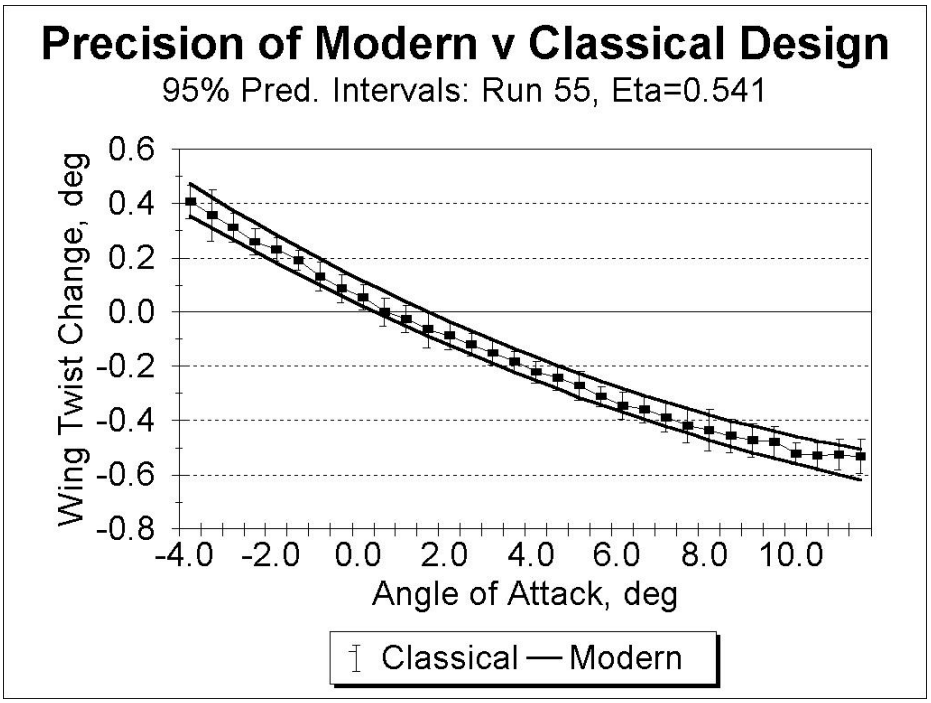

Figure 38. Wing twist obtained in OFAT and MDOE testing.

Figure 39. Close-up view of an arrow wing model with PSP coating (the leading-edge region is buffed for boundary layer transition trip dot application).

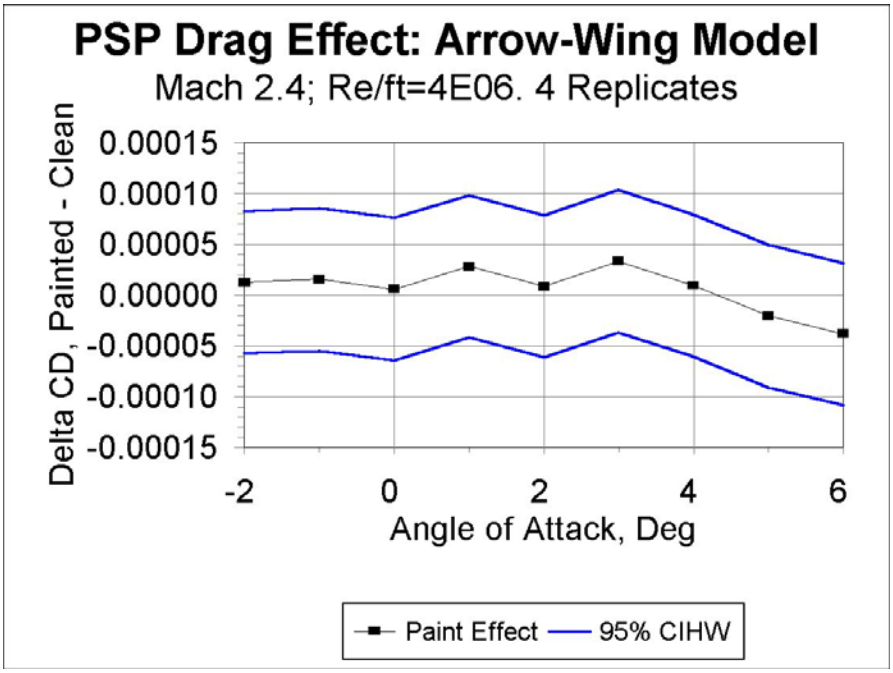

Figure 40. PSP effects on drag coefficient using MDOE design with four replicates.

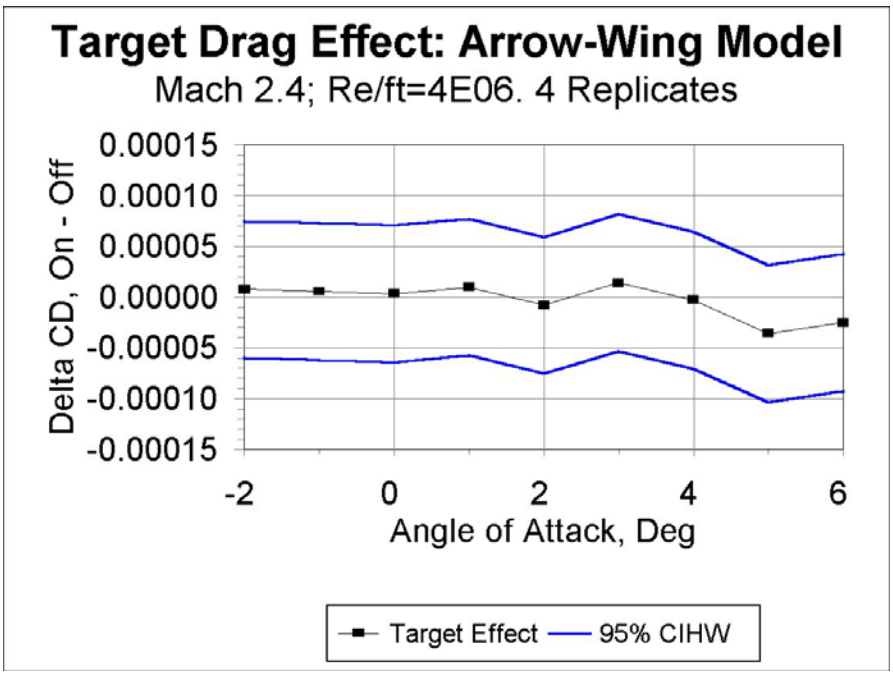

Figure 41. VMD target effects on drag coefficient using MDOE design with four replicates.

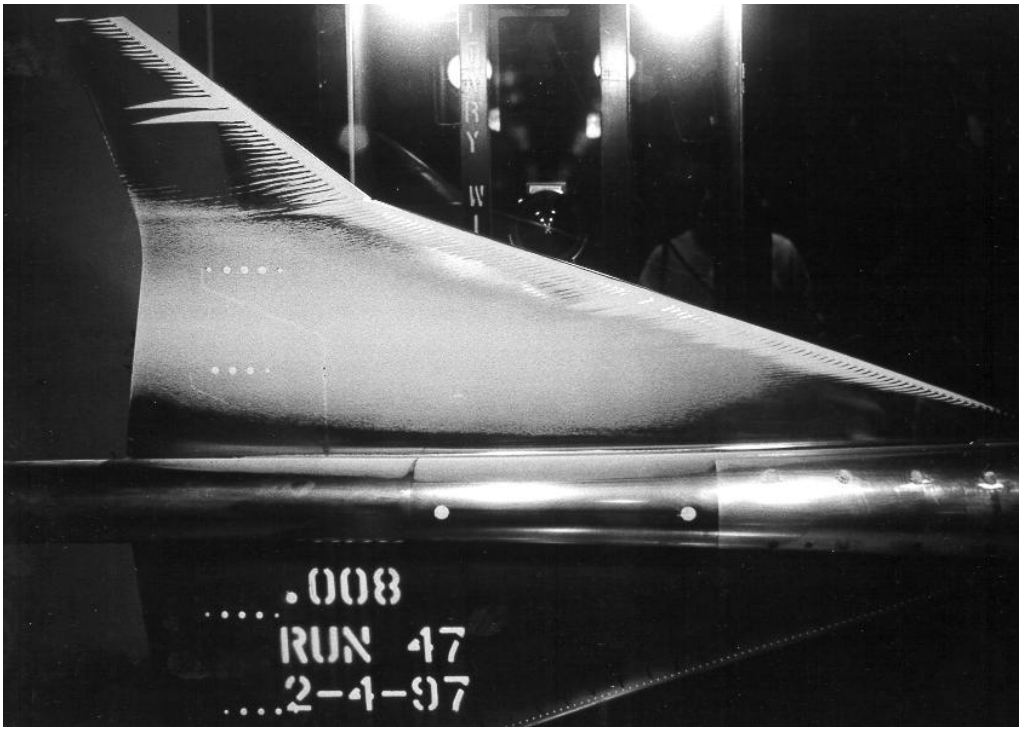

Figure 42. Surface sublimation pattern on a slender wing at Mach = 2.4 in UPWT Test Section 2.

Figure 43. UV oil pattern on a slender wing model at Mach = 2.4 and α = 4.5 degrees in UPWT Test Section 2.

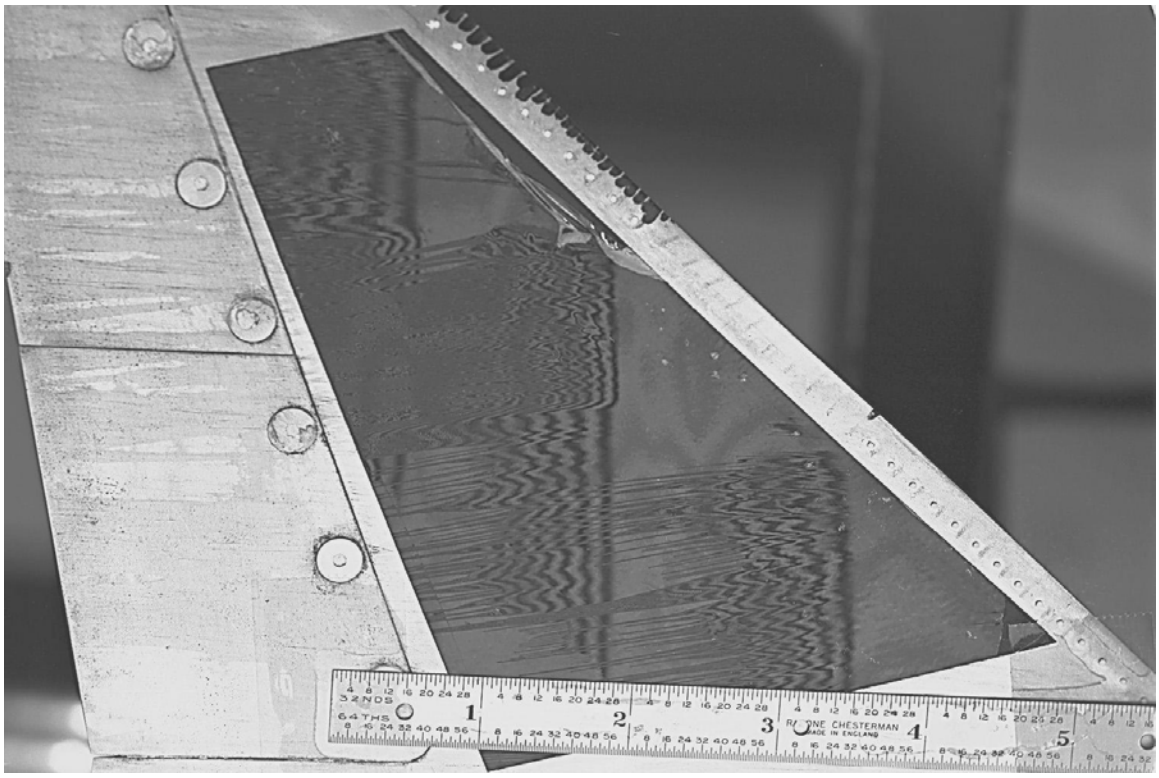

Figure 44. Oil film interferometry image at Mach = 2.4 in UPWT Test Section 2.

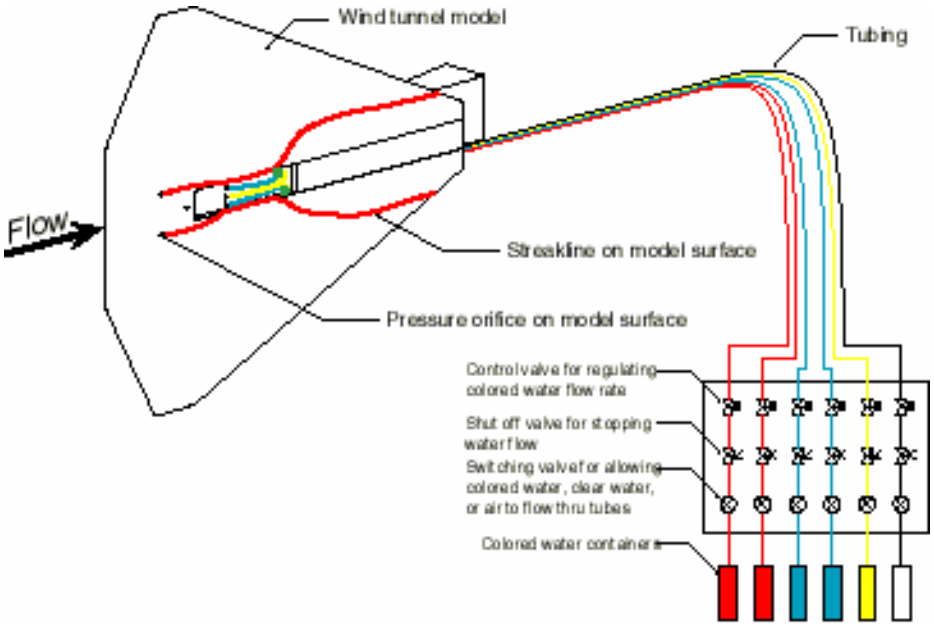

Figure 45. Sketch of colored water injection system at UPWT.

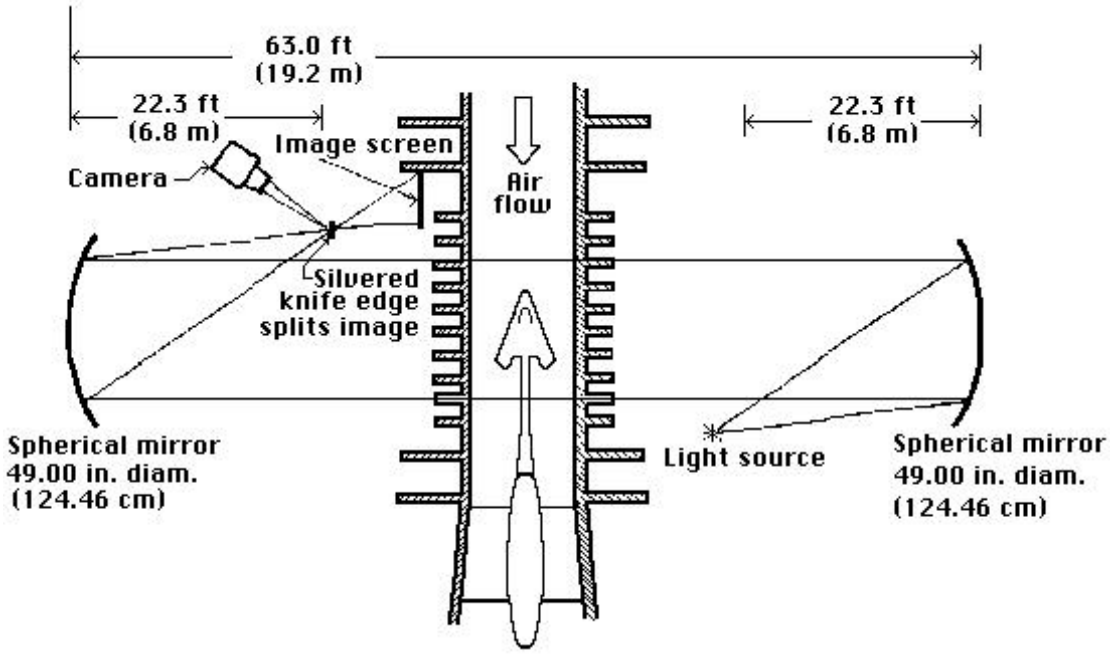

Figure 46. Sketch of the UPWT schlieren system.

(a) Mach = 2.16, α = 0 degrees.

Figure 47. Schlieren flow visualization images on a 2%-scale X-33 model in UPWT Test Section 2.

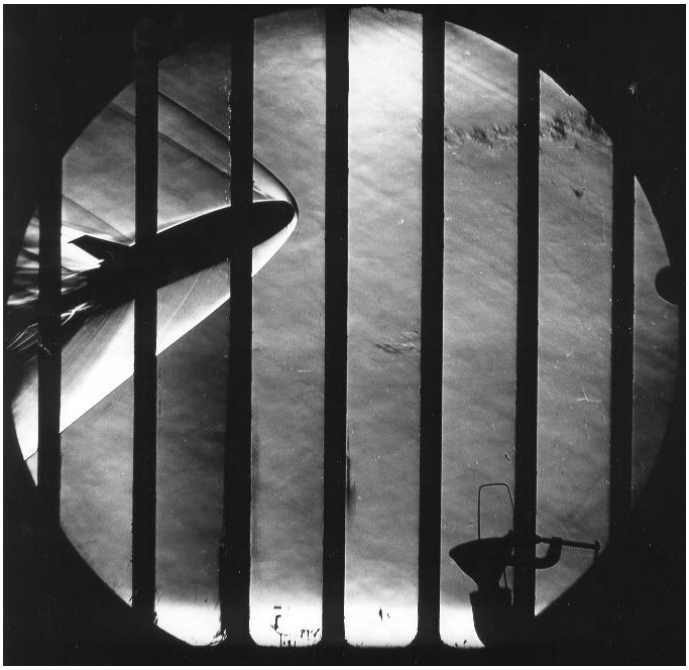

(b) Mach = 2.16, α = 24 degrees.

Figure 47. Concluded.

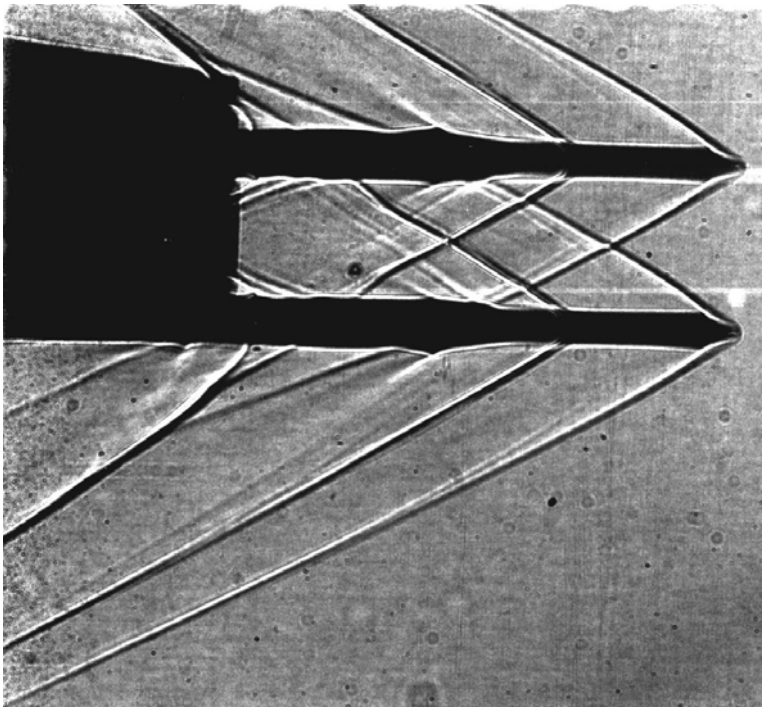

Figure 48. Shadowgraph image of cone probe device in UPWT Test Section 2.

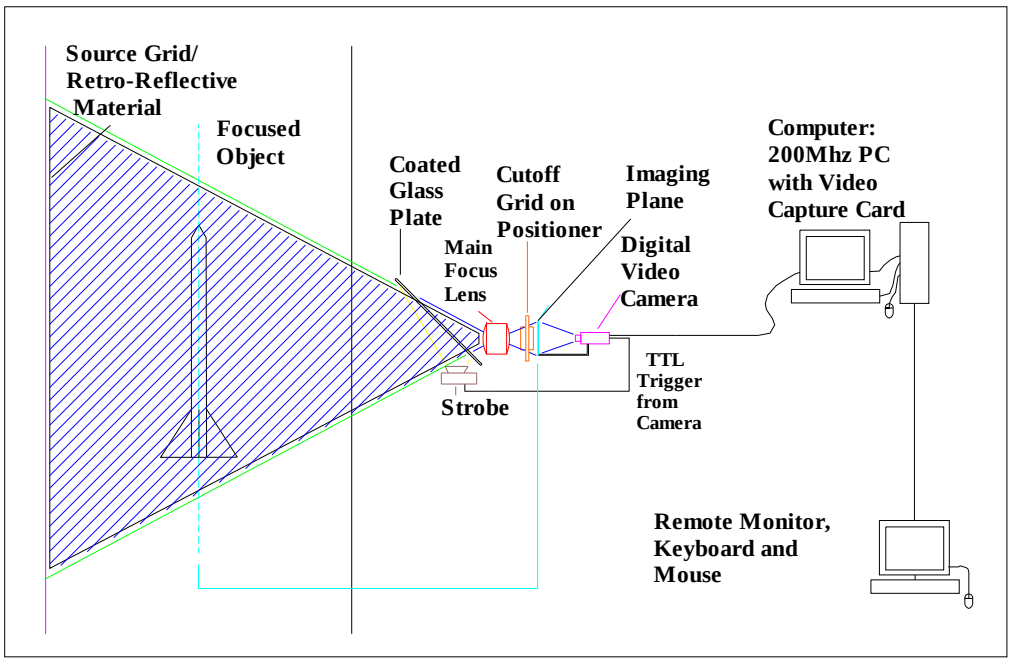

Figure 49. Sketch of focusing schlieren system for UPWT Test Section 1.

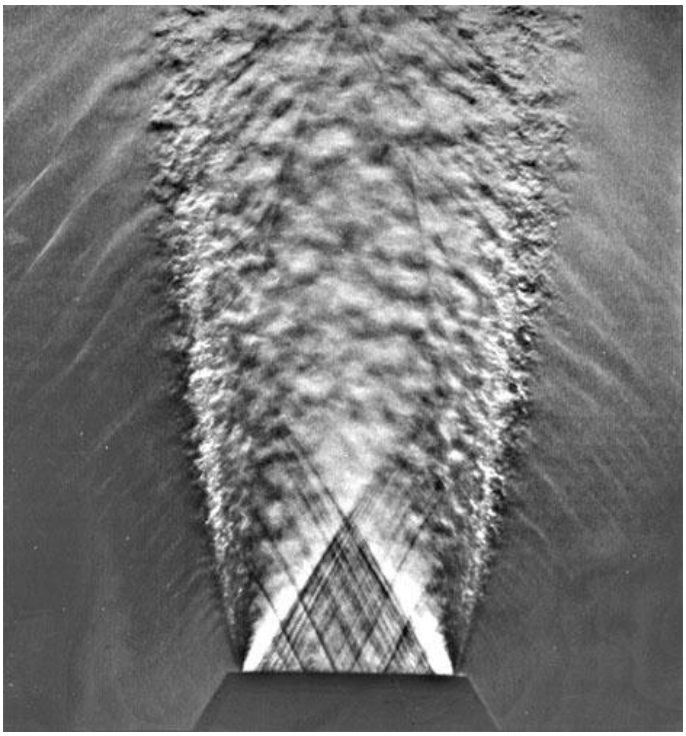

Figure 50. Focusing schlieren visualization of jet exhaust flow (reference 55).

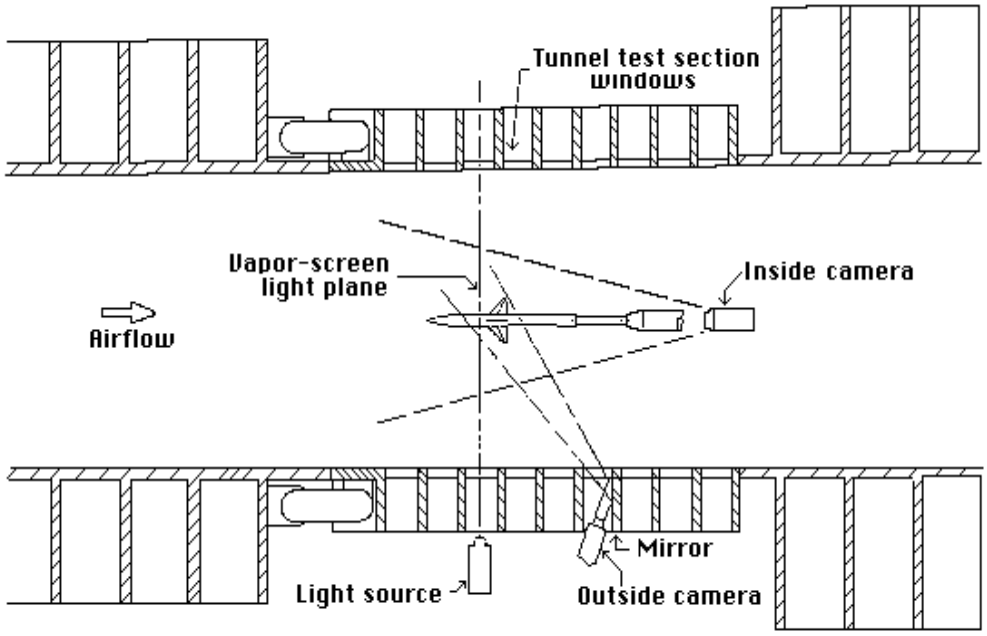

Figure 51. Sketch of UPWT vapor screen setup.

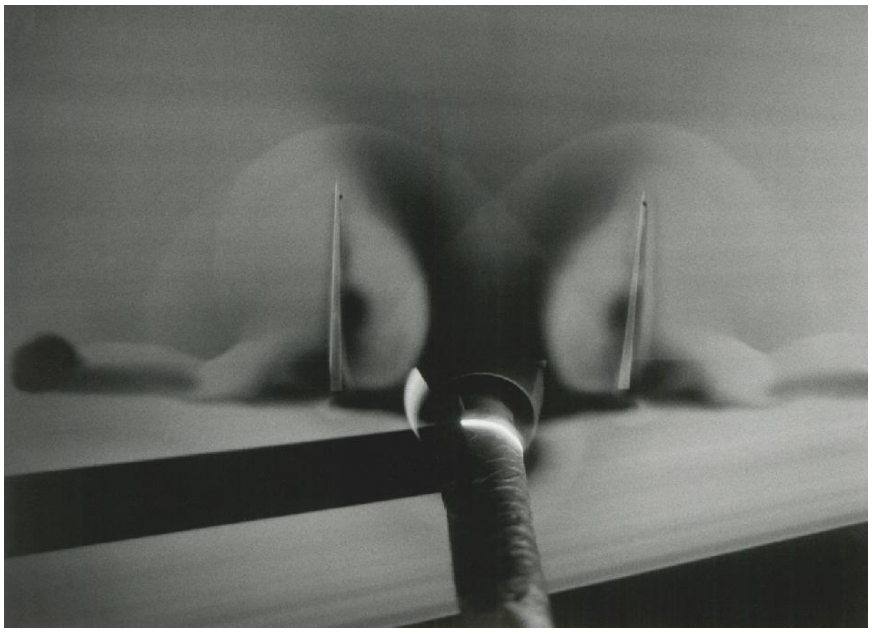

(a) 65-degree cropped delta wing with LEX and twin vertical fins at Mach = 1.6 and $\alpha = 12^{o}$.

Figure 52. Laser vapor screen flow visualization images from UPWT Test Section 1.

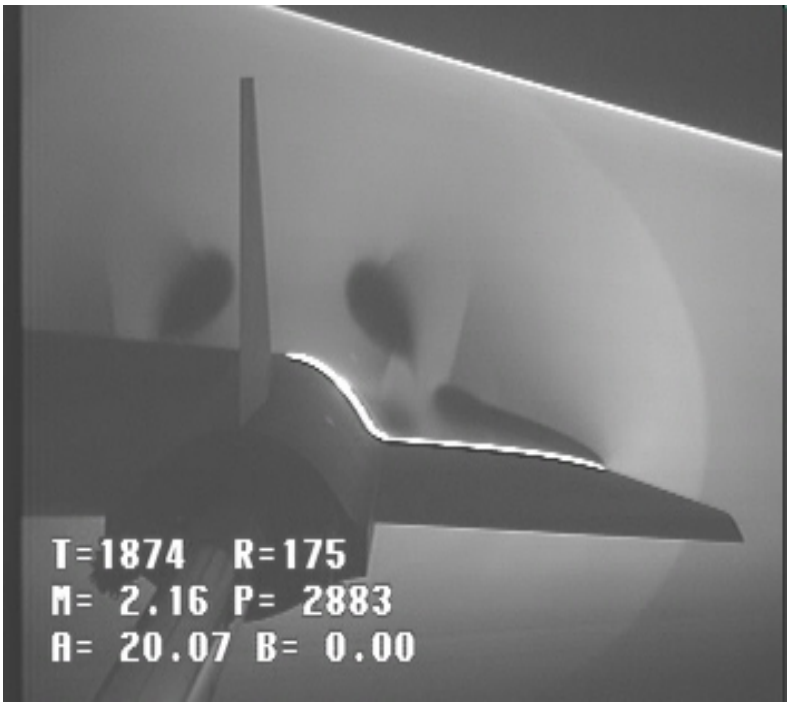

(b) Forebody and wing vortex flows on MTVI model at Mach = 2.16 and $\alpha = 20^{o}$.

Figure 52. Concluded.

Figure 53. Still and video camera installation for vapor screen flow visualization in UPWT Test Section 1.

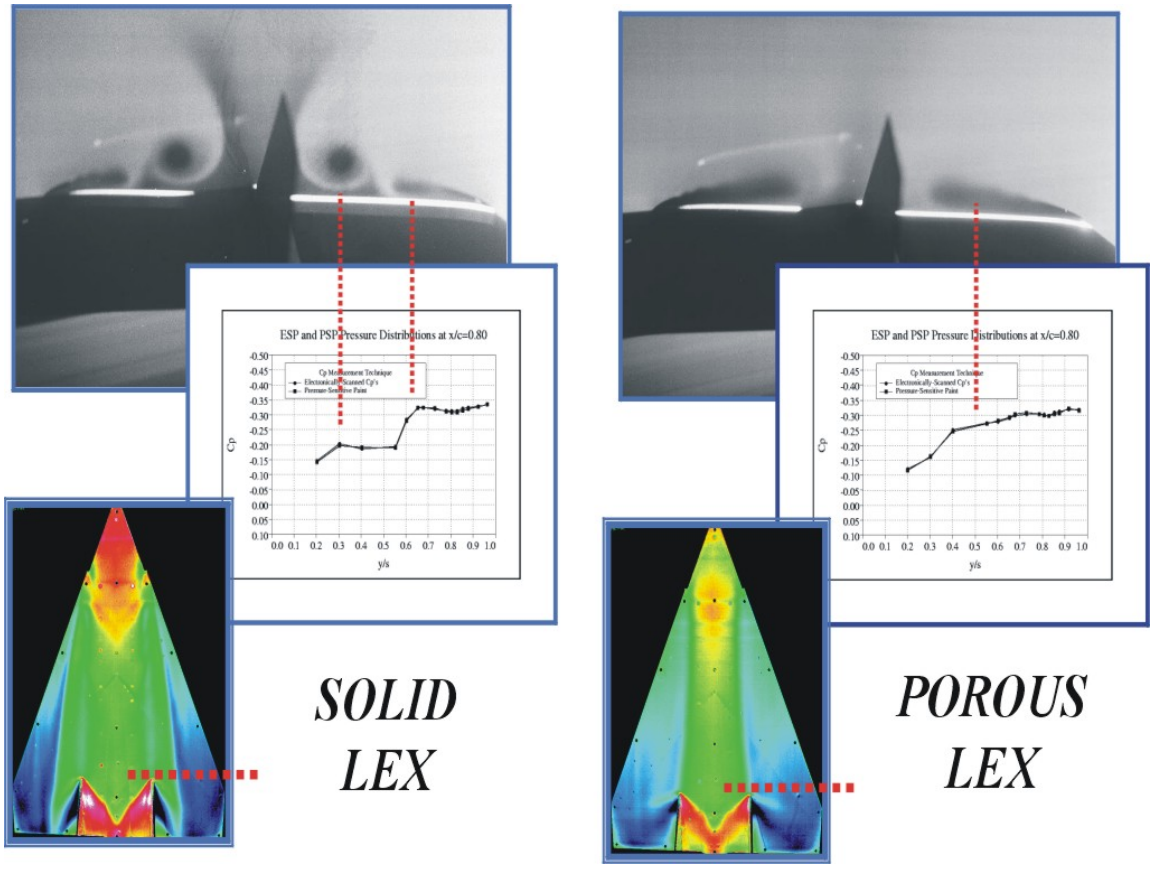

Figure 54. Correlation of LEX porosity effect in laser vapor screen images with wing surface static pressure distribution trends at Mach = 1.6 and $\alpha = 8^{o}$ in UPWT Test Section 1.

Figure 55. Generic missile model with instrumented fins in UPWT Test Section 2.

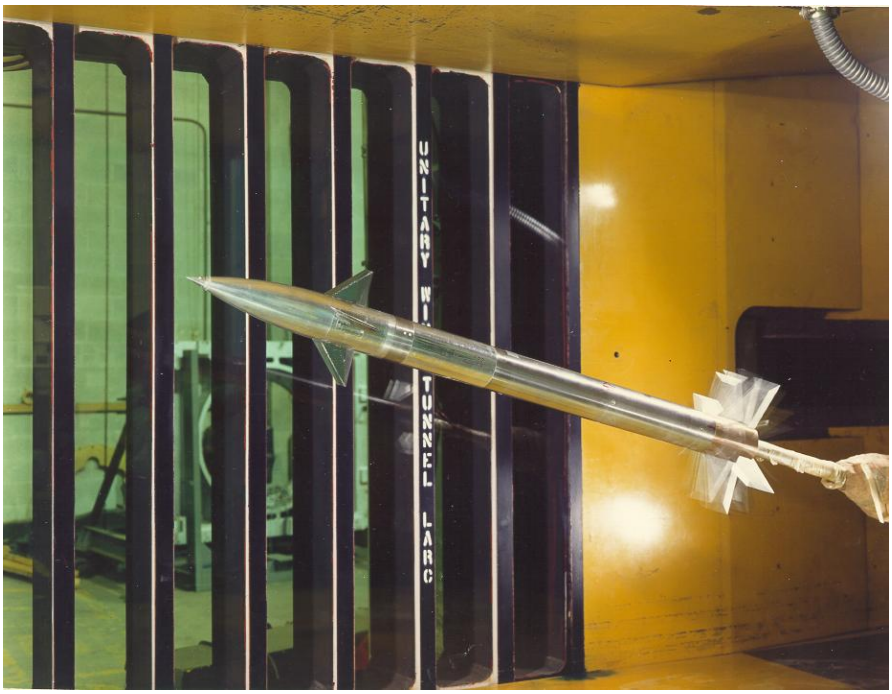

Figure 56. Generic missile model with rolling tail aftbody in UPWT Test Section 1.

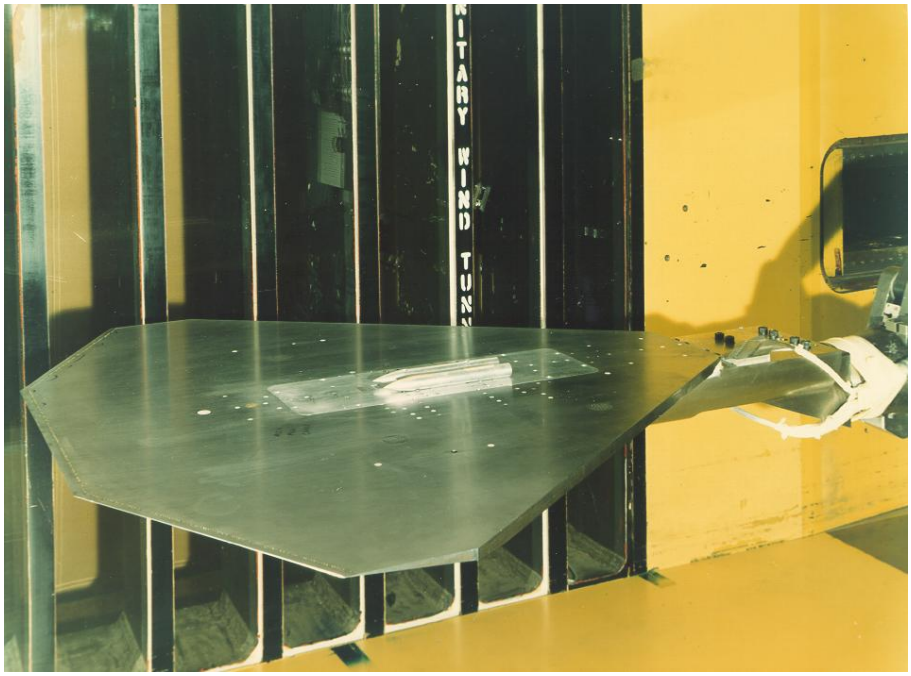

Figure 57. Flat-plate store carriage drag model installed in UPWT Test Section 1.

Figure 58. Flutter panel fixture mounted to the side wall in UPWT Test Section 1 (view looking downstream).

Figure 59. Sonic boom pressure measurement setup in UPWT Test Section 1.

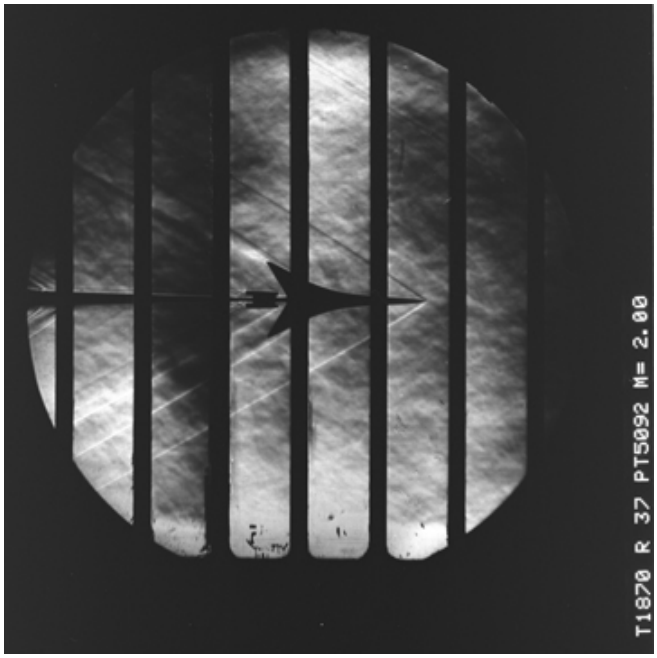

Figure 60. Sonic boom model shock wave image in UPWT Test Section 1 at Mach = 2.0.

Figure 61. 2.5%-scale X-33 model installed on the NASA LaRC dynamic stability system in UPWT Test Section 1.

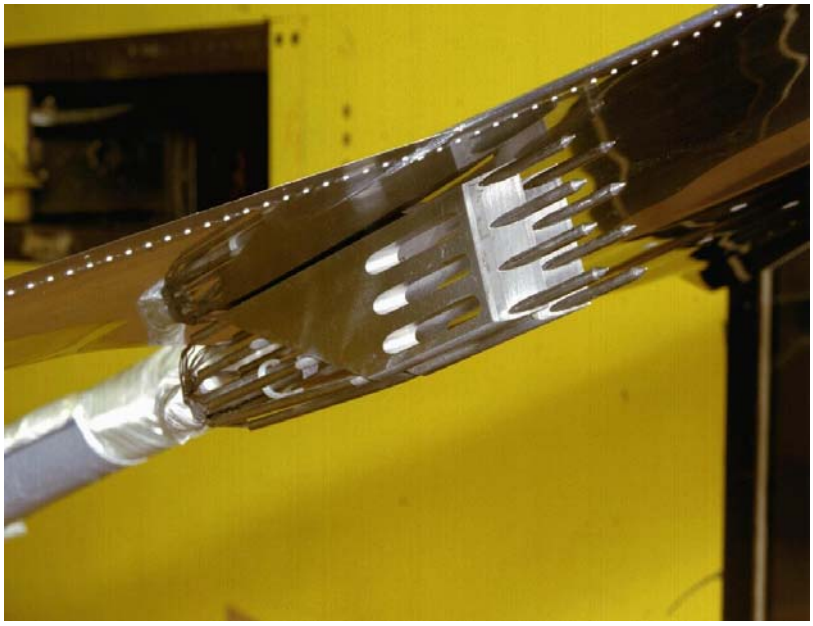

Figure 62. Close-up image of inlet survey rake installed on the lower surface of a slender wing-fuselage model in UPWT Test Section 2.

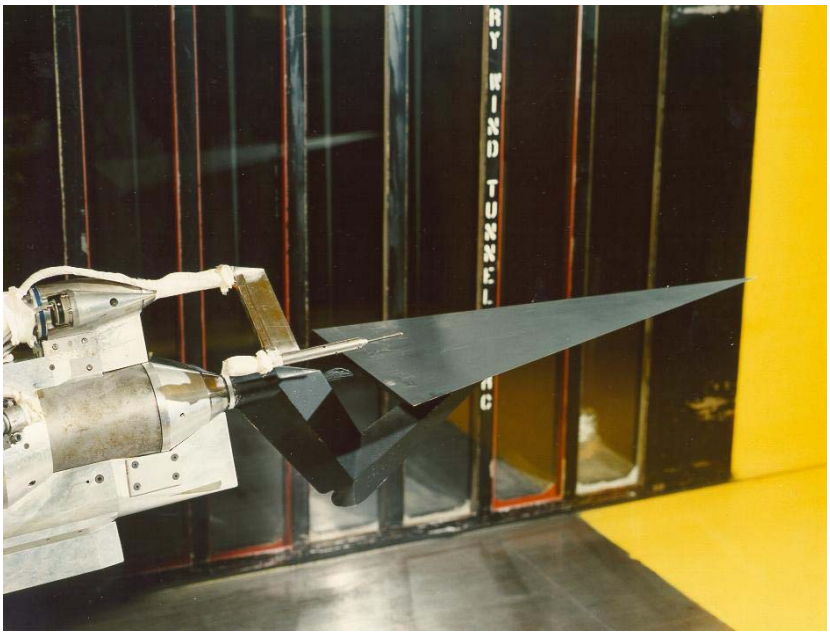

Figure 63. 75-degree delta wing with flow field survey apparatus in UPWT Test Section 2.

Figure 64. Supersonic transport model with flow field survey apparatus in UPWT Test Section 1.

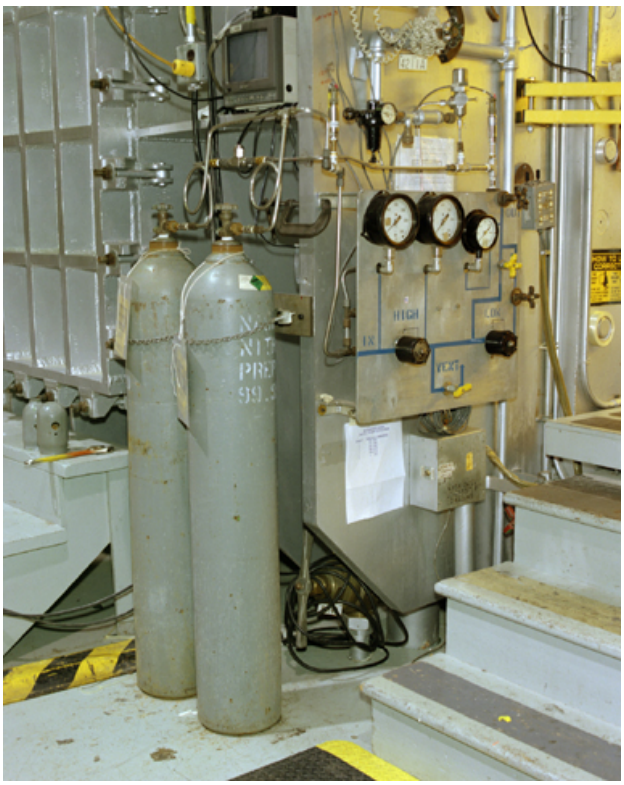

Figure 65. UPWT nitrogen gas delivery system for reaction control system (RCS) testing.

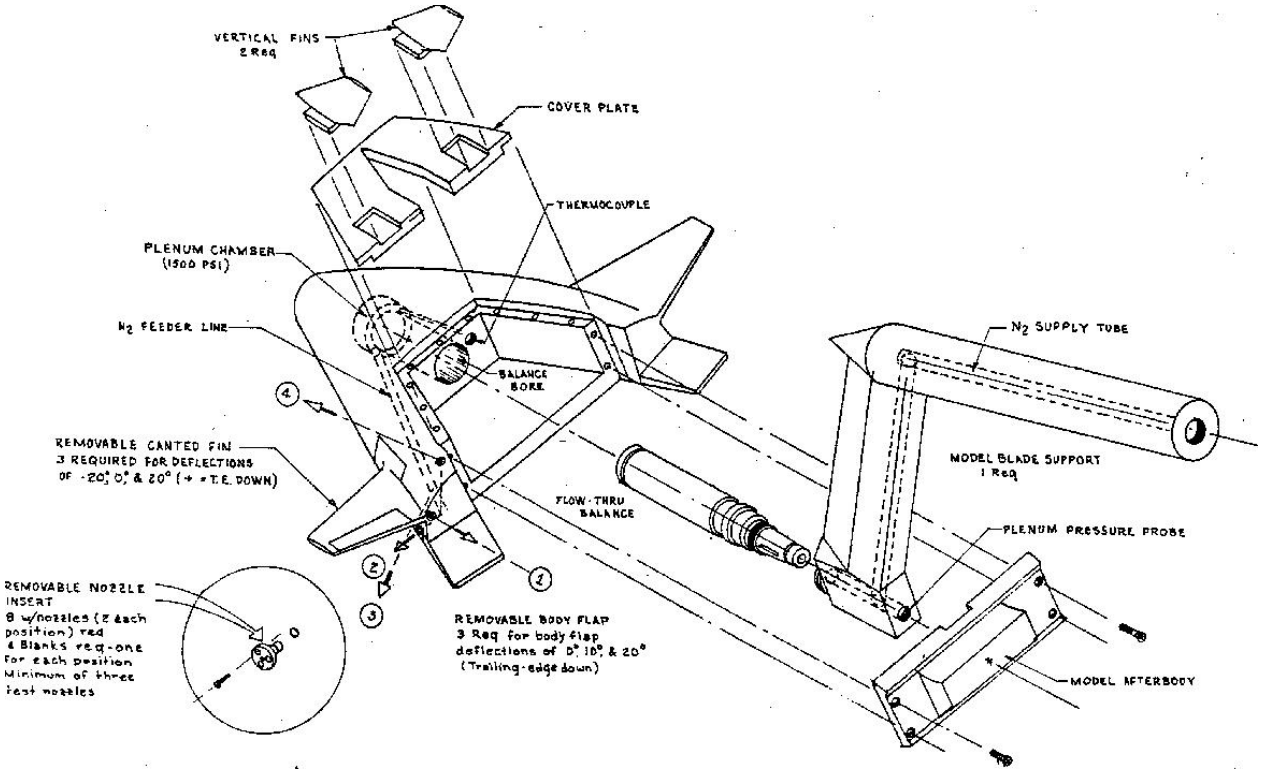

Figure 66. Exploded view of 1%-scale X-33 RCS model with flow-through balance and offset sting.

(a) Side view.

(b) Plan view.

Figure 67. Photographs of the 1%-scale X-33 RCS model installed in UPWT Test Section 2.

	Test	Mach	Re/ft (10^{-6})	Run	β, deg	P_{jet}, psi	LH/RH δ_{bflap}, deg	LH/RH δ_{elev}, deg	LH Nozzle
○	1713.	4.60	2.49	502.	-0.01	403.	0/0	0/0	3A, Down-firing
□	1713.	4.60	2.49	501.	0.00	508.	0/0	0/0	3A, Down-firing
◇	1713.	4.60	2.49	500.	-0.01	565.	0/0	0/0	3A, Down-firing
△	1713.	4.60	2.49	499.	0.00	726.	0/0	0/0	3A, Down-firing
◺	1713.	4.60	2.49	498.	0.00	949.	0/0	0/0	3A, Down-firing

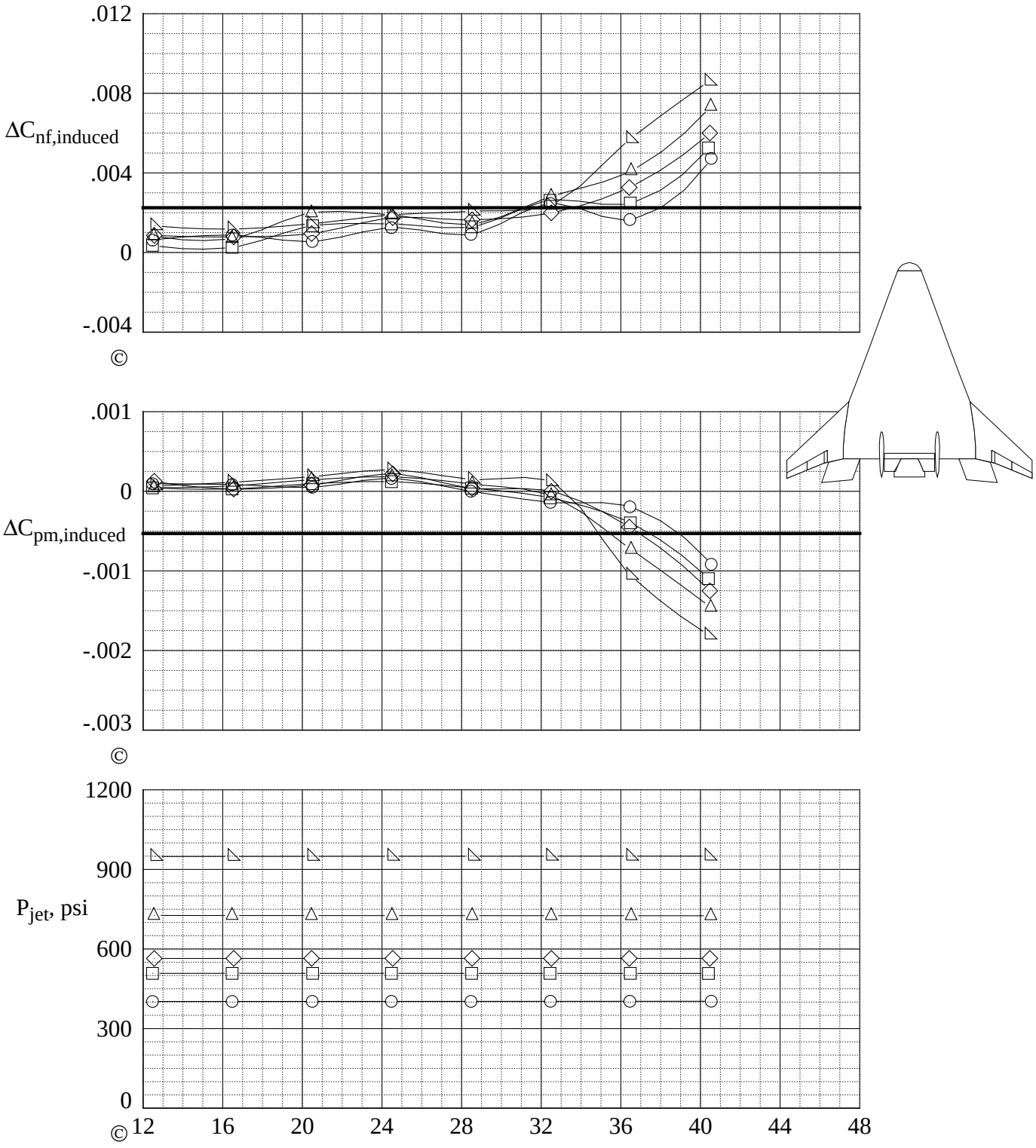

Figure 68. RCS jet-induced coefficient increments on the 1%-scale X-33 RCS model in the UPWT Test Section 2 at Mach = 2.5.

Figure 69. UPWT high angle-of-attack apparatus installed in Test Section 1. (Calibration plate shown on lower surface is installed for wind-off calibrations only.)

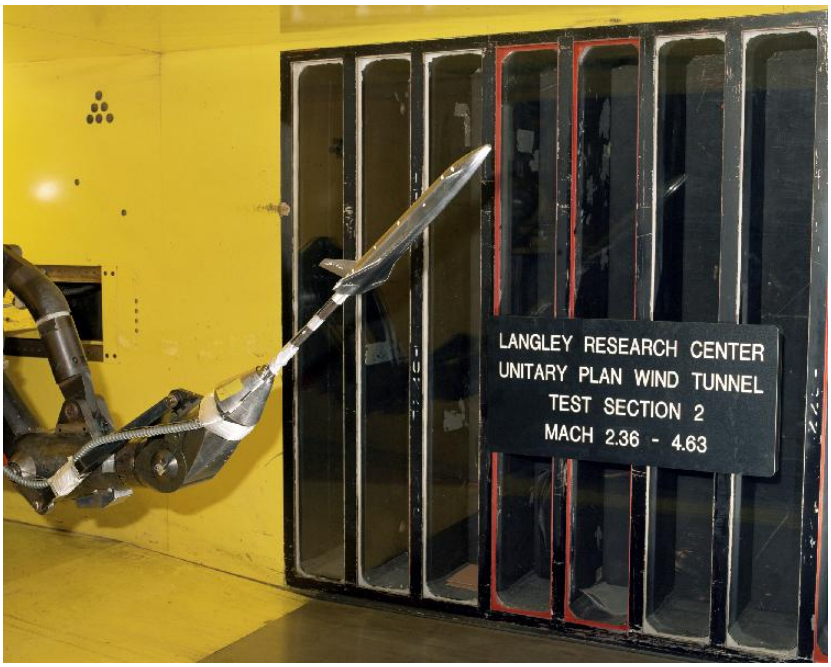

Figure 70. 1.75%-scale glideback booster model installed on the high angle-of-attack apparatus in UPWT Test Section 2.

Figure 71. 6%-scale Hyper-X stack configuration installed in UPWT Test Section 1.

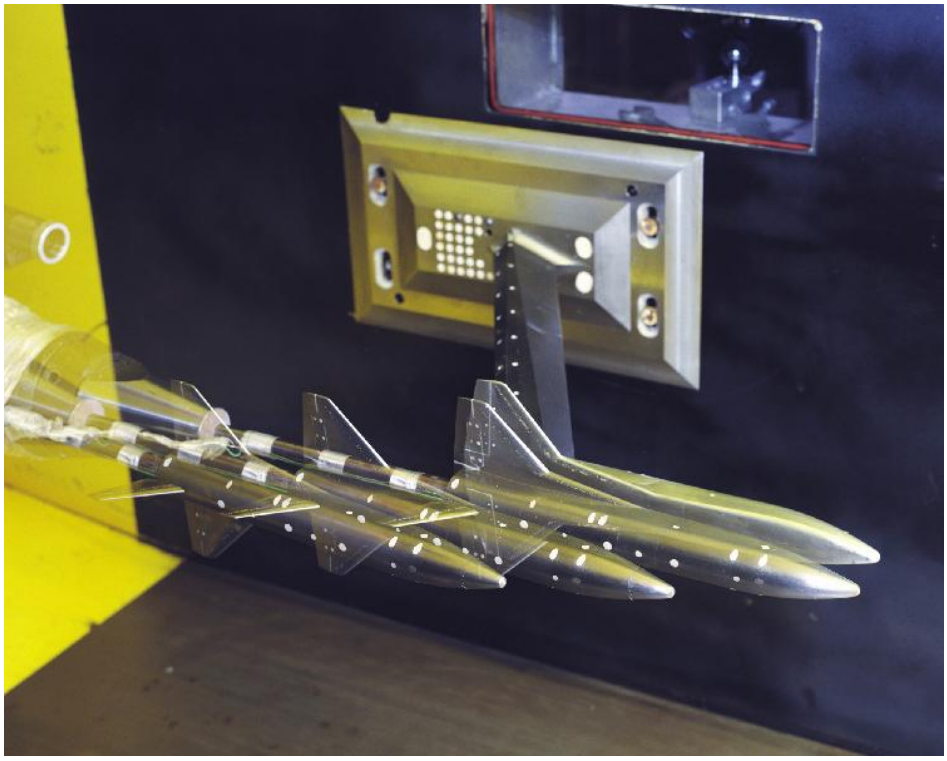

Figure 72. Multiple-exposure photograph of UPWT stage separation setup.

Figure 73. Simulated captive bimese arrangement using the UPWT stage separation setup.

Figure 74. Simulated spatial positioning in a stage separation trajectory.

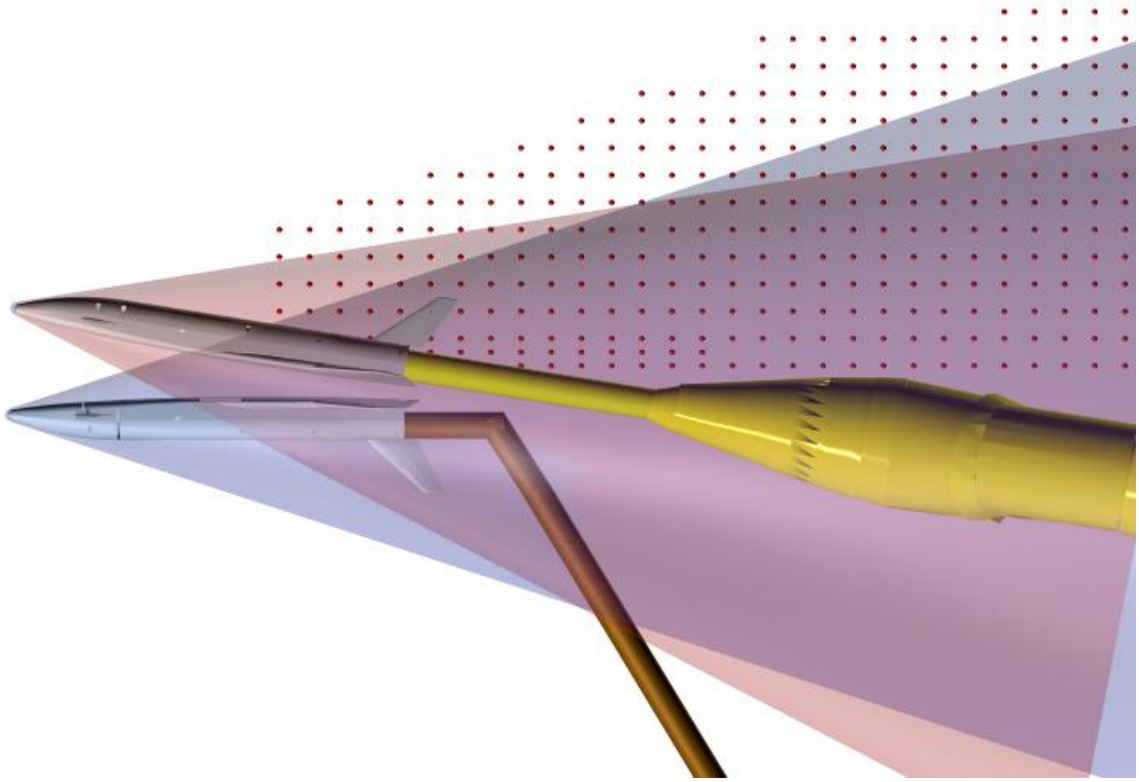

Figure 75. Preliminary Virtual Facilities rendering of the UPWT stage separation setup.

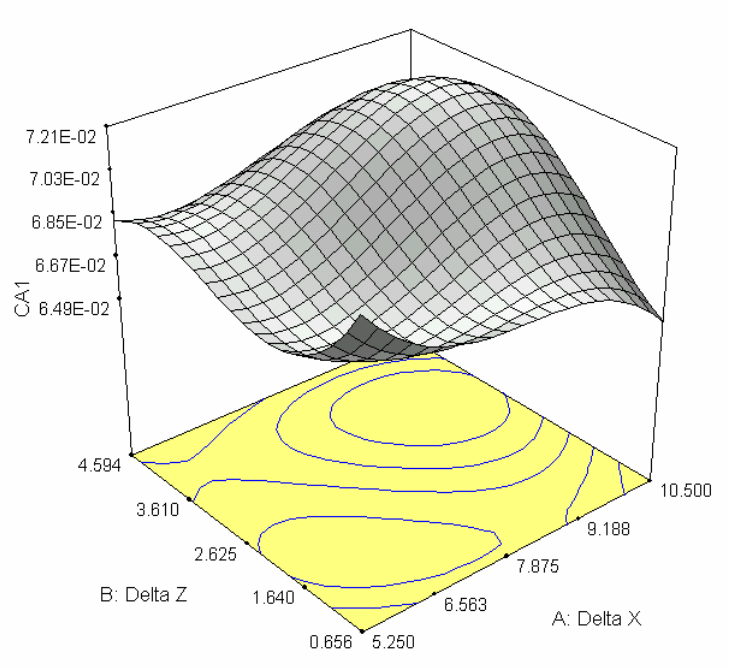

Figure 76. Orbiter model axial force response surface in a selected subspace at $\alpha = 2.5^{o}$.

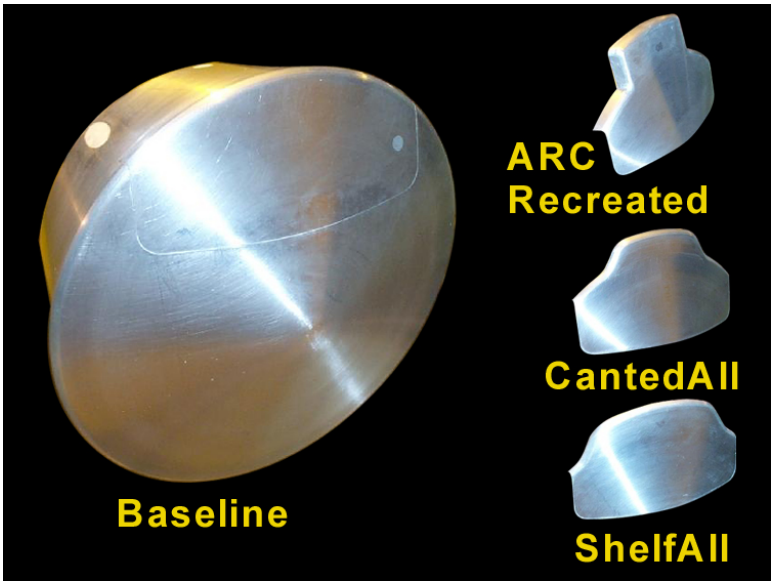

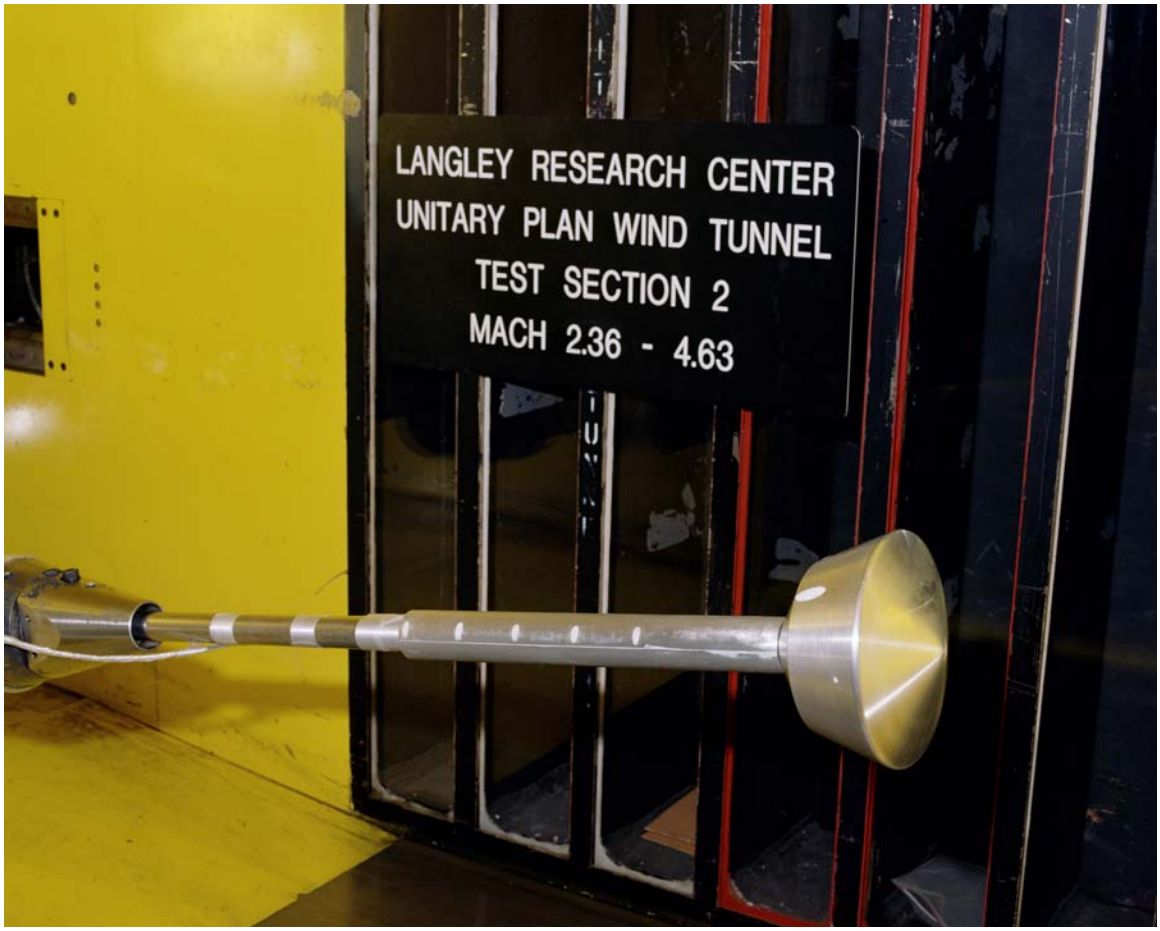

Figure 77. Mars Smart Lander model installed in UPWT Test Section 2.

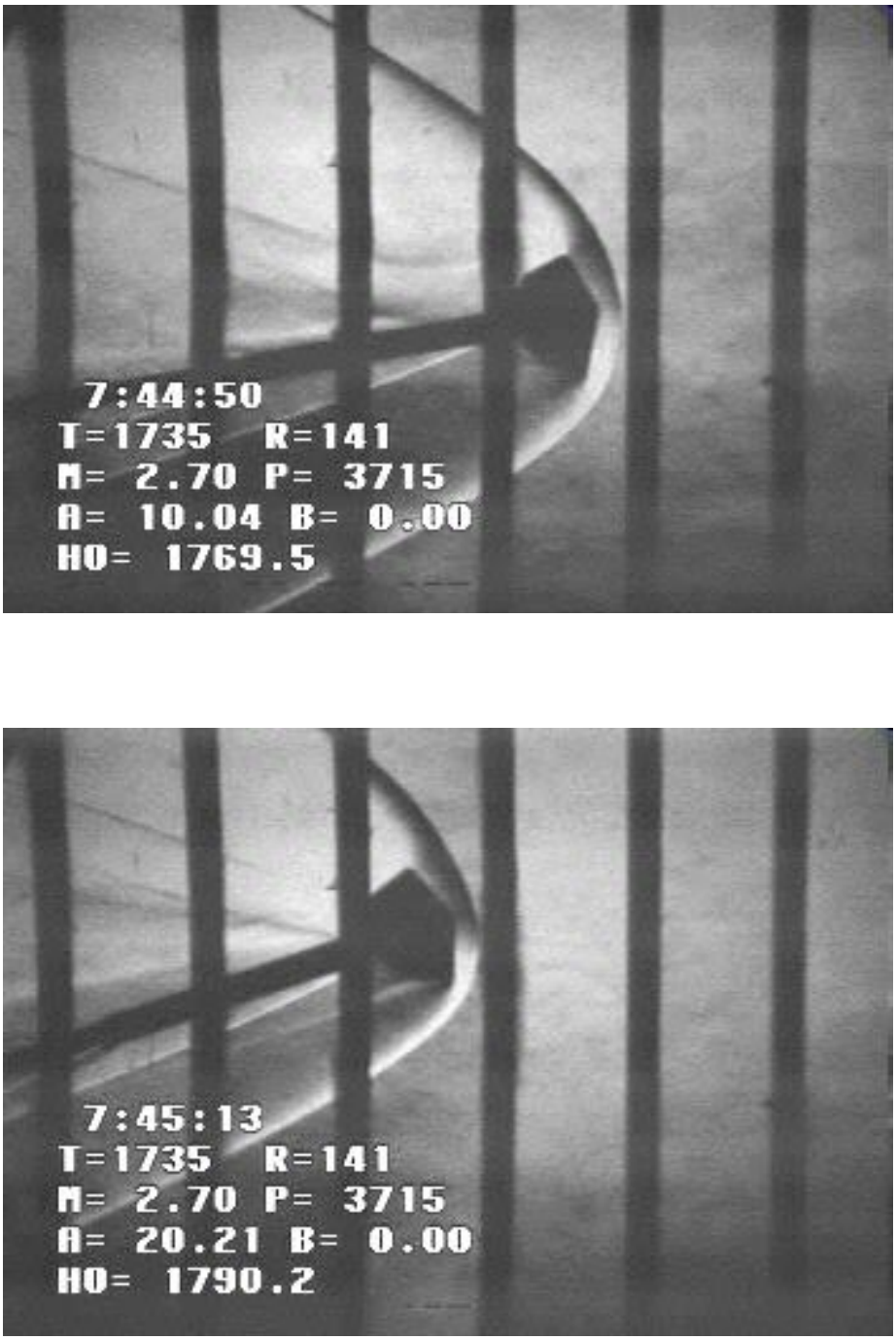

Figure 78. Schlieren flow visualization images of a Mars lander model at Mach = 2.7 in UPWT Test Section 2.

REPORT DOCUMENTATION PAGE

Form Approved
OMB No. 0704-0188

1. REPORT DATE *(DD-MM-YYYY)*	2. REPORT TYPE	3. DATES COVERED *(From - To)*
01- 08 - 2007	Technical Memorandum	

4. TITLE AND SUBTITLE
Overview of Supersonic Aerodynamics Measurement Techniques in the NASA Langley Unitary Plan Wind Tunnel

5a. CONTRACT NUMBER

5b. GRANT NUMBER

5c. PROGRAM ELEMENT NUMBER

6. AUTHOR(S)
Erickson, Gary E.

5d. PROJECT NUMBER

5e. TASK NUMBER

5f. WORK UNIT NUMBER
136905.02.04.04.01.04

7. PERFORMING ORGANIZATION NAME(S) AND ADDRESS(ES)
NASA Langley Research Center
Hampton, VA 23681-2199

8. PERFORMING ORGANIZATION REPORT NUMBER
L-19380

9. SPONSORING/MONITORING AGENCY NAME(S) AND ADDRESS(ES)
National Aeronautics and Space Administration
Washington, DC 20546-0001

10. SPONSOR/MONITOR'S ACRONYM(S)
NASA

11. SPONSOR/MONITOR'S REPORT NUMBER(S)
NASA/TM-2007-214894

12. DISTRIBUTION/AVAILABILITY STATEMENT
Unclassified - Unlimited
Subject Category 02
Availability: NASA CASI (301) 621-0390

13. SUPPLEMENTARY NOTES
An electronic version can be found at http://ntrs.nasa.gov

14. ABSTRACT

An overview is given of selected measurement techniques used in the NASA Langley Research Center (NASA LaRC) Unitary Plan Wind Tunnel (UPWT) to determine the aerodynamic characteristics of aerospace vehicles operating at supersonic speeds. A broad definition of a measurement technique is adopted in this paper and is any qualitative or quantitative experimental approach that provides information leading to the improved understanding of the supersonic aerodynamic characteristics. On-surface and off-surface measurement techniques used to obtain discrete (point) and global (field) measurements and planar and global flow visualizations are described, and examples of all methods are included. The discussion is limited to recent experiences in the UPWT and is, therefore, not an exhaustive review of existing experimental techniques. The diversity and high quality of the measurement techniques and the resultant data illustrate the capabilities of a ground-based experimental facility and the key role that it plays in the advancement of our understanding, prediction, and control of supersonic aerodynamics.

15. SUBJECT TERMS
Aerodynamics; Modern design of experiments (MDOE); Electronic pressure scanners; Flow measurements; Flow visualization; Strain gage balances; Supersonic; Test techniques; Virtual diagnostics; Wind tunnel

16. SECURITY CLASSIFICATION OF:			17. LIMITATION OF ABSTRACT	18. NUMBER OF PAGES	19a. NAME OF RESPONSIBLE PERSON
a. REPORT	b. ABSTRACT	c. THIS PAGE			STI Help Desk (email: help@sti.nasa.gov)
					19b. TELEPHONE NUMBER *(Include area code)*
U	U	U	UU	107	(301) 621-0390